Impact of a mixed water methanol feed on olefin formation during the MTO process

Yentl Pauwels

Supervisor: Prof. dr. ir. Veronique Van Speybroeck
Counsellors: Dr. Kristof De Wispelaere, Simon Bailleul

Master's dissertation submitted in order to obtain the academic degree of
Master of Science in Chemical Engineering

Department of Applied Physics
Chair: Prof. dr. ir. Christophe Leys
Faculty of Engineering and Architecture
Academic year 2015-2016

UNIVERSITEIT GENT

This research was conducted at the Center for Molecular Modeling.

Acknowledgements

The last five years have been challenging, interesting and above all educative. I gained knowledge and insight in the field of chemical engineering and now, at the end of my academic program, I am ready for the industry. Therefore, I would like to thank all of the people that have been involved in this route and helped me to tackle the obstacles. During my last year at the university of Ghent I chose to do my master thesis at the research group CMM. Not only was I interested in molecular modeling, the dynamics of the group convinced me of this choice. I would like to thank the CMM research group for giving me the opportunity to do my research.

I enjoyed the ambiance between the group members and therefore I would like to thank all the CMM'ers. In specific I would like to thank my supervisor Veronique Van Speybroeck and counselors Kristof De Wispelaere and Simon Bailleul for their commitment and great advice. They always provided constructive feedback, new insights and new future challenges. Thanks to their suggestions new routes were explored, bringing me to the result I show today.

Furthermore, I would like to thank my thesis friends Senne, Titus, Pieter, Klaas and Michiel. Not only did they create a great atmosphere in our thesis room, they were always eager to listen to my progress and above all they provided a listening ear while expressing my frustrations. They also helped by passing through their experience of working with LaTeX.

I also want to thank my class mates for the great five years of study we had. I will see you around. At last I want to thank my family and friends for their support in everything I do.

Yentl Pauwels
Ghent, June 1st 2016

Impact of a mixed water methanol feed on olefin formation during the MTO process

Yentl Pauwels

Supervisors: prof. dr. ir. Veronique Van Speybroeck
Counsellors: dr. ir. Kristof De Wispelaere, ir. Simon Bailleul

Master's dissertation submitted in order to obtain the academic degree of
Master of Science in Chemical Engineering

Faculty of Engineering and Architecture – Ghent University
Center for Molecular Modeling
Academic year 2015–2016

Abstract

Due to the interest in renewable feedstock, the Methanol-to-Olefin (MTO) process was developed as an alternative for the conventional steam cracking process to produce light olefins. In this process a methanol source originating from a carbon-rich feedstock is converted into hydrocarbons using zeolite catalysts. The hydrocarbon pool mechanism is nowadays generally accepted where a pool of organic species acts as co-catalyst in the reaction mechanism. In the archetypal H-SAPO-34 catalyst, polymethylbenzenes are identified as the major HP species. For such aromatic compounds the side-chain and paring mechanism was proposed. Impact of water may eventually tune the product selectivity towards lower/ higher olefins.

In this work the effect of water is investigated on the paring mechanism by ab inito molecular modeling techniques to obtain information on the dynamic behavior of the process. The contraction reaction steps are studied by evaluation of the expansion of the unit cell, the stability of the intermediates and additional water molecules within the framework. Furthermore, metadynamics techniques are used to calculate the free energy barrier of the reactions to asses the reactivity of some carbocationic intermediates.

Keywords: Methanol-To-Olefin process, H-SAPO-34, paring mechanism, ab initio molecular dynamics, metadynamics

Impact of a mixed water methanol feed on olefin formation during the MTO process

Yentl Pauwels
Supervisor: prof dr. ir. Veronique Van Speybroeck
Counsellors: dr. ir. Kristof De Wispelaere and ir. Simon Bailleul

Abstract—**Molecular modeling of chemical reactions is an important technique in chemical engineering for mechanism elucidation and process optimization. Hereby, ab initio molecular dynamic modeling is a valuable tool to obtain information on the dynamic behavior of the process and is often used in the research towards the very complex Methanol-to-Olefin (MTO) process. Together with metadynamics techniques it gives information about reactions and free energy barriers. Both techniques have been used in this master thesis to analyze the effect of water on the paring mechanism of the MTO process. It was found that at low water loadings, water destabilizes the intermediate. This effect diminishes at high water loadings where water is more clustered resulting in a decrease of the energy level. Thus, it is suggested that the overall effect of water is that it can help the formation of propylene at high water loading, in order to overcome the large energy barriers of this route.**

Keywords—**Methanol-to-Olefin process, H-SAPO-34, paring mechanism, ab initio molecular dynamics, metadynamics**

I. Introduction

In view of the depleting oil reserves, researchers try to find alternatives for the production of ethylene and propylene. For this purpose the Methanol-to-Olefins (MTO) process, in which a methanol source originating from a carbon-rich feedstock can be converted into hydrocarbons using zeolite catalysts, was developed.[1] The complex MTO mechanism is currently still under investigation, but the hydrocarbon pool (HP) mechanism is nowadays generally accepted.[2] Herein, a pool of organic molecules present in the zeolite acts as a co-catalyst in the reaction mechanism.[3] In the archetypal H-SAPO-34 catalyst, polymethylbenzenes are identified as the major HP species.[4] For such aromatic HP compounds a distinction can be made between two proposed pathways: the side-chain and the paring mechanism.[5] In this contribution we will focus on propylene formation in H-SAPO-34 via the paring mechanism, which is characterized by subsequent ring contraction and expansion reactions of the aromatic HP molecules, as depicted in Figure 1. The first step that was investigated is the contraction reaction of the heptamethylbenzenium cation (heptaMB$^+$) to the pentamethyl-isobutyl-cyclopentadienyl cation (5-iC_3-CP^+). The latter species was found to be in equilibrium with the bicyclic molecule pentamethyl-dimethylcyclopropyl-cyclopentenyl cation (5-3-CP$^+$). In a second reaction the carbon-carbon bound between the ring and isopropyl group is broken and a hydride transfer takes place resulting in the formation of propylene and the pentamethylcyclopentadienyl cation (PMCP$^+$).

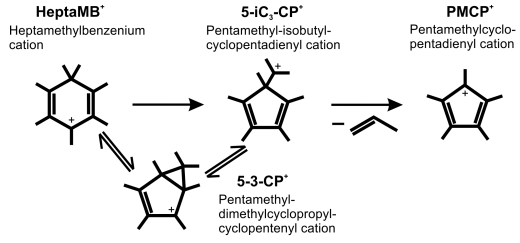

Figure 1: Overview of the investigated reactions within the paring cycle in H-SAPO-34.

An objective in the research towards the MTO process is to obtain a better control of the ethylene/propylene ratio. One of the strategies that has been proposed (and industrially applied) is the addition of water/steam to the feed which increases the ethylene selectivity and catalyst lifetime.[6, 7]

To elucidate the effect of water on the feasibility of the paring mechanism, a detailed mechanistic study on the paring cycle is performed with state-of-the-art molecular simulation techniques encompassing first principle molecular dynamics and metadynamics. A H-SAPO-34 unit cell is considered and in order to evaluate the behavior of the water molecules, different degrees of water loading are added as schematically shown in Figure 2. The chosen reaction steps are tested by evaluating the framework flexibility and this is linked to the contraction/expansion of the intermediate molecule. Furthermore the position of the water is evaluated and linked to possible interaction with the framework or the intermediate.

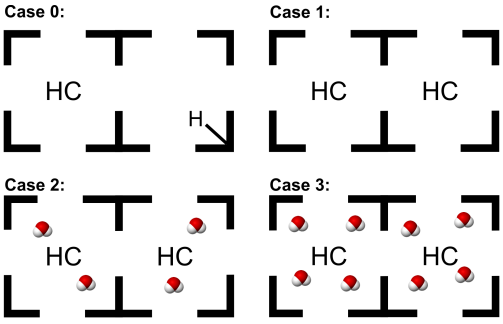

Figure 2: Schematic representation of the four simulations that have been performed concerning one of the intermediates of the paring cycle.

II. Computational methods

All simulations are performed using CP2K with a GTH basis set and pseudopotentials. Furthermore, the combined GPW basis set approach is used with the revPBE functional and Grimme D3 dispersion corrections are added. An empty H-SAPO-34 unit cell containing 110 atoms is used for which periodic boundary conditions are applied in order to get a full representation of the catalyst topology. The catalyst is activated by the substitution of two Si substitutional defects such that two Brønsted acid sites are obtained per unit cell. Ab initio molecular dynamics (AIMD) simulations have been performed with a timestep of 0.5 fs in the NPT ensemble at 623 K and 1 atm. The system was first equilibrated with the CSVR thermostat and thereafter a 50 ps production run with a chain of five Nosé-Hoover thermostats was obtained. The pressure was controlled by a MTK barostat. For the metadynamics simulations the same basis set and functionals are used but these simulations are performed in the NVT ensemble at 623 K using a chain of five Nosé-Hoover thermostats. A timestep of 0.5 fs was taken and Gaussian hills of 5.0 kJ/mol were added every 50 steps. The width of the Gaussian hills was set to 0.02.

III. Results and discussion

I. Analysis methods for the AIMD simulations

The effect of water, the behavior and stability of the carbocationic intermediate is studied by performing several analyses on the results of the AIMD simulations for the three considered intermediates of the paring mechanism. First of all, the volume of the framework is studied because this might act as driving force for the contraction step to proceed. Together with the variation of the unit cell volume, the change in the unit cell parameters in all three directions, indicated on Figure 3, are analyzed to elucidate possible anisotropy in these variations. Furthermore, the mobility of the solvent molecules and aromatic HP species within the zeotype framework are studied and visualized in order to see the preferred position of the water molecules. Herein, clustering of the water molecules is of course evaluated. In this master thesis clustering was considered to be present if the distance between two oxygen atoms of water molecules is less than 3.5 Å. For the analysis of the mobility of the aromatic species within the framework, two angles are defined as indicated in Figure

3. α is the angle between the plane spanned by the ring carbon atoms of the hydrocarbons and the vector spanned by six of the T-atoms of the framework. β is the angle defined between the ring carbon atoms of the hydrocarbons and the vector spanned by four of the T-atoms of the framework that are perpendicular to the previous framework atoms. 2D histograms are made based on these two angles to visualize hotspots in the orientation of the intermediate. The position of the aromatic species is than linked to the previous results. Lastly, the energy profile of the calculations obtained from AIMD calculations is investigated. However, no activation barriers are calculated, the energy profile gives an idea of the driving force for the reaction to proceed.

In case 1, 2 and 3, as denoted in Figure 2, an intermediate is placed in each cage to prevent unwanted diffusion of water molecules to a neighboring cage. However by periodicity still an empty cage is created. Some of the solvent molecules diffused to this area further denoted as the empty cage.

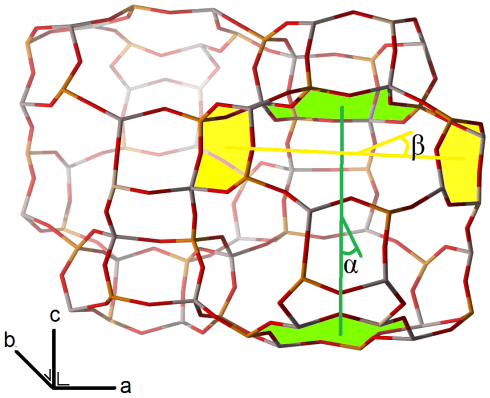

Figure 3: Representation of H-SAPO-34 with indicated α and β angle as well as with the a, b, c directions.

In the subsequent metadynamics simulations, energy (in the form of Gaussian hills) is added to the free energy surface in function of a limited number of collective variables (CV) in order to overcome the reaction barrier. Based on these Gaussian hills the free energy surface can be reconstructed. This allows studying the reactivity of some intermediates occurring in the paring cycle.

II. Behavior and stability of paring cycle reaction intermediates

Analysis of the framework flexibility showed that loading H-SAPO-34 with heptaMB$^+$ at 623 K and 1 atm results in the elongation of the framework in the c-direction relative to an empty catalyst framework (see Figure 4). This result could be related to the position of the intermediate within the framework which was preferentially positioned along the c-axis.

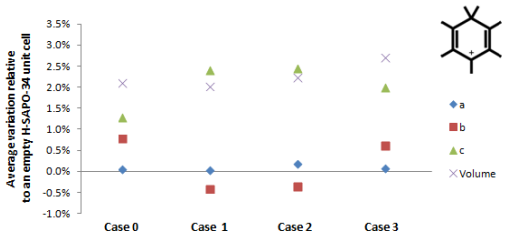

Figure 4: Average variation of unit cell parameters and volume relative to an empty H-SAPO-34 unit cell at 623 K and 1 atm of heptaMB$^+$ for a 50 ps MD simulation.

After loading of the systems with water (case 2), the anisotropy remained with its strongest elongation in the c-axis. At low water loading, the orientation of heptaMB$^+$ is not much effected by the solvent molecules due to the position of the solvent in the empty cage. However with an increased water loading (case 3) it was found that the framework elongation became less anisotropic and more solvent molecules are positioned close to heptaMB$^+$ and to the framework. Thus, it is concluded that at higher water loading, molecules are more attracted to the intermediate and the framework. Furthermore, an increased water loading leads to an increased water clustering. In case 2, 50 % of the water molecules does not form a cluster, 30 % forms dimers and 20 % trimers. These values shifts with higher loadings since all water molecules are clustered. In case 3, 68 % forms a dimer, 15

% trimers, 11 % tetramers and 6 % pentamers. So a clear trend to higher cluster formation is seen with higher water loading which should not be surprising.

It is suggested that the position of the solvent molecules influences the position and orientation of the intermediate thus affecting the unit cell of the framework.

During the AIMD simulation of 5-3-CP$^+$ all the H-SAPO-34 unit cell parameters variations are positive and the prominent elongation in the c-direction is not present (see Figure 5). The unit cell volume decreases from case 2 to case 3 and the elongation is less anisotropic in case 3. Both for case 2 as for case 3 more water molecules are constrained to 5-3-CP$^+$ than for the heptaMB$^+$ as was seen visually. Furthermore, in case 2 the clustering consists only of dimers (72 %). 28 % does not form any cluster. In case 3, 66 % of the water molecules forms dimers, 20 % trimers, 9 % tetramers and 4 % pentamers. Again, the variety of clustering increases with increasing water loading.

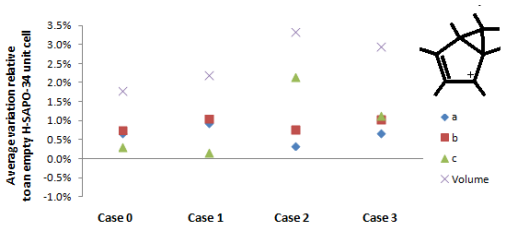

Figure 5: Average variation of unit cell parameters and volume relative to an empty H-SAPO-34 unit cell at 623 K and 1 atm of 5-3-CP$^+$ for a 50 ps MD simulation.

Besides a difference in the unit cell variations, there is also an energy difference between both intermediates. As shown in Figure 6, the energy difference between heptaMB$^+$ and 5-3-CP$^+$ increases at first (when two water molecules are added in each cage compared to case 0 where no water molecules are present) but this difference diminishes when four water molecules are added in each cage. The effect of water on the energy profile is thus relatively outspoken but at high water loadings the effect completely cancels out again. It should be noted that a simulation of 50 ps is rather short to do accurate energy calculations because of the rather large energy variations over time.

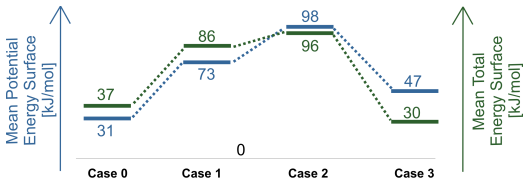

Figure 6: Energy profile for the different cases of 5-3-CP$^+$ relative to heptaMB$^+$ at 623 K and 1 atm during a 50 ps MD simulation.

It is concluded that in case of 5-3-CP$^+$ at low water loading, more water molecules are positioned close to the intermediate compared to heptaMB$^+$. This results in a different behavior of the framework flexibility and result in a destabilization of the energy profile. At high water loadings, the clustering increases, resulting in a decrease of the energy profile.

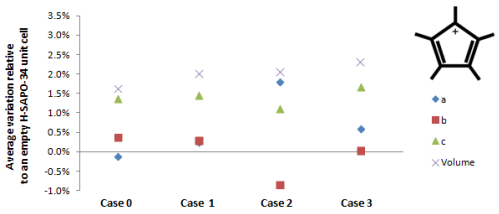

Figure 7: Average variation of unit cell parameters and volume relative to an empty H-SAPO-34 unit cell at 623 K and 1 atm of PMCP$^+$ for a 50 ps MD simulation.

The last evaluated intermediate is PMCP$^+$. In Figure 7 its unit cell parameter is given. When no water molecules are present, the elongation is the strongest in the c-direction and all the variations are positive. However, when water molecules are added (in case 2), the strongest elongation is seen in the b-direction with a contraction in the a-direction. This position of the intermediate is shown in Figure 8. At low water loading, no molecule is positioned in the so

called empty cage. Furthermore, in case 2 93 % of the water molecules forms dimers and only 7 % remain unclustered.

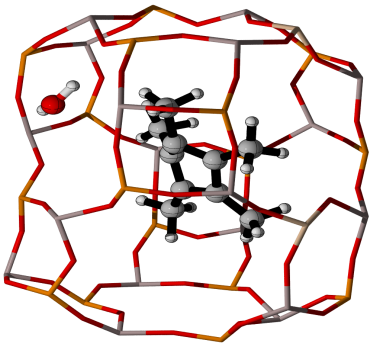

Figure 8: Snapshot of the position of $PMCP^+$ (α = 25, β = 8) in case 2 in H-SAPO-34 in a 100 ps MD simulations at 623 K and 1 atm.

When more water molecules are added in case 4, everything is clustered with a distribution of 52 % dimers, 24 % trimers, 17 % tetramers and 7 % pentamers. The amount of clustering is higher compared with the clustering for the other two considered intermediates. Furthermore, the intermediate positions is given in Figure 9 in which the 5-3-CP^+ is mobile within both α and β.

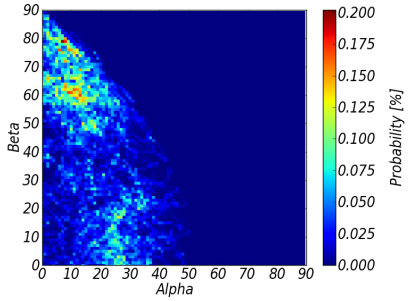

Figure 9: Probability density distribution of the position of 5-3-CP^+ in case 3 in H-SAPO-34 in a 50 ps MD simulations at 623 K and 1 atm in the two cages.

At last, the probability distribution of the shortest distance between both Si-atoms and all C-atoms is shown in Figure 10 which shows a broader distribution for higher water loading. Although, not shown here, this result did not appear for $heptaMB^+$ and 5-3-CP^+.

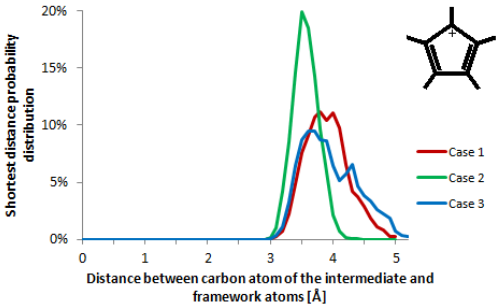

Figure 10: Shortest probability distribution of the distance between Si of the framework and a carbon atom of $PMCP^+$ in H-SAPO-34 in a 50 ps MD simulation at 623 K and 1 atm for the three cases

It is suggested that competition between the water molecules and the intermediate to locate itself towards the Si-atom result at high water loadings in a decrease of the energy level as was seen in the results of 5-3-CP^+.

III. Reactivity of paring cycle reaction intermediates

During the metadynamics simulations, only the first reaction step (i.e. the contraction of $heptaMB^+$) is shown here. In order to perform metadynamics calculations collective variables (CV) were defined which induce the transition from the reactant to the product state and back. The 2D free energy surface of the contraction reaction is given in Figure 11. The two regions corresponding with 5-iC_3-CP^+ (C) and 5-3-CP^+ (B) are both visualized. It can be immediately seen that $heptaMB^+$ (A) is far more stable than the five-ring molecules. However these results are preliminary as yet no sufficient barrier recrossing has been achieved of the result.

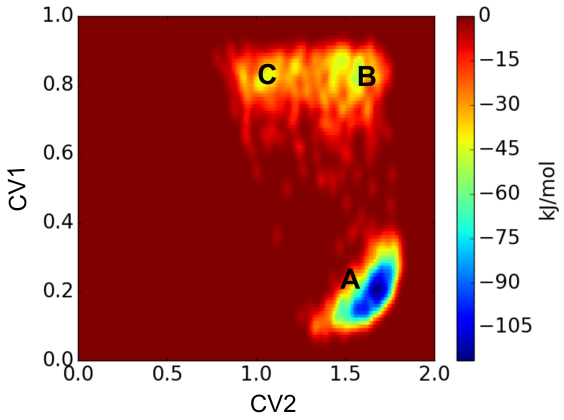

Figure 11: 2D FES obtained from the metadynamics simulation of the ring contraction of heptaMB$^+$ at 623 K and 1 atm in case 0. A) heptaMB$^+$ B) 5-3-CP$^+$ C) 5-iC_3−CP$^+$.

IV. Conclusion and future outlook

From the analyses performed, it is concluded that adding water molecules lead to a competition between the water molecules and the considered intermediate to interact with the active site of the framework. This results in a lower stability of the intermediates. However, when further increasing the water loading the amount of clustering increases. Taking into account the increased amount of clustering, it can be assumed that due to the clustering there is less competition between the water molecules and the carbon atoms to interact with the framework stabilizing the system. Thus, it is suggested that the overall effect of water on the paring cycle is that it can help the formation of propylene at high water loading, in order to overcome the large energy barriers of this route.
The incomplete obtained 2D free energy profile shows its lowest energy around -105 kJ/mol. Although further analysis of the free energy profile is needed. An alternative mechanism in which first expansion proceeds before contraction take place seems promising and could be interesting for future work.[8]

Acknowledgements

This work was performed at the Center for Molecular Modeling under the supervision of prof. dr. ir. Veronique Van Speybroeck, dr. ir. Kristof De Wispelaere and ir. Simon Bailleul. I would like to thank them for this support and guidance. The computational resources and services used were provided by Ghent University (Stevin Supercomputer Infrastructure).

References

[1] Olsbye, U. and Svelle, S. and Bjørgen, M. and Beato, P. and Janssens, T. V. W. and Joensen, F. and Bordiga, S. and Lillerud, K. P. Conversion of Methanol to Hydrocarbons: How Zeolite Cavity and Pore Size Controls Product Selectivity. *Angew. Chem., Int. Ed.*, 51 (2012) 5810–5831

[2] I. M. Dahl and S. Kolboe On the reaction mechanism for hydrocarbon formtation from methanol over sapo-34. Isotopic labeling studies of the co-reaction of ethene and methanol *J. Catal.*, 149 (1994) 458–464

[3] D. M. McCann, D. Lesthaeghe, P. W. Kletnieks, D. R. Guenther, M. J. Hayman, M. Waroquier, J. F. Haw A complete catalytic cycle for supramolecular methanol-to-olefins conversion by linking theory with experiment. *Angew. Chem., Int. Ed.*, 47 (2008) 5179–5182

[4] B. Arstad and S. Kolboe The reactivity of molecules trapped within the SAPO-34 cavities in the methanol-to-hydrocarbons reaction. *J. Am. Chem. Soc.*, 123 (2001) 8137–8138

[5] K. Hemelsoet, J. Van der Mynsbrugge, K. De Wispelaere, M. Waroquier, V. Van Speybroeck Unraveling the Reaction Mechanisms Governing Methanol-to-Olefins Catalysis by Theory and Experiment. *ChemPhysChem*, 14 (2013) 1526–1545

[6] K. De Wispelaere, C. S. Wondergem, B. Ensing, K. Hemelsoet, E. J. Meijer, B. M. Weckhuysen, V. Van Speybroeck, and J. Ruiz-Martinez Insight into the effect of water on the methanol-to-olefins conversion in h-sapo-34 from molecular simulations and in situ microspectroscopy. *ACS Catal.*, 6 (2016) 1991–2002

[7] Wragg, D. S. and Johnsen, R. E. and Norby, P. and Fjellvag, H. The adsorption of methanol and water on SAPO-34: in situ and ex situ X-ray diffraction studies *Microporous Mesoporous Mater.*, 134 (2010) 210–215

[8] B. Arstad, S. Kolboe , and O. Swang Theoretical study of the heptamethylbenzenium ion. intramolecular isomerizations and c2, c3, c4 alkene elimination. *I. Phys. Chem. A*, 109 (2005) 8914–8922

Contents

List of abbreviations

AIMD	Ab initio molecular dynamics
BO	Born-Oppenheimer
bpd	Barrels per day
CN	Coordination number
CSVR	Canonical sampling through velocity rescaling
CV	Collective variable
D	Deuterium
DFT	Density functional theory
DFT-D	Density functional theory - dispersion
DME	Dimethyl ether
DMTO	Dimethyl ether/ methanol to olefin process
GC-MS	Gas chromatography-Mass spectroscopy
GGA	Generalized gradient expansion
GPW	Gaussian and plane waves
GTO	Gaussian type orbitals
$HeptaMB^+$	Heptamethylbenzenes
HexaMB	Hexamethylbenzenes
HP	Hydrocarbon pool
IR	Infrared
IZA	International Zeolite Association
LCAO	Linear Combination of Atomic Orbitals
LDA	Local-density approximation
MD	Molecular dynamics
MTD	Metadynamics
MTG	Methanol-to-Gasoline
MTO	Methanol-to-Olefins
MTP	Methanol-to-Propylene
NMR	Nuclear Magnetic Resonance
PBC	Periodic boundary conditions
PBE	Perdew, Burke, Enrzerhof
PMB	Polymethylbenzene

PES	Potential Energy Surface
PW	Plane waves
SAPO	Silicoaluminophosphate
STO	Slater type orbitals
syngas	Synthesis gas
TIGAS	Topsøe integrated gasoline synthesis
UV–VIS	Ultraviolet–visible spectroscopy
QM/MM	Quantum mechanics/molecular mechanics
ZSM	Zeolite Socony Mobil

List of symbols

a	ms^-2	Acceleration of the nuclei
E	kJ/mol	Total energy
F	N	Forces on the nuclei
$\widehat{H}_{el}$	J	Hamiltonian
K	kJ/mol	Kinetic energy
k_b	J/K	Boltzmann constant
m	kg	Mass of the nuclei
r	Å	Position of the nuclei
t	s	Time
T	K	Temperature
U/V	kJ/mol	Potential energy
x	Å/Å^3	Unit cell parameter (a, b, c or volume)
$\bar{x}$	Å/Å^3	Unit cell parameter (a, b, c or volume)
α	[-]	Angle
β	[-]	Angle
$\Delta_r H^\circ$	kJ/mol	Reaction enthalpy at 298 K

Chapter 1

Introduction

In view of the depletion of oil reserves,[1] researchers try to find alternatives for the production of ethylene and propylene,[2] since the demand for ethylene and propylene is still increasing.[3] Alternative resources e.g. methanol, biomass and CO_2 have been investigated and discussed for many years.[4,5] For this purpose the Methanol-to-Olefins (MTO) process was developed as an alternative for the conventional steam cracking process to produce light olefins. In this process a methanol source originating from a carbon-rich feedstock - such as natural gas or coal - can be converted into hydrocarbons using zeolite catalysts.[4] Although research on alternative fuels gain more and more attention, one can conclude that the oil reserves will still supply the earth for many years. Therefore, the key to the commercial success of the MTO process will be its viability against traditional resources. A high oil price will be beneficial for the MTO process and vice versa. BP estimated in 2014 that at the current production rates the earth will be able to produce oil for the next 53 years.[6] The proved oil reserves of the main five producing countries are graphically presented in Figure 1.1. Proven oil reserves are defined as those that have a reasonable certainty of being commercially recoverable under existing economic and political conditions, with existing technology.[7,8] Unfortunately, the oil price dropped enormously in 2015 due to the concurrence with shale gas (see Figure 1.2).[9] In the US the cost-advantaged light feedstock (natural gas or shale gas) is mostly used in steam cracking (often called ethane crackers) instead of the oil derivative naphta. Ethane crackers result in the production of predominately ethylene. Propylene on the other hand is produced as a byproduct in steam cracking with naptha as feedstock. The change of feedstock to ethane has resulted in an increasing demand for propylene production and the production of shale gas further disrupted the ethylene/propylene balance. The ethylene demand is estimated to increase from 140 million tonnes in 2014 to 196 million tonnes by 2023 and the propylene demand is estimated to increase from 90 million tonnes in 2014 to 130 million tonnes by 2023.[10]

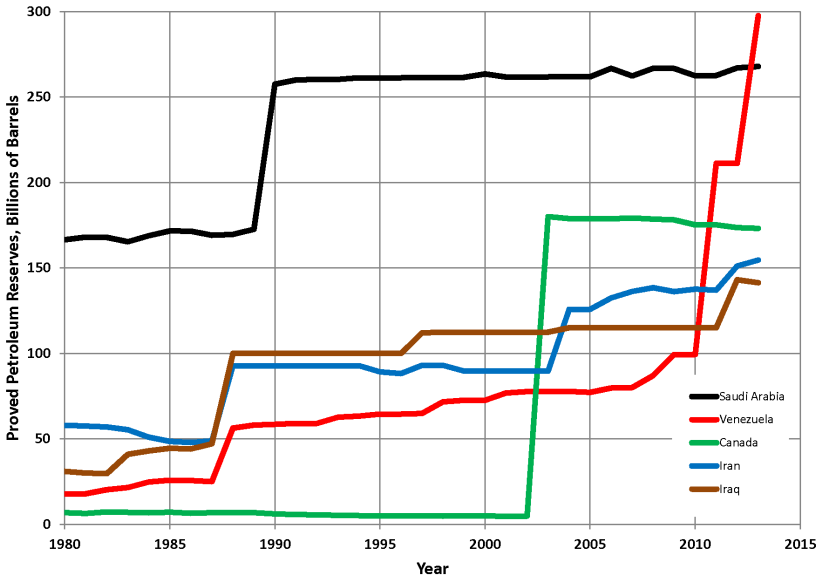

Figure 1.1: Proven oil reserves of the top five producing countries.[7]

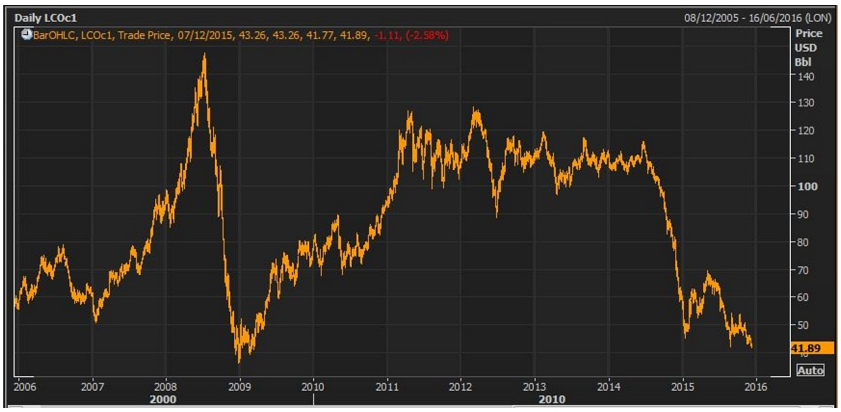

Figure 1.2: Oil Price per barrel from 2005 until 2016.[9]

1.1 History of the methanol conversion process

Research to alternative energy fuels and in specific to methanol production was spurred by the 70's oil crisis and the discovery of a new acidic aluminosilicate zeolite called H-ZSM-5.[11] It was found that the combination of its acidity and shape selectivity properties lead to the ideal catalyst for industrial use. In 1973 a Mobil research group found the ability of H-ZSM-5 to convert methanol into hydrocarbons similar to high-octane gasoline[12]. This resulted in the Methanol-to-Gasoline (MTG) process and has been further developed by Mobil.[13]

Following, New Zealand selected the MTG process in 1979 over the Fischer-Tropsch process (commercialized as the SASOL process[14]) for the production of gasoline from natural gas. Even though the MTG technology was not proven at the time and the SASOL process was already commercialized, the plant went in operation in 1986 and produced 600,000 tonne gasoline a year, which was one third of the national demand of gasoline. Unfortunately, just after the installation the oil price dropped so steep that the plant was shut down and only the methanol production remained, continuing operation as such until today. In the eighties a MTG pilot set-up was build in Wesseling, Germany. This reactor using a H-ZSM-5 catalyst could produce 16 tonne of gasoline per day.[15]

Worth mentioning here is an alternative process for the MTG process, called the TIGAS (Topsøe integrated gasoline synthesis) process. The main difference being the immediate production if a mixture of methanol and dimethylether (DME) in the TIGAS process, without producing methanol separately. This process has a higher efficiency and overcomes the problem of condensation and re-evaporation of methanol.[16] Although the process looked promising, research is no longer focused on the MTG process because of a diminished importance of gasoline production.

Research focus has shifted to the production of light olefins: the MTO process. It was developed after the discovery of H-SAPO-34 by researchers at Union Carbide (now UOP).[17] The structure of this catalyst is characterized by it small windows that increase the selectivity towards light olefins, such as ethylene and propylene. At the end of the eighties the oil price increased again and new pilot set-ups were built. In 1996, UOP (in corporation with Norsk Hydro) announced that their MTO process was ready for the construction of a 250,000 tonne olefins per year plant. Total Petrochemicals further improved the industrial process by combining the UOP/Hydro process with an olefin cracking unit to further increase the selectivity towards light olefins. A pilot set-up was build in 2009 in Felluy, Belgium with a capacity of 10 tonne per day of methanol feed.[18,19]

Researchers at Lurgi came up with a new route to increase the yield of propylene, called the Methanol-to-Propylene (MTP) process. Herein the unwanted molecules such as ethylene and butylene are recycled to the reactor resulting in a high selectivity towards propylene (70 %). This process was build in China in 2010 with a production capacity of 500 ktonne/y and 185 ktonne/y of gasoline as major by-product.[20]

A similar process to the MTO process is the DMTO (dimethyl ether/methanol to olefins) process developed by researchers at Dalian Institute of Chemical Physics. The used catalyst is H-SAPO-34 and it includes a recycle of C_4^+ olefins to increase the yield towards ethylene and propylene. This process was built in Baotou, China in 2010 with a pro-

duction capacity of 600 ktonne/y of ethylene and propylene.[21] China has interest in the MTO process due to its large reserves of coal resulting in an annual capacity of ten million tons of methanol per year.

Summarizing: Over the years, several pilot set-ups have been built and commercial set-ups have been installed (mainly in China). Herewith the UOP/Norsk Hydro MTO, Lurgi's MTP and Dalian's DMTO processes seem economically interesting. European research is however not necessarily focused on the coal production in China. European researchers try to find an alternative, economically feasible process instead of the conventional crude oil process. In Figure 1.3 the effect of the gas price on the methanol production cost is given. In an industrialized location the feedstock price for natural gas is high, resulting in a high overall cost. A methanol production plant located in a remote area with low natural gas feedstock costs will have a lower production cost. Economy of scale can further reduce the overall methanol production cost. Depending on the oil price this technology can concur with the conventional crude oil process.

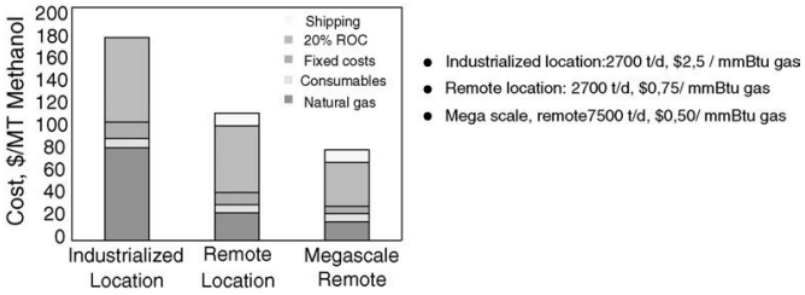

Figure 1.3: Effect of gas price (location) and scale on methanol production costs.[22]

1.2 From feedstock to methanol

The MTO process is part of a broader process by which olefins can be produced via the formation of methanol. In a first step natural gas (or any other carbon resource such as coal) is reformed to synthesis gas (syngas) (see equation 1.1). Methane is a major compound of natural gas and its reforming reaction is given in equation 1.2. Further hydrogenation of carbon monoxide results in the formation of carbon dioxide and hydrogen, see equation 1.3. Syngas is composed of hydrogen and carbon monoxide and to a minor extent carbon dioxide and water. It was first used for lighting and heating in the nineteenth century by coal gasification. Not until the beginning of the twentieth century the opportunities towards fuels and chemical synthesis from syngas were seen.

$$C_nH_m + nH_2O \rightleftharpoons \frac{n+m}{2}H_2 + nCO \tag{1.1}$$

$$CH_4(g) + H_2O(g) \rightleftharpoons 3H_2(g) + CO(g) \quad \Delta_r H^\circ = 206.2\ kJ/mol \tag{1.2}$$

$$CO(g) + H_2O(g) \rightleftharpoons CO_2(g) + H_2(g) \quad \Delta_r H^\circ = -41.2\ kJ/mol \tag{1.3}$$

The produced syngas will be used in a next step to form crude methanol (impure methanol).[23] The reactions are shown in Equation 1.4-1.6 which are all exothermic.

$$CO(g) + 2H_2(g) \rightleftharpoons CH_3OH(g) \quad \Delta_r H^\circ = -90.5\ kJ/mol \tag{1.4}$$

$$CO_2(g) + 3H_2(g) \rightleftharpoons CH_3OH(g) + H_2O(g) \quad \Delta_r H^\circ = -49.3\ kJ/mol \tag{1.5}$$

$$CO(g) + H_2O(g) \rightleftharpoons CO_2(g) + H_2(g) \quad \Delta_r H^\circ = -41.2\ kJ/mol \tag{1.6}$$

These two processes, from feedstock to syngas and from syngas to methanol can be combined in one step in an industrial set-up. The set-up shown in Figure 1.4 is an example of the two steps set-up.[23] Herein, the feedstock is first desulphurized and water is removed.

Steam reforming of desulfurized gas is the general production technique for syngas, with partial oxidation of natural gas as an alternative.[24] Steam reforming of natural gas is exothermic and thus intermediate cooling is needed. The overall conversion is increased by dissipating the heat. Two reactor types are used: the adiabatic or the isothermal reactor. Adiabatic reactors contain multiple beds with cooling equipment in between the layers. Isothermal reactors, on the other hand, make use of continuous cooling. More recent technologies to form syngas are hydrogenation of carbon dioxide or biomass gasification.[25,26]

A second reactor, the methanol reactor, will produce methanol from the obtained syngas. The resulting crude methanol contains a lot of side-components that have to be removed by distillation. In a first distillation column the most volatile components (light alcohols) are removed, in a second distillation unit water and higher alcohol components are removed. The first processes towards methanol took place at high temperatures (350 ℃) and high pressure (250 - 350 bar) and used ZnO/Cr_2O_3 catalysts. In 1966, ICI developed a new process towards methanol over the more active catalyst, $Cu/ZnO/Al_2O_3$ using lower temperatures (220 - 275 ℃) and lower pressures (50 - 100 bar).[23]
The process has been further optimized such that nowadays a yield of 1 kg of MeOH is obtained per liter of catalyst with a selectivity of more than 99.5 % for methanol, whereby the catalyst has a lifetime of 3-5 years under normal operating conditions.

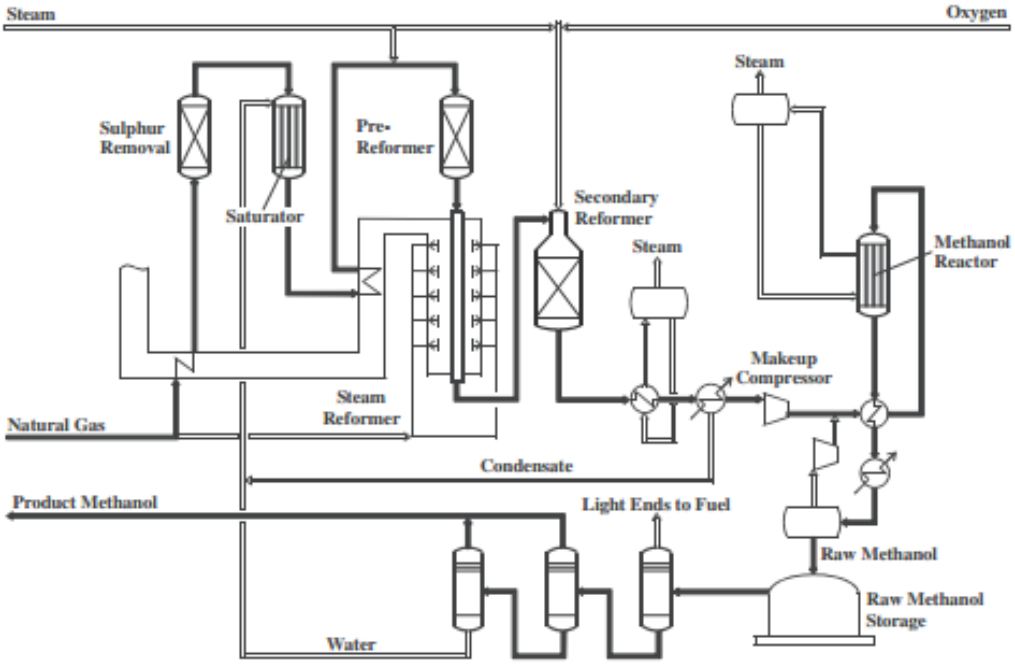

Figure 1.4: Schematic flow diagram of the methanol production starting from natural gas via two-step reforming.[24]

1.3 Olefin production processes

After methanol is produced, it reacts further towards the desired olefins in the so called MTO process. The MTO process was developed in both a fixed bed set-up and in fluidized bed reactors with continuous catalyst regeneration.[27] In the fluidized bed, the vaporized methanol is mixed with the zeolite catalyst to form a suspension, which is charged to the bottom of the riser where reaction can occur.[28] In the fixed bed, tubular reactors packed with catalyst are used. Due to fast deactivation of the catalyst, regeneration is frequently needed in a fixed bed set-up whereas in a fluidized bed there is a continuously regeneration of the catalyst. The increasing coke deposits continuously changes the product distribution.[29] In Figure 1.5 the UOP/Hydro fluidized MTO set-up is shown. It consists of two main parts: the reaction section in which the methanol is converted into olefins and the separation section where the olefin-range products are separated from each other. The reactor operates at a pressure of 2 - 4 bar and a temperature of 350 - 550 °C.[18]

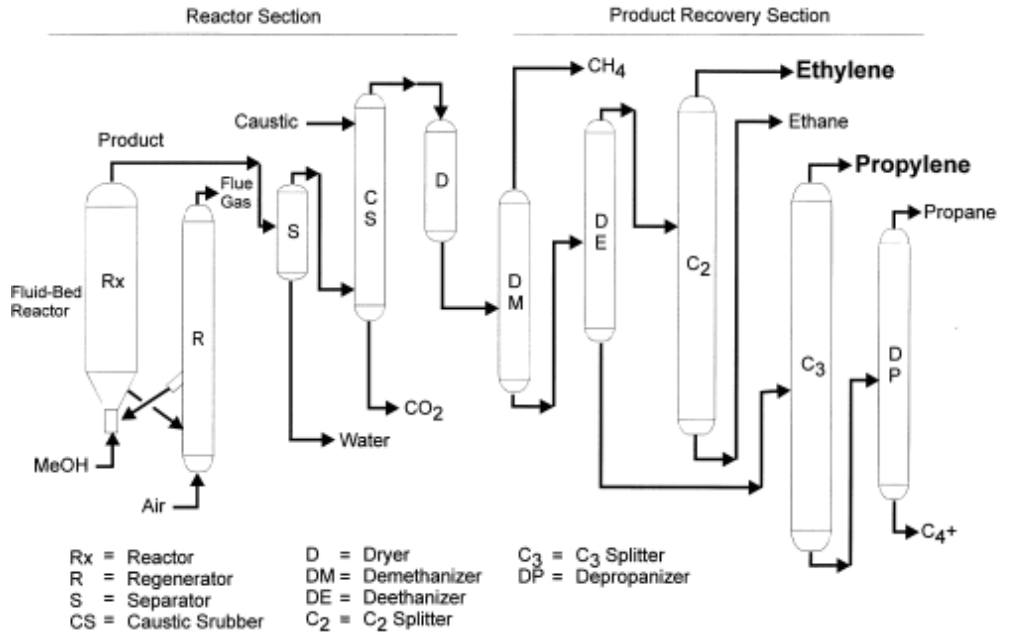

Figure 1.5: Schematic flow diagram of the UOP/Hydro MTO process for olefin production.[18]

The Lurgi's fixed bed process is shown in Figure 1.6. The reactor consists of parallel fixed bed reactors containing H-ZSM-5 catalyst. It operates at 460 - 480 ℃ and atmospheric pressure. Earlier MTO applications were often focused on the production of ethylene, whereas now propylene becomes more important. Therefore, the Lurgi set-up is interesting since it has a high selectivity towards propylene (70 %).[20]

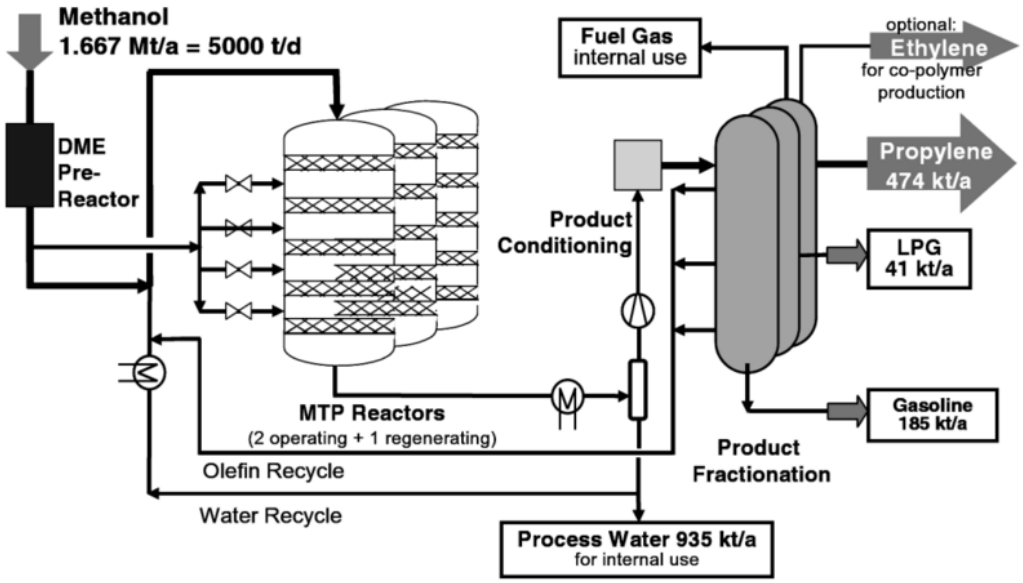

Figure 1.6: Schematic flow diagram of Lurgi's MTP process.[20]

The more recently developed DMTO process is schematically given in Figure 1.7. Just like the UOP/Hydro MTO process, it makes use of a fluidized bed reactor. The reactor outlet is immediately quenched and water is removed from the effluent. It also uses recycle streams to increase the selectivity towards light olefins.[30]

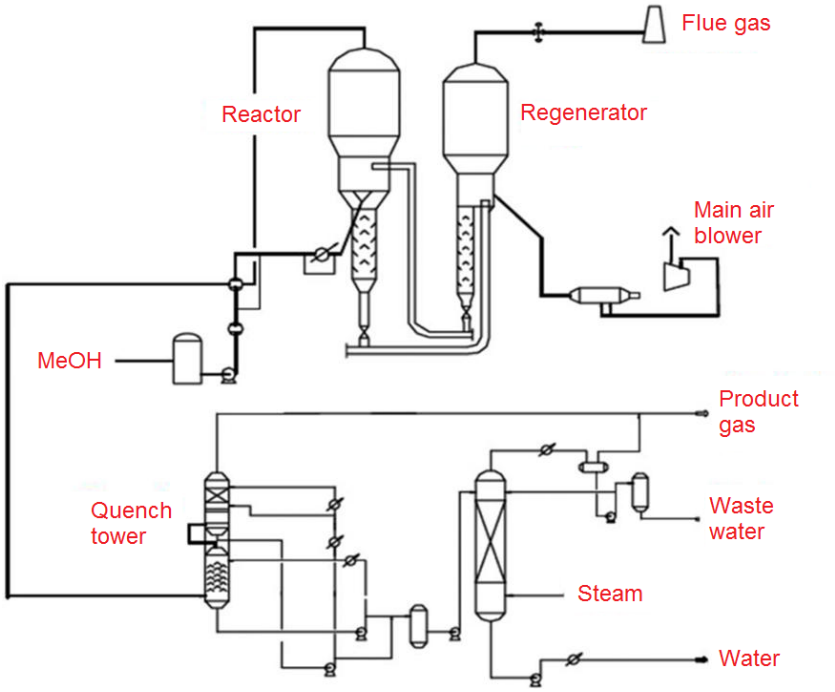

Figure 1.7: Schematic flow diagram of the DMTO process.[30]

Chapter 2

The Methanol-to-Olefins process

In this chapter, more in-dept information about the MTO mechanism is provided. The Methanol-to-Olefins process is a complex process. Even today, the mechanism is not fully unraveled and it is still under investigation. For a more elaborated overview of the MTO process over the years, I refer to instructive review papers of Olsbye et al. and Hemelsoet et al.[21,31,32]

2.1 Direct coupling

The main aim of the early research on the MTO mechanism was to discover how the initial C-C bond was formed and led to the proposition of direct mechanisms: the oxonium ylide mechanism[33], the carbene mechanism[34], the carbocationic mechanism etc.[16] However, it was experimentally seen that the olefin formation only took place after a certain amount of time on stream (a so called induction period). These first proposed direct mechanisms never could describe this induction period. Furthermore, the theoretical results failed to give a realistic model because of too highly activated reaction steps.[16,35] As an alternative, a mechanism based on a hydrocarbon pool species (HP) has been proposed which is explained in more detail in the next paragraph. The HP mechanism is nowadays the generally accepted mechanism.

2.2 The hydrocarbon pool mechanism

The first alternative mechanism was proposed by Dessau et al.[36,37] According to them the final product can only be formed after the formation of a critical amount of alkenes. Several other mechanisms were proposed and led to the indirect mechanism of Dahl and Kolboe.[38] A pool of organic molecules present in the framework structure initiates the reaction and thus act as a co-catalyst in the reaction mechanism. The active center of

the zeolite/zeotype material thus consists of an inorganic Brønsted acid site and organic active HP species.[39] These hydrocarbon pool species undergo several methylation steps by methanol, methoxides or dimethyl ether and finally eliminate light olefins.[40] The organic species make reactions possible that would otherwise require high energy barriers.

A schematic overview of the MTO process is given in Figure 2.1. In the first phase, the carbon rich feedstock is converted into methanol as discussed in the previous chapter. Researchers do agree that in the second phase an equilibrium reaction takes place to form a mixture of methanol, water and dimethyl ether. Dependent on the reaction conditions two routes are established for the production of this mixture: the associative and dissociative route. In associative routes, methanol monomers react with each other leading to the formation of methanol dimers. In dissociative routes, methanol dehydrates to form methoxy species.[41] Secondly it was experimentally seen that a kinetic induction period takes place before in a third step the primary olefin products can be formed. In a fourth step the primary products are converted into a mixture of hydrocarbons leading to a broad product distribution.[42] Finally, coke species are formed and the catalyst is deactivated due to blocking of the active sites. The precise product distribution and underlying reaction mechanism is dependent on the process conditions and vary with the choice of catalyst. The two most important catalysts from an industrial viewpoint are H-SAPO-34 and H-ZSM-5 and will be further discussed in the next chapter.[32]

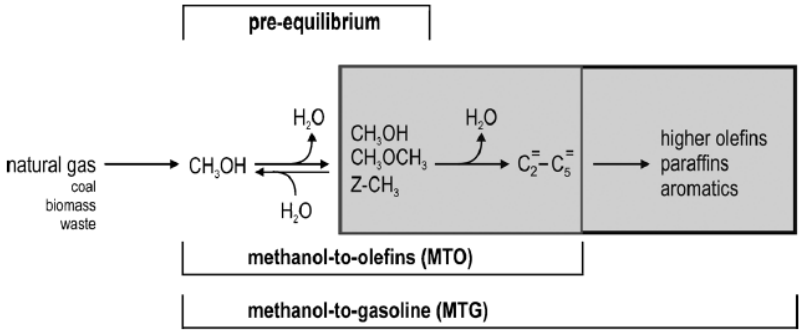

Figure 2.1: Conversion of natural gas into methanol and subsequent olefins.[32]

2.2.1 Nature of the HP species: alkenes and aromatics

Initially the nature of the HP species was unclear and has been the topic of many research. Two categories of organic species are identified as possible co-catalyst: alkenes and aromatics. Once initial light olefins are formed, they can further react to larger alkene and aromatic species, i.e. the HP species. For both types of HP species an olefin production pathway was proposed: the alkene and aromatic cycle. Figure 2.2 gives an

overview of the two routes for the production of olefins co-catalyzed by hydrocarbon pool species. Two pathways were proposed based on aromatic HP species: the side-chain and the paring mechanism. The paring mechanism was first introduced by Sullivan et al. (in 1961)[43] while the side-chain mechanism was first introduced by Mole et al. (in 1983)[44] and was further developed by Haw et al.[45] Both mechanisms start with the methylation of an aromatic ring until a gem-methylated molecule is formed (i.e. two methylgroups substituted on one carbon atom of the ring structure).[42,45]

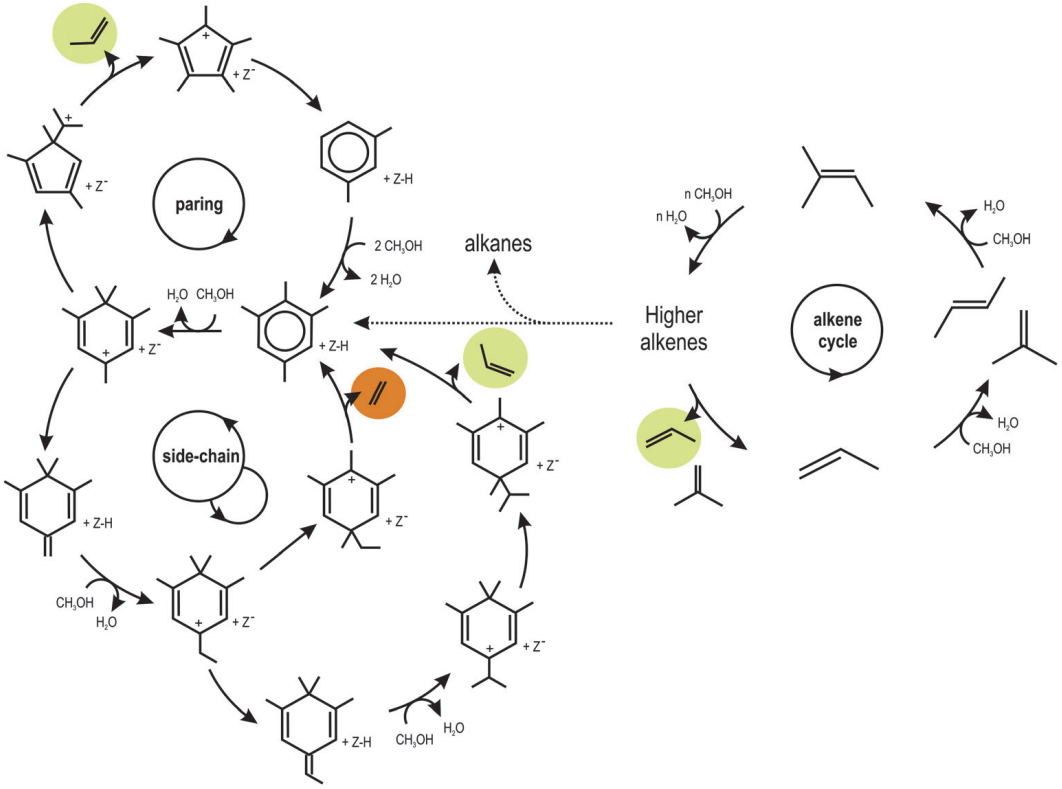

Figure 2.2: Representation of the dual-cycle mechanism which occurs in H-ZSM-5, i.e. both the aromatic and alkene pathway occurs.[46]

The catalyst type will result in different HP species which will affect the product distribution. It was found that a low acidity of the zeolite/zeotype material and narrow pores favor the alkene pathway with isobutene as main HP species leading to the formation of high alkenes (C_4^+). On the other hand, large pores favor polymethylbenzene (PMB) intermediates as the characteristic hydrocarbon pool species and lead to the formation of C_2-C_4 olefins and aromatics.[44] In H-SAPO-34 and H-Beta mostly methylated benzenes were identified as the main HP species. In the archetypal H-SAPO-34 catalyst, polymethylbenzenes are the major HP species. This can be explained by the large cages of H-SAPO-34. Olefin formation will occur via the aromatic cycle.[47] For H-ZSM-5 the dual-cycle concept was proposed, i.e. both the alkene (with higher olefins as HP species)

and aromatic cycle (with polymethylbenzenes as HP species) are active. Furthermore, the propylene formed in the aromatic cycle can act as co-catalyst in the alkene cycle and propylene can oligomerize to polymethylbenzene as can be seen in Figure 2.2.[46,48]

Research by Song et al.[49] showed that both the reactivity and the selectivity of polymethylbenzenes towards propylene increases with the number of methyl substituents favoring four to six methyl groups. This result was confirmed by research of Hemelsoet et al.[32,50] Xylene and trimethylbenzene lead to the formation of mostly ethylene, whereas tetramethylbenzenes and PMB lead to the formation of mostly propylene. Haw and coworkers defined methylnaphtalenes as alternative HP species.[42]

Ab initio modeling in H-SAPO-34 performed by Van Speybroeck[51] et al. suggested heptamethylbenzenium cation (heptaMB$^+$) as starting active molecule formed by methylation of hexamethylbenzene (hexaMB), which is identified as the main hydrocarbon pool molecule. Based on carbon labeling of methanol within H-SAPO-34 Arstad et al.[52] also suggested hexaMB as main hydrocarbon pool species. Toluene was suggested as the second most reactive HP molecule. Herein, Arstad et al.[52] performed fundamental gas phase studies that reproduced the experimental findings regarding the activity and selectivity of different PMBs. Lesthaeghe et al.[35] proved the importance of taking the molecular sieve structure (H-SAPO-34) into consideration of the gem-methylation of PMBs using the QM/MM (Quantum mechanics/molecular mechanics) method. It was found that the chabazite topology is ideal to stabilize methylbenzenium cations.

2.2.2 First step within the side-chain and paring mechanism: gem-methylation of methylbenzenes

The first step for the side-chain and the paring mechanism is identified as the gem-methylation of methylbenzenes. The methylation step can occur via two mechanisms: the stepwise and concerted mechanisms.[53,54,55] In the stepwise mechanism, a methanol is dissociated into a surface-bound methoxide and a water molecule before the actual methylation step takes place. In the concerted mechanism a methanol molecule is physisorbed at the Brønsted site followed by methylation and water elimination in a single step. Methylation steps take place in both aromatic as alkene cycles and have generally been accepted as crucial steps within the MTO mechanism to incorporate methanol into the hydrocarbon pool. Methylation steps are one of the few reactions that can be investigated via direct kinetic measurements.[56,57] However, there still remain questions concerning the stepwise or concerted pathway. Furthermore, the process conditions will have a major influence.[55,58]

2.2.3 Side-chain mechanism

The side-chain mechanism is characterized (as seen in Figure 2.2) by the formation of an exocyclic double bond of an aromatic HP molecule by deprotonation followed by side-chain methylation and side-chain elimination reactions leading to the formation of both ethylene and propylene (see Figure 2.2). Herein, De Wispelaere et al. proposed a catalytic side-chain route for ethylene and propylene production in H-SAPO-34. A complete route for ethylene, propylene and butene was found without free energy barriers higher than 100 kJ/mol.[59]

2.2.4 The paring mechanism

Via experimental and theoretical results the side-chain route gained more and more support. But, the side-chain rout was not able to describe some specific labeling structures that were found in labeled methanol experiments. Mixed labeled products were detected, which could not be described by the side-chain mechanism as shown in Figure 2.3. This led to the hypothesis that a contraction/ expansion pathway would be part of the whole mechanism resulting in the scrambling of ^{13}C between ring and methyl positions.

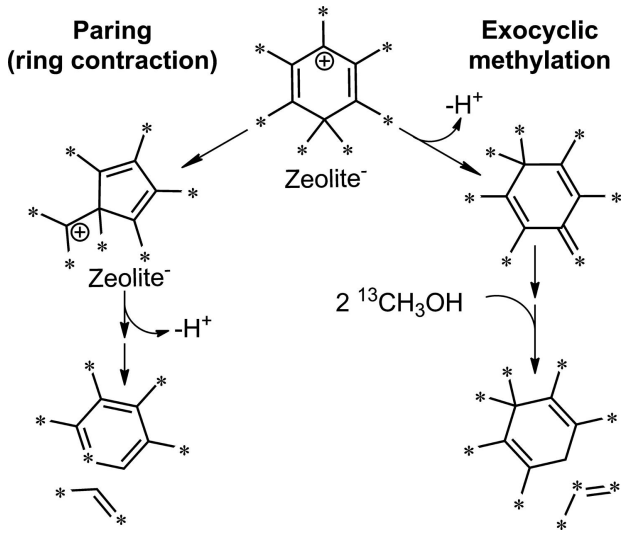

Figure 2.3: Labeling patterns in the formation of propylene via the paring or exocyclic mechanism (i.e. the side-chain mechanism). Stars signify labelled carbon atoms.[60]

The paring mechanism is characterized by ring contraction of six-ring to five-ring carbenium ions, hydride shifts resulting in the formation of propylene and finally ring expansion of the five-ring to a six-ring. A complete catalytic cycle of the paring mechanism for isobutene formation is given in Figure 2.5.[50] Alternatively, a ring expansion/contraction route was explored via the formation of the tropylium ion. This will be discussed in

more detail in the following paragraphs.

Although several research groups investigated the mechanism, still a lot of questions remain. The ring expansion exhibits high energy barriers and it is not yet clear if the proposed route as indicated in Figure 2.2 is completely feasible.

Experimental indications for the paring mechanism

Research towards the mechanism has been performed by pulse experiments and isotopic labeling. An exchange between ring ^{12}C and methyl ^{13}C carbon atoms is assumed to be an indicator for the paring mechanism. Alternatively, H/D exchange can be used. However, these techniques are not conclusive for the determination of the specific reaction pathway. Therefore, also first principle modeling has been performed to distinguish between the different reaction pathways and will be discussed in the next paragraph. The coexistence of different concurring pathways make isotopic labeling an uncertain technique towards the unraveling of reaction mechanisms. In this section an overview of different studies in different zeolites will be discussed.

Wang et al.[39] performed carbon isotopic labeling experiments of the methanol feed within H-ZSM-5. By performing GC-MS analysis C_5 and C_6 rings were detected and more specifically C_5 cyclic species with ethylgroups on the ring. The formation of the cyclic C_5 cations was further verified by Wang et al. by liquid state NMR spectroscopy. From these experiments it was concluded that ring contraction occurs on the protonated methylbenzenes and a mechanism with ethylcyclopentenyl intermediates should be considered. In Figure 2.4 observed ethylcyclopentenyl cations are given. The first and third intermediate were already observed in 2000 by Haw et al. by NMR experiments.[45,50] NMR studies on H-ZSM-5 performed by Haw et al.[21] detected 1,3-dimethylcyclopentenyl carbenium ion as most observed molecule retained on the bed. More methylated 6-ring molecules were observed in H-Beta which has larger pores than H-ZSM-5.

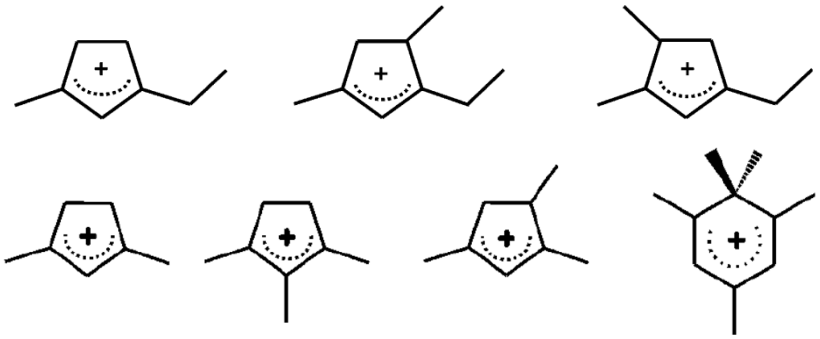

Figure 2.4: Intermediates detected by NMR experiments on H-ZSM-5 by Wang et al.[39,61]

Theoretical calculations on the paring mechanism

The complete catalytic paring cycle involves a sequence of elementary steps: methylations, ring contraction, shift of a hydride or methyl group, elimination of side alkyl groups and regeneration of methylbenzenes as shown in Figure 2.5. The main bottleneck is identified as these last two steps, i.e. the elimination of side alkyl groups and regeneration of methylbenzenes from 5-ring structures.[62]

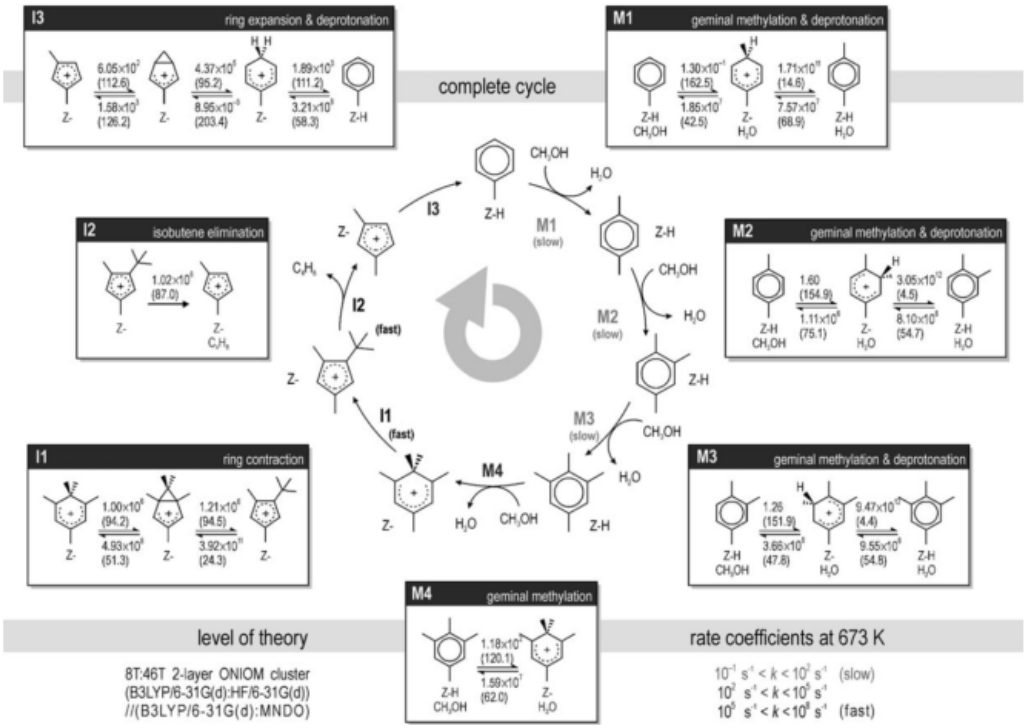

Figure 2.5: Complete Catalytic Cycle of the paring mechanism in H-ZSM-5. Calculated rate constants at 673 K are given in s^{-1} and reaction barriers at 0 K (in brackets) are given in kJ mol^{-1} [50]

Computational investigations by Wang et al.[62] in H-SAPO-34 lead to the proposition of bicyclic species (i.e. two neighboring ring structures) while other researchers do not consider these bicyclic species as valuable intermediates.[50] The mechanism is shown in Figure 2.6, where the bicyclic species are labeled as M3, M4/C3 and M7/C4. The research was performed by period DFT (Density Functional Theory) calculations with a PBE-D approach.

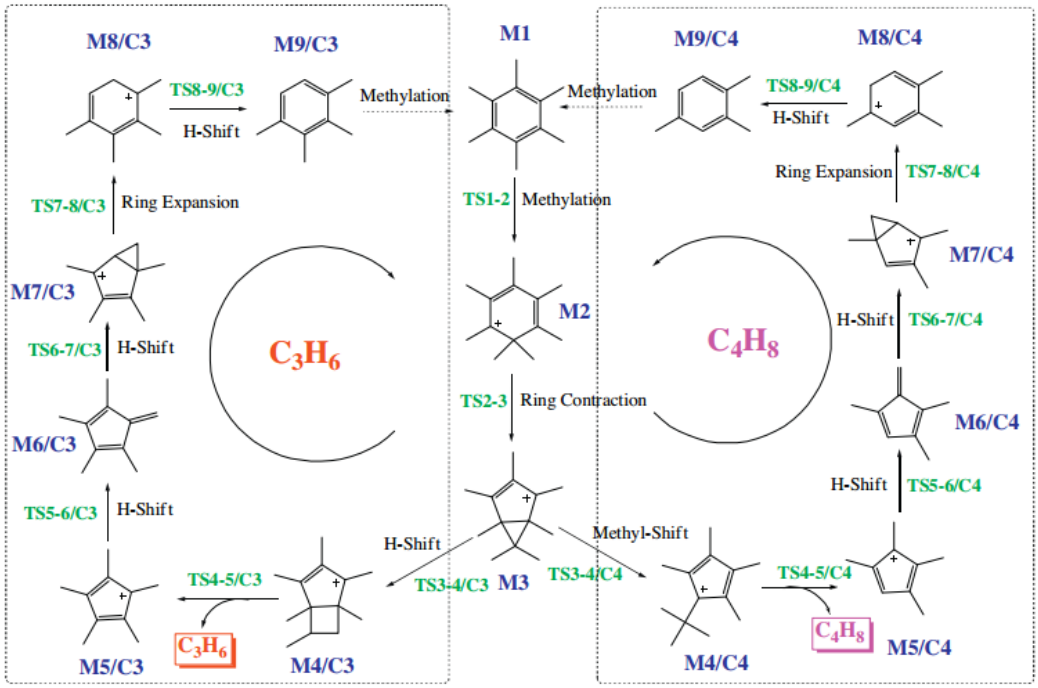

Figure 2.6: Catalytic cycle of the paring hydrocarbon pool mechanism for the MTO conversion starting from hexaMB in acid zeolite or zeotype catalyst.[62]

The paring route starts with the formation of heptaMB$^+$(M2) by gem-methylation of hexaMB (M1), which is slightly endothermic (33 kJ/mol). The first bicyclic molecule that is formed is heptamethylbicyclohexenyl cation (M3). In the next step, the butylene and propylene formation cycles differ. While in the propylene formation, a H-shift leads to the formation of the second bicyclic molecule: hexamethylbicycloheptenyl cation (M4/C3). It was calculated that a reaction barrier of 259 kJ/mol is needed for this reaction step. Subsequently, the pentamethylcyclopentadienyl cation (M5/C3) is formed. No transition state was recognized which is rather odd as this is seen as the limiting reaction step in other energy schemes. Subsequently hexaMB is again obtained by two H-shifts step followed by a ring expansion, again a H-shift and some methylation steps. These last steps are exothermic reactions. In the formation of isobutene, instead of an H-shift, a methyl shift will result in the split off of the olefin. Again, H-shift followed by ring expansion, again a H-shift and methylation steps will result in the regeneration of hexaMB. Although the research is interesting some questions rise concerning the energy calculations as only the enthalpy is taken into account and thus entropy is neglected. This is however a major drawback as entropy effects are of major importance within zeolite catalysis.[63,64] The energy profile is shown in Figure 2.7. Apparently, no transition state could be detected in the step leading to the formation of propylene (from M4 to M5/C3). Although, no explanation or further details are mentioned in the paper.[62]

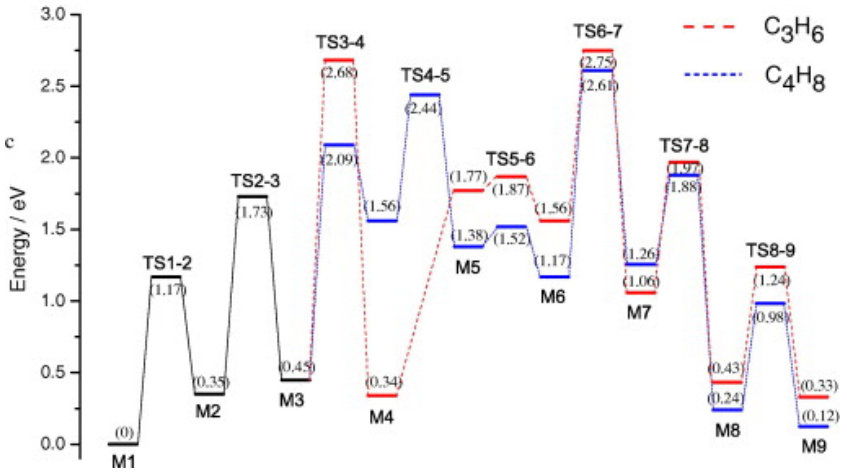

Figure 2.7: Energy profile of the paring hydrocarbon pool mechanism for the MTO conversion in HexaMB/H-SAPO-34. The relative energy of each state referred to M1 is listed in parenthesis.[62]

Also Arstad et al.[65] suggested bicyclic species (3-ring and 5-ring) in the MTO mechanism within H-SAPO-34 in which the bicyclic species have an energy of 53 kJ/mol compared to heptaMB$^+$. Arstad et al. calculated that the first step, in which heptaMB$^+$ cation is formed from hexaMB, is the most difficult reaction with the highest transition state barrier (299 kJ/mol). In this step the aromaticity disappears. The computational calculations were performed with B3LYP/6-311G(d,p) level of theory. All reported energies were calculated using the B3LYP/cc-pVTZ//B3LYP/6-311G(d,p)+ZPE level of theory. Remark the difference between the calculated 53 kJ/mol (transition state energy of 299 kJ/mol) by Arstad et al. and the calculated 33 kJ/mol (transition state energy of 113 kJ/mol) by Wang et al. The computational method is thus very important for the accuracy of the calculations. It is however stated in this review paper that the cluster method is known to give too high activation energies. The second most difficult step is the expansion reaction from the 5 to the 6-ring with a transition state energy of 293 kJ/mol.

Other theoretical calculations compared the reaction pathway starting from heptaMB$^+$ cation and protonated xylene.[66] It was clearly seen that for heptaMB$^+$ cations lower energy barriers were obtained. Furthermore, there is a hypothesis that also ethylene could be formed via the paring mechanism. It was suggested that the amount of methyl groups will influence whether ethylene or propylene will be formed.[67]

An alternative for the contraction-expansion paring mechanism

Arstad et al.[65] proposed a pathway similar to the known paring route for the formation of ethylene via a ring expansion instead of ring contraction. The ring expansion mechanism is shown in Figure 2.8 were it can be seen that first the bicyclic molecule is formed that reacts further to a seven membered ring: protonated hexamethylcycloheptatriene (tropylium ion).[68]

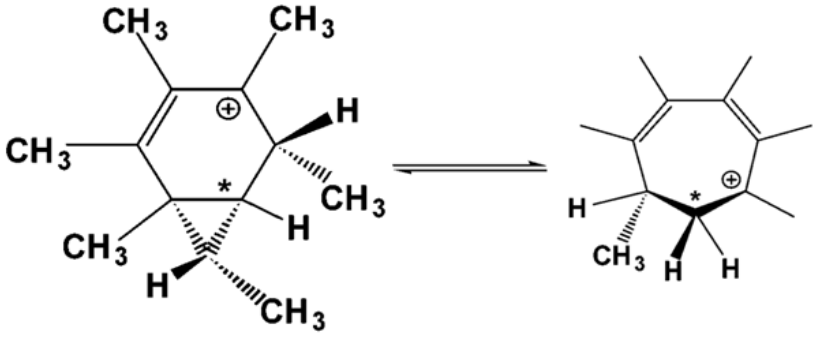

Figure 2.8: Ring expansion reaction as proposed by Arstad et al.[65]

Nevertheless, no further investigation on this mechanism has been performed so far.

The paring mechanism in other zeolite topologies

Also other zeolite structures seem to produce olefins via the paring mechanism. Bjørgen et al. suggested the paring mechanism as dominant mechanism for H-Beta zeolite, in which mainly propylene and isobutene are formed.[69,70] In H-ZSM-5, the dual cycle concept is proposed, in which olefins are formed via aromatic and alkene HP species. The paring route is suggested as the dominant pathway for the production of isobutene.[50] Furthermore, it was suggested by Ilias et al.[71] that ethylene could be formed via the paring cycle in H-ZSM-5 based on isotopic labeling experiments. Westgård Erichsen et al.[72] investigated the paring route in the H-SSZ-24 zeolite. With its large pores it favors aromatic HP species leading to high selectivities towards aromatics and C_2-C_4 olefins. The results show that both ethylene and propylene contained a single ^{13}C originating from a heptaMB$^+$ cation. Furthermore, butenes were eliminated from the ring structure via either one or two labeled carbon atoms. The occurrence of one labeled carbon can be explained by the paring cycle. However, the occurrence of a second labeled carbon in the C4 olefin should be linked to another unidentified mechanism. This all leads to the suggestion of another cation than the pentamethylcyclopentenyl carbenium ion which perhaps might not be an intermediate in the reaction. It can be concluded from this

paper that some parts concerning the paring reaction is doubted, although alternatives are not yet established.

To conclude, identified scrambling of labeled C-atoms identified 5-ring species (pentamethylcyclopentenyl carbenium ion). Computational investigations towards the paring mechanism suggests a contraction-expansion mechanism. The energy barriers given by the researchers depend on the selected level of theory. Nevertheless, it can be concluded that the breaking of the aromaticity requires a lot of energy as well as the split-off of the olefin product.

2.3 The MTO catalyst

Zeolites are crystalline aluminosilicates with a porous structure containing channels and cavities in the order of molecular dimensions.[73] Zeolites are formed in nature in the presence of volcanic activity,[74] but, the success of zeolites in chemical and petrochemical industry only started after the synthetic pathway was explored. Zeolites have been of great use in the chemical industry. Its uniform pore diameter makes it often the preferable choice over the more conventional catalysts. Zeotype materials are comparable to zeolites but exist beside Si, Al and O also of other elements e.g. P. The most known structures for zeolites or zeotype materials are faujasite, mordenite, MFI and chabazite (e.g. H-SAPO-34) topologies. A full list of catalyst topologies and further details can be found on the IZA database.[75]

The introduction of synthetic faujasite structures e.g. zeolites X and Y in fluid catalytic cracking in 1962, was of great importance in the development of the zeolite industry. In the years after this discovery, zeolites became of general use in the petrochemical industry, as well as in the research towards the Methanol-to-Olefin process. The largest industrial applications of zeolites can be found in the detergency industry in which zeolites are used to remove Ca^{2+} and Mg^{2+} ions from hard water and thus act as ion-exchange reagent.[74] Other applications of zeolites within oil refining are Fluid Catalytic Cracking and Hydrocracking.[76]

The product distribution and the underlying reaction mechanism of the MTO process is dependent on the used catalyst. The influence of the zeolite is twofold: on the one hand there is the influence of the Brønsted acid sites, on the other hand there is the framework structure of the zeolite. Besides the topology of the catalyst, process conditions will influence the product distribution as well.

2.3.1 Framework structure

The framework characteristics, namely structure, pore size, chemical composition and crystallite size determine the reactant, transition and product selectivity.[77] In the case of Methanol-to-Olefins conversion, reactant selectivity will be less important due to the small size of the methanol molecule compared to the pore size of the zeolite. The free diameter of methanol is 2.8 Å compared with an opening window of 7, 5.5, 4 Å for large-, medium and small pore sizes for zeolites, consisting of respectively 12-ring, 10-ring and 8-ring (number of T atoms) windows. Hereby T is the number of tetrahedral atoms such as Al or Si forming the window. The transition and the product shape selectivity on the other hand are of importance in the MTO process. For example, the selectivity of the pores will take care of the inability of the large alkene and aromatic compounds to diffuse out of the pores of the zeolite.[77]

2.3.2 Acidity

As mentioned before, the acidity of the zeolite plays an important role in the catalytic activity where both the acid strength and the acid site density are determining. The acidity of the zeolite is mostly determined by Brønsted acid hydroxyl groups. The stronger the Brønsted acid site, the higher its catalyst activity because it will donate its proton to other species more easily. Research towards these hydroxyl groups has been performed by IR spectroscopy studies. It was found that the hydroxyl groups absorb in the range of 3800-3600 cm^{-1}.[21]

2.3.3 Zeolite topologies

The most investigated zeolites/zeotype materials are H-ZSM-5 (MFI topology) and H-SAPO-34 (Silico-aluminophosphate catalyst, chabazite topology). Both topologies are shown in Figure 2.9 together with other topologies that are frequently used during MTO research. The product distribution of the two zeolites is very different. The small pore size of H-SAPO-34 will lead to light olefin production (ethylene/propylene). Instead, for ZSM-5 larger products can be obtained (e.g. methylbenzene, isobutane and isopentane) and a low amount of light olefins will be obtained (see Figure 2.11).[42] Although, the research is mostly concentrated on H-ZSM-5 and H-SAPO-34, one should keep in mind that the commercialization of new 'ideal' catalyst are often more challenging than the more simple and easy producible catalyst.[32]

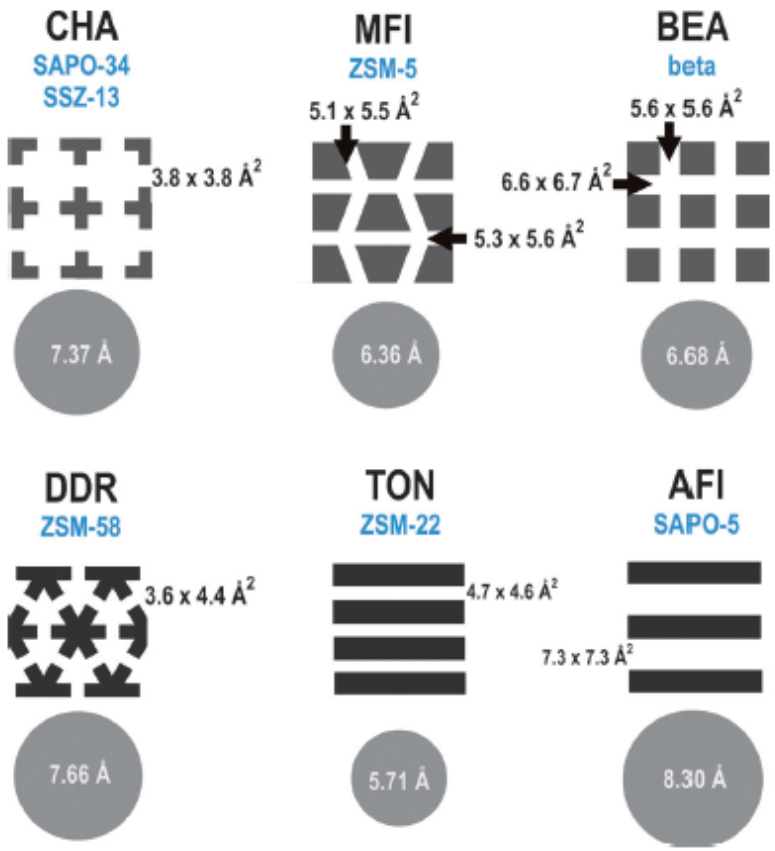

Figure 2.9: Schematic representation of the CHA and MFI and other topologies with given pore sizes. In grey, the maximum diameter of a sphere which can be included is given. The numbers refer to pure silica zeolites and are taken from the IZA (International Zeolite Association) database.[32]

H-SAPO-34

H-SAPO-34, a silicoaluminophosphate based zeotype catalyst, is a 8-ring zeolite with a CHA topology as can be seen in Figure 2.10. It exhibits a 3D-network consisting of large cavities (10.0x6.7 Å^2) and small 8-ring windows (3.8x3.8 Å^2). The Brønsted acid sites originate from framework substitution and in the case of H-SAPO-34 a silicon can be inserted in a alumniphosphate structure by substitution of a single phosphor atom by a silicon-atom. Alternatively, silicon islands can be formed in the H-SAPO-34 structure by substitution of two neighboring P and Al atoms by two Si atoms or by a combination of the two.[32] These different substitutions will lead to different acid strengths of the catalyst.[78,79]

Due to the small pore size of H-SAPO-34, a broad distribution of molecules can be formed in the cages, but only the small molecules can diffuse out of the catalyst leading

to a high selectivity towards ethylene and propylene (see Figure 2.11). For example benzene will fit in the cages, but cannot diffuse through the window from one cage to another. Consequently, this leads to a high olefins (ethylene and propylene) selectivity. The MTO process based on H-SAPO-34 is industrialized by Norsk Hydro/UOP.[22,80]

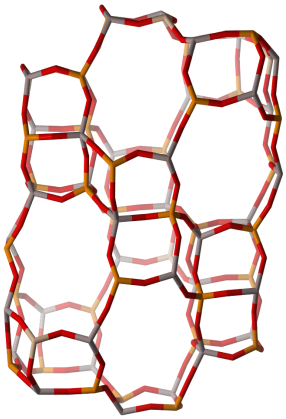

Figure 2.10: Framework structure of H-SAPO-34.[81]

H-SAPO-34 has been proven to be a very selective catalyst towards light olefins with a selectivity over 80% to $C_2^= - C_4^=$. This can also be seen in Figure 2.11, where a comparison is made with H-ZSM-5. A disadvantage of H-SAPO-34 is its rapid deactivation compared to H-ZSM-5.[82,83] Catalyst deactivation is very important for the commercialization of the process. Over time, PMBs are converted into methylnaphtalenes and can convert further to phenantrene structures and other heavy aromatic structures (i.e. coke). These aromatics are too big to diffuse through the channels and are stuck in the cages. This limits the smaller molecules to diffuse towards the cages blocking further reaction. When a catalyst bed is deactivated, the selectivity towards ethylene increases, while the total olefin yield decreases.[42] The selectivity towards ethylene and propylene reaches its maximum at 5.7 wt% of coke content.[83] Furthermore, coke compounds can adsorb on the active sites, thereby deactivating the catalyst (i.e. poisoning of the catalyst active centres).[26]

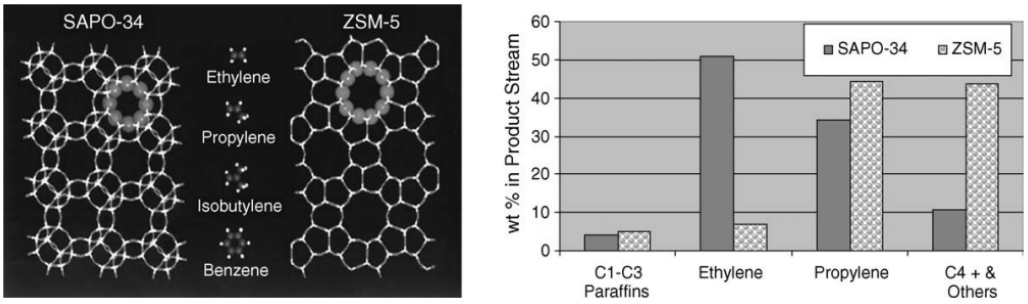

Figure 2.11: Framework structure of H-SAPO-34 and ZSM-5 with its corresponding product distribution.[22]

The size of the pores and diffusion limitations are determining for the coking rate. Alvaro et al. stated that catalysts with small crystal sizes have a lower deactivation rate due to the higher amount of accessible cages near the surface. Therefore, attempts to control the size of H-SAPO-34 have been carried out. Small H-SAPO-34 crystals have been obtained mainly by fractionation of the zeotype material.[26]

H-ZSM-5

ZSM-5 is a 10-ring zeolite used in the petrochemical industry for the synthesis of ethylbenzene, the isomerization of xylenes and the disproportionation of toluene.[84] The framework structure of ZSM-5 with MFI topology is shown in Figure 2.12. It exhibits a 3D-network of sinusoidal (zig-zag) (5.1x5.5 $Å^2$) and straight (5.3x5.6 $Å^2$) channels see Figure 2.11.[53] When used as an MTH catalyst, the medium size pores lead to a broad product distribution, since light olefins, isobutene, isopentene and even methylbenzenes can diffuse out of the catalyst.[32] It was found that in H-ZSM-5 ethylene is mainly formed in the aromatic cycle while propylene and higher olefin are mainly formed in the alkene cycle.[39] Furthermore, the product distribution is hardly dependent on the operating conditions. The deactivation process in H-ZSM-5 is related to blocking of the pores due to the adsorption of polyaromatics on the channel intersection and outer surface.

To create a Brønsted active site a defect is created in the framework by replacing a Si atom by an Al atom. This introduces a negative charge which is then compensated by a proton thereby creating its Brønsted active site. H-ZSM-5 is also used in an industrial environment in the synthesis of ethylbenzene, the isomerization of xylenes and the disproportionation of toluene.[84]

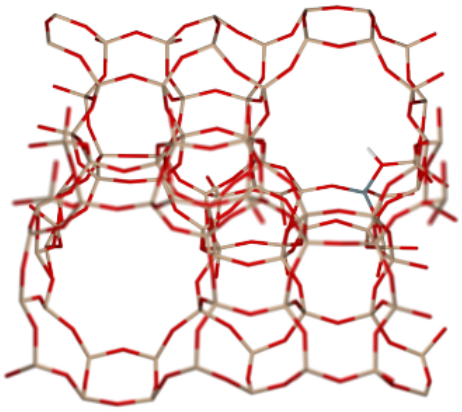

Figure 2.12: Framework structure of ZSM-5.[81]

Other topologies

H-SAPO-34 and H-ZSM-5 are the most important studied catalysts in the light of the MTO process and have respectively a CHA and MFI topology. Another important catalyst type is the BEA type material. BEA type catalysts consist of intersecting straight channels which are slightly larger compared to H-ZSM-5 (see Figure 2.9). Due to its large pores it minimize steric constraint and transition-state selectivity. Therefore, it is a suitable catalyst to gain knowledge about the activity and selectivity of specific reaction intermediates that can immediately be fed to the catalyst.[32] H-beta is an example of this topology and consist of a 12-ring structure with three dimensional channels of size 6.6x6.7 and 5.6x5.6 $Å^2$.[69,85]

On the contrary of the MFI, BEA or CHA topology TON and AFI topologies consist of a 1D channel system. H-ZSM-22 is an example of the TON topology. It consists of one-dimensional 10-ring channels of size 4.6x5.7 $Å^2$. Research on H-ZSM-22 showed that the aromatic cycle contributes in a minor extent to the total mechanism and mainly reaction proceeds via the alkene cycle resulting in a low yield of ethylene. H-ZSM-22 has a high selectivity for branched C_5^+ in combination with a low selectivity towards aromatics.[86,87] An example of the AFI topology is H-SAPO-5. It consists of one-dimensional 12-ring channels of size 7.3x7.3. Its more bulky nature with less steric constraint has the consequence that bulky molecules easily diffuse out of the pores. The AFI topology is not suited for industrial MTO applications but is used in research as model for H-SAPO-34 because it has no diffusion limitations.[88]

2.4 Effect of a mixed water methanol feed on zeolite catalyzed reactions

An objective in the research towards the MTO process is to obtain a better control of the ethylene/propylene ratio and other higher olefins. One of the strategies that has been proposed (and industrially applied) to modify the product selectivity and catalyst lifetime is the addition of water/steam. Insight in the effect of water on the molecular level can result in a better control of the product distribution. However, the effect of water on zeolite-catalyzed reactions is still not fully known. Although water is part of the feed of the methanol and is formed as byproduct in the conversion of methanol towards olefins, it was often ignored in previous simulations.[89] Without any separation or addition of water, crude methanol contains between 12 and 20 wt% of water.[12] Due to the interest in biomass (which contains between 8.6 and 10 mol% water[90]) the effect of water is now investigated.

2.4.1 Understanding effect of water in industry

Before the latest research will be explained, a more in-dept look is taken to some of the written patents concerning the MTO process and the effect of water. Already in 1981, the effect of water was recognized.[91] It was reported that water has a favorable effect on the ethylene selectivity and reduced the formation of butene. On the other hand, the activity of the manganese aluminosilicate catalyst decreased under the imposed reaction conditions and regeneration was only possible for a few times. This problem was solved by careful dehydration of the methanol before recycling but required a lot of energy. On the other hand, water has been recognized to slow down the catalyst deactivation by minimizing the coking rate.[92] In 2008, the equilibrium mixture between methanol, dimethyl ether and water was fully understood but water was mostly removed to some extent. Water can significantly increase the potential for hydrothermal damage of the catalyst. Furthermore, the presence of water results in an increased flow rate requiring larger sized vessels and processing and operating equipment.[93]

Lurgi claimed more recently, in 2013, its process plant for producing synthetic fuels from oxygenates. Herein, water is recycled and afterwards removed from the first stage of the process.[94,95] In 2015, UOP claimed a process for increasing conversion efficiency of oxygenates to olefins. Herein, methanol is converted to DME and water, with an intermediate where water is removed. The effluent consisting of methanol and DME is then further converted to olefins. They developed a configuration in which the oxygenate feed can be transferred to a methanol/DME feed.[96] Thus water is often removed for further processing in the technologies used nowadays. An objective is to couple both

the methanol plant and the MTO unit without separation of water, which would finally result in a lower equipment and operation cost.[97]

2.4.2 Effect of water on ethylene selectivity and coke formation

In 1991, Marchi and Froment[98] investigated the catalytic conversion of methanol to light alkenes on H-SAPO molecular sieves. They concluded was that water results in a higher alkene production rate and a lower coking rate. In this paper a mixture of 30/70 wt% of methanol/water has been suggested at a temperature of 700 K for an optimal efficiency of the catalyst H-SAPO-34.[98] In 2001, Song et al.[67] related the increased ethylene selectivity to the transition state shape selectivity. Ethylene formation occurs via the smallest transition state and is therefore favorable at high water loadings. Hunger et al.[99] on the other hand, stated that addition of water results in an equilibrium shift between methanol, water and DME towards methanol which results in a higher selectivity towards ethylene.

The slower deactivation of the catalyst has been related by Marchi and Froment[98] to the competitive adsorption between water, light olefins and oligomer molecules on the acid sites. Due to the adsorption of polar water molecules on these strong acidic sites, the formation of large aromatic species is inhibited resulting in a larger induction period. This conclusion has also been stated by Wragg et al.[100] and was confirmed with UV-VIS microspectroscopy studies combined with molecular simulations as discussed by De Wispelaere et al. show that the induction period increases with a higher water content as shown in Figure 2.13.[101,102] It was found that methanol and water have an adsorption enthalpy of respectively -90 kJ/mol and -75 kJ/mol at 330 °C. Calculations led to the conclusion that two methanol molecules can already deprotonate the Brønsted acid site. On the other hand, several water molecules are needed to form a cluster and to deprotonate the Brønsted acid site. This cluster formation leads to a decreased activity of the methanol due to a lower probability of methanol protonation.

The competition at the Brønsted acid site between water and methanol as studied by De Wispelaere et al. was also linked with the competition with proylene.[101] A competition was found between water and propylene adsorption on the Brønsted acid site and this behavior increased with increased water loading. Thus, in the presence of water, propylene will have a lower coverage on the surface, this will decrease the probability of propylene to react further towards cyclic HP species, which will result in a slower catalyst deactivation.[101]

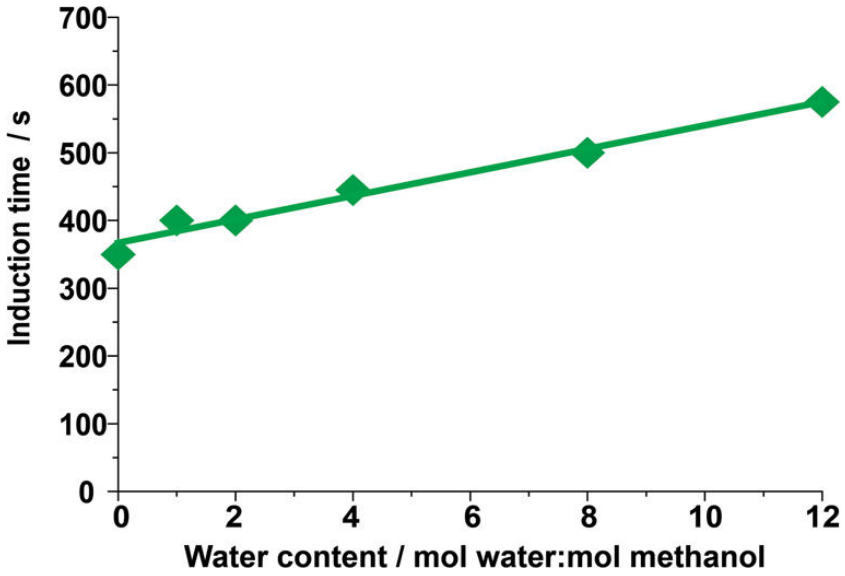

Figure 2.13: Induction period observed by UV-VIS microspectroscopy in function of the water loading on single H-SAPO-34 crystals.[101]

Wu and Xianchun suggested that the optimum water content in the feed is between 73 and 80 mol%.[103] Gayubo et al. suggested that water results in a decrease of the acid strength in the presence of water and at elevated temperatures. This effect gets more remarkable at higher water content and higher temperatures.[104] Other papers stated that co-feeding of water increases the olefin selectivity, reduces the coke formation and prolonged the catalyst life time.[105,106,107] These insights have been obtained by pulsed experiments and GC-analysis. In general, computational studies on the effect of water are rather limited.

2.4.3 Kinetic modelling study

A kinetic modeling study has been performed on the MTO process by Vera-Castaneda[108] et al. The thermodynamical mechanism that describes the overall reaction sequence is given in Figure 2.14.[97] It is a simplified model which does not include surface species etc. It contains the dehydration of methanol towards DME, consecutive reactions for the production of olefins, the decomposition of methanol to carbon monoxide and hydrogen and further hydration towards carbon dioxide and hydrogen. The hydrogenation of methanol and ethylene to respectively methane and ethane are also included.[108]

$$2MeOH \overset{k_{r1}}{\Leftrightarrow} [(CH_3)_2O] + H_2O$$
$$2[(CH_3)_2O] \xrightarrow{k_{r2}} C_2H_4 + 2MeOH$$
$$2MeOH \xrightarrow{k_{r3}} C_2H_4 + 2H_2O$$
$$C_2H_4 + DME \xrightarrow{k_{r4}} C_3H_6 + MeOH$$
$$C_3H_6 + DME \xrightarrow{k_{r5}} C_4H_8 + MeOH$$
$$C_4H_8 + DME \xrightarrow{k_{r6}} C_5H_{10} + MeOH$$
$$MeOH \xrightarrow{k_{r7}} CO + 2H_2$$
$$CO + H_2O \xrightarrow{k_{r8}} CO_2 + H_2$$
$$MeOH + H_2 \xrightarrow{k_{r9}} CH_4 + H_2O$$
$$C_2H_4 + H_2 \xrightarrow{k_{r10}} C_2H_6$$

Figure 2.14: Reaction mechanism for the MTO process.[97]

The kinetic reaction mechanism for the MTO process as proposed by Vera-Castaneda (see Figure 2.14) has been further used to see the effect of water. The result are shown in Figure 2.15. With an increasing molar ratio of water to methanol, the conversion decreases but the ethylene yield increases. This can be explained by the equilibrium between methanol, DME and water which is pushed towards methanol, consequently resulting in a higher ethylene production.[97]

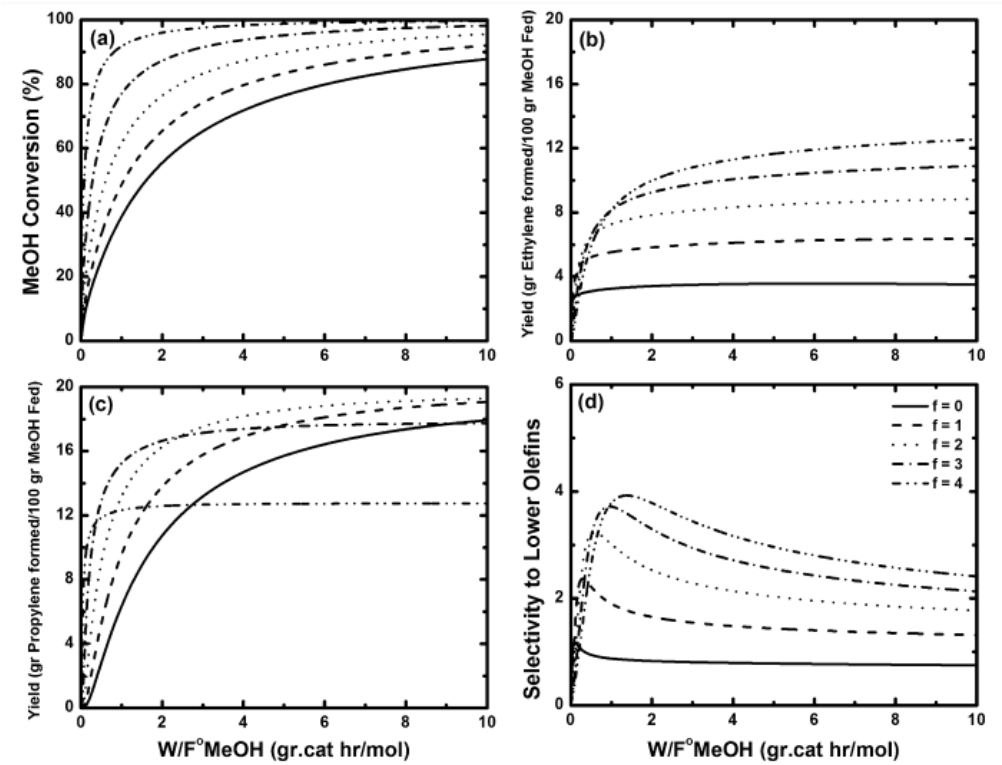

Figure 2.15: The effect of the water to methanol (f=W/M) molar ratio on the (a) methanol conversion, (b) ethylene yield, (c) propylene yield and (d) selectivity towards light olefins in an ideal fixed bed reactor.[97]

To conclude, the hydrocarbon pool mechanism can describe the induction period that is experimentally seen. Herein, two routes were proposed: the aromatic and alkene route. Dependent on the zeolite topology, one of the routes can be favored or not. In H-SAPO-34, the aromatic route is considered as the pathway for the formation of ethylene and propylene. The aromatic route again consists of two cycles: the side-chain and paring cycle. The paring cycle is considered in this thesis. The route was developed in order to explain the scrambling that was experimentally seen. A lot of research have been performed on identifying HP species and from this the paring cycle was developed together with computational studies. The previous mentioned studies indicate that addition of water in the catalyst pores has a complex nature and will influence the reaction with different phenomena such as adsorption, diffusion and reactivity.

2.5 Objective of the master thesis

In this master thesis the paring mechanism and moreover the effect of water on it will be investigated. Experimentally, it was found that water results in a higher alkene rate and a lower coking rate. These results were explained by the competition between water and light olefins on the Brønsted acid site.[98] This was also found by De Wispelaere et al.[101] during computational investigation of the effect of water. In the paring mechanism there is no H-transfer between the acid site and the intermediate. Therefore, the effect of water is less straightforward and its role is rather unclear. The study of solvent molecules is rather limited, especially the effect of water on the paring mechanism and it is aimed to unravel the effect of water on the reaction mechanism.

Initially, in this master thesis ab initio molecular dynamics simulations are carried out on different intermediates without any solvent molecules present. These calculations are followed by calculations with different degrees of water loading. A schematic overview of the water loadings is presented in Figure 4.2. Several analyses will be performed on the obtained MD simulations. Due to the dynamic nature of the zeolite, the volume of the unit cell will be investigated because the volume change might influence the reaction kinetics. Is there a contraction of the unit cell volume that stimulates the contraction step of the paring cycle? Is there a contraction in one specific direction? Furthermore, the effect of water will be studied on the energy level of the intermediate, its position within the framework and on the position of the aromatic species. By doing all this, it is aimed to link both experimental and theoretical results.

Besides, AIMD simulations metadynamics simulations will be performed to calculate the free energy barriers between the different intermediates. The computational details will be given in the next chapter.

Chapter 3

Computational methods

In this master thesis a theoretical approach is used to gain more insight in the methanol-to-olefins process, thus no experimental input is used. The obtained results and knowledge are the consequence of molecular modeling techniques. Quantum mechanical techniques are necessary to describe the changes of the electronic bonding pattern during chemical reactions. Both ab initio molecular dynamics (AIMD) and metadynamics (MTD) simulations will be performed.

3.1 Quantum mechanical methods

In quantum mechanics, the electronic structure of a molecular system is determined. The time independent Schrödinger equation describes the energy eigenfunction of the electronic many-body problem and is solved by applying the Born Oppenheimer (BO) approximation:

$$\widehat{H}_{el}\psi = E\psi \tag{3.1}$$

$$\widehat{H}_{el} = (\widehat{T}_e + \widehat{V}_{en} + \widehat{V}_{ee}) + \widehat{V}_{ne} \tag{3.2}$$

Herein, the Hamiltonian is an operator describing the total energy of the system. The Born Oppenheimer approximation supposes that the nuclei are infinitely heavy such that the nuclear kinetic energy can be neglected. For the remaining electronic Hamiltonian H_{el} the interactions are split up. In the above equation T is the notation for the kinetic energy and V for the potential energy between electrons e and nuclei n. Still, the nuclear-electron interaction term appears. Different methods exist to solve for this. The Hartree-Fock method and the DFT method will be discussed. The DFT method is used in this master thesis. [109]

3.1.1 Hartree-Fock

The Hartree-Fock (HF) method is an ab initio method which describes the many-body problem as a single Slater determinant. The Hartree-Fock method uses the Born-Oppenheimer (BO) approximation and the mean field approximation. This means that the motion of electrons no longer depends on the motion of nuclei and the motion of nuclei no longer depends on the detailed motion of the electrons but only on an average property. Atomic energies within HF always underestimate the exact solution. The difference is equal to the electronic correlation energy E_c. By introducing more correlations for this term the energy converges to the exact solution (post Hartree-Fock). The wave function is considered as the fundamental quantum variable that is able to describe any property of the system.[109]

3.1.2 Density Functional Theory

The Density Functional Theory (DFT) is an alternative method to solve the electronic many-body problem. It stills assumes the BO approximation but instead of solving the time independent wave function the electronic density is introduced and defined as the fundamental quantum mechanical variable. The Kohn-Sham equation is the analogous of the Schrödinger equation in the DFT method. It describes a fictitious system of non-interacting electrons that generate the same density as any given system of interacting electrons. There now exists a Slater determinant that exactly reproduces the true electronic ground state density. The density function completely defines the system in the ground state and any property can be described by this function. The problem is now reduced to obtain a good approximation for the exchange correlation energy functional, which is determined on a semi-empirical way. This results in the risk of overshooting on the contrary of HF which always underestimate the exact solution.

Calculations using the DFT method have gained great success with applications ranging from material science to chemistry and biochemistry. It is a valuable method to describe interacting electrons. It makes use of the simple three-dimensional electron density function instead of the complex many-dimensional wave function. A disadvantage of DFT is that it often fails to describe the exchange-correlation function. These errors than originate from delocalization error of approximate functionals.[110] There exist different classes of functionals that are often used for DFT calculations: Local functionals (Local-density approximation, LDA), Semi-local functionals (e.g. generalized gradient expansion, GGA), Hybrid functionals, Meta-GGA functionals. An overview of the hierarchy of the functionals, defined as the Jacob's ladder, is given in Figure 3.1. The first level estimates the exchange-correlation energy only based on the electron density. The second level takes also the gradient of the electron density into account. The third level

of exchange-correlation functionals are based on ρ, $\bigtriangledown\rho$ and the non-interacting kinetic energy density τ. The fourth level of exchange-correlation functionals are based on ρ, $\bigtriangledown\rho$ and the kinetic energy density ϵ_x. The upper level of the Jacob's ladder also accounts for unoccupied levels.

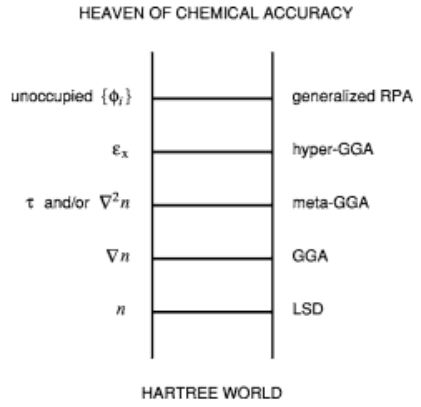

Figure 3.1: Jacob's ladder of density functional approximations for the exchange-correlation energy. (n=ρ) [111]

DFT-D

The disadvantage of the DFT method is that it does not account for dispersion interactions. Dispersion interactions are defined as the attractive part of the van der Waals interaction and are those interactions between atoms and molecules that are not directly bounded to each other. It is used for zeolite catalyzed reactions to describe interaction of the zeolite framework with the observed molecules. The most known method to account for these interactions are the Grimme dispersion interactions which are also used in this master thesis. Hereby, it applies an extra empirical potential C_6R^{-6} on the system. [112,113]

3.1.3 Basisset

In order to solve the electron-many body system derived from the Schrödinger equation, the molecular orbitals need to be rewritten in function of a chosen basisset. Every molecular orbital can be rewritten as a linear combination of atomic orbitals i.e. the LCAO approach. These atomic orbitals can then be further rewritten as a linear combination of one or more Slater type orbitals (STOs). The STOs are however computationally complex and are approximated by functions that can be integrated more easily. In theory, an infinite linear combinations must be taken in order to describe the MO correctly. This is however not possible and the linear combination will be chosen dependent on the required accuracy.

A suitable basisset instead of STOs are Gaussian type orbitals (GTO). Herein, a distinction is made between the core and the valence electrons. The valence electrons are estimated with a higher accuracy, i.e. a linear combination of more GTO compared to the core electrons. The GTO are then defined as the basis set for the molecular system.

Besides GTO also plane waves (PW) can be used to describe the molecular system. PW uses the Fourier series expansion of the atomic orbitals called the plane wave to define the molecular system. PW as basisset has gained lot of interest to applications with a periodic system. The main disadvantage of the technique is that a lot of plane waves are necessary to describe the rapid variations of the wave functions close to the nuclei and that PWs are very memory demanding. On the other hand PWs are atomic position independent which reduces the complexity of the calculation.[114]

In this thesis a third basisset is used, i.e. Gaussian and plane waves[114] (GPW) method which is implemented in the program package CP2K.[115] The method uses an atom-centered Gaussian type basis to describe the wavefunction, but uses an auxilary plane wave basis to describe the density.[116]

3.2 Zeolite models

The MTO mechanism is studied for many years. In the earlier years the catalyst topology was never considered due to the computational difficulty.[52] These calculations were valuable in their time frame, but nowadays it has been clear that the framework composition must be taken into account. Later on, the importance of the topology was recognized and gas phase calculations without any consideration of the catalyst topology were replaced by finite cluster models. Herein, the catalyst topology was considered on a limited basis. However, in order to fully account for the zeolite model the model must be extended. An alternative approach is the periodic cluster model. This approach will also be used in the master thesis.

3.2.1 Finite cluster model

In the finite cluster model, part of the catalyst topology is cut out of the zeolite model. Hereby bonds are broken and the dangling bonds have to be saturated with auxiliary atoms e.g. hydrogens. Because these hydrogen atoms would result in a higher flexibility of the zeolite cluster compared to a realistic zeolite framework, an infinite mass is applied to the hydrogen atoms such that the zeolite cluster is constrained in space. This technique limits the problem significantly. However this results in a decrease of the

accuracy. Often, DFT calculations on the finite cluster model are performed to provide a good starting structure for periodic calculations in which the entire catalyst topology is considered.[117]

3.2.2 Periodic model

A zeolite topology is characterized by unit cells that are periodically repeated (see Figure 3.2). The periodic model calculations are limited to only one unit cell but is afterwards periodically extended. The advantage of this model is that the full zeolite nature is considered with its channels and pores. The disadvantage is however that the amount of T-atoms is often higher for the periodic model than for the extended finite cluster model resulting in a higher computational demand. It has been intensively debated whether the periodic model or the extended finite model is the best choice. We can conclude that both methods have their strengths and weaknesses.[32]

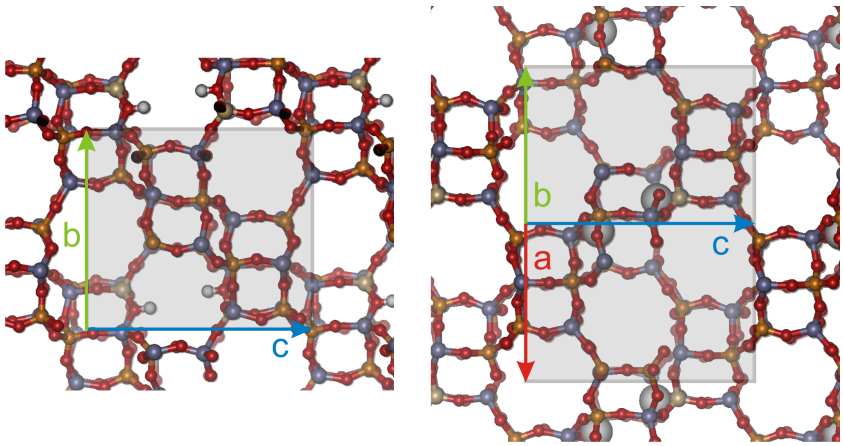

Figure 3.2: H-SAPO-34 unit cell (shaded area) containing two acid sites taken from De Wispelaere et al.[101]

3.3 The molecular dynamics approach

In order to calculate the dynamics of reactions, static or dynamic methods can be used. Early research on the MTO mechanism made use of static methods. Nowadays both techniques are used. With static calculations only the reactant, product and transition state energy is calculated. Static ab initio modeling of the molecule is performed in order to find the absolute minimum on the PES at 0 K. In principal, in order to find the reaction velocity all trajectories on the potential energy surface must be calculated. However, this is not computationally feasible and the transition theory is applied. By this, the calculations are limited to three complexes: the reactant, product and transition state. These are then related to its microscopic properties by means of the calculation

of partition functions.

On the contrary, the dynamic research is able to probe a larger part of the potential energy surface (PES). In general the PES is very complex with dimensions of 3N-6 for molecules for N atoms. There are 3N degrees of freedom associated with the positions of each atom. However due to symmetry reasons after global translation (three degrees of freedom) and global rotation (three degrees of freedom) the PES has 3N-6 dimensions. Although the molecular dynamics approach is clearly much more computationally expensive, it is used to describe heterogeneous complex systems were many local minima exist. Furthermore, the MTO process takes place at elevated temperatures were probably different states will be occupied and the static approach will not be sufficient to cover this.[81,118]

In this work much attention is given to this static approach, the focus in the following paragraphs will be on the molecular dynamic approach. Molecular dynamics and metadynamics simulations are used to account for the dynamics of the system such as the presence of solvent molecules, the movement of the zeolite, entropy and temperature effects. These computational methods are used together with visualization techniques in order to provide a three-dimensional representation under a given set of reaction conditions.

3.3.1 Molecular dynamics

In the ab initio molecular dynamics (MD) approach the physical movement of a molecular system is followed over time. Molecular Dynamics is a deterministic method in which the state of the system at any future time is calculated based on its current state. A schematic overview of the iterative procedure is given in Figure 3.3. The simulation starts with an initial structure at t=0. The forces (F) on all atoms in their current position (r) are calculated as the derivative of the potential energy (V) to its position. By applying Newton's second law the motion of the molecules during the time interval Δ t is calculated:

$$F = -\frac{\partial V}{\partial r} \tag{3.3}$$

$$\overrightarrow{F} = m\overrightarrow{a} \tag{3.4}$$

The new velocities and positions can be calculated with the formula given in Figure 3.3 at time t+Δ t. The iterative procedure is repeated until the sample time is considered to be sufficient. The choice of the timestep is crucial for the accuracy of the calculation. On the one hand, the time step must be small enough to be able to describe small events,

on the other hand, a small time step will require a large computational time.[118]

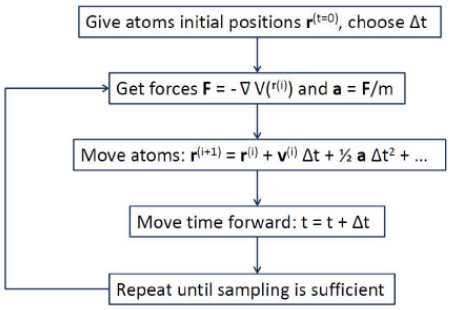

Figure 3.3: Schematic overview of the procedure followed in Molecular Dyanmics[109]

Within MD two approaches are used to solve the electronic many-body problem after each time step:

- Born-Oppenheimer MD
- Car-Parrinello MD

In Born-Oppenheimer MD only the BO surface is taken into account. Thus only movement of the particles on this BO surface is considered. Whereas, in Car-Parrinello MD small deviations from the BO surface are allowed.[118] Molecular dynamic methods should result in a better understanding of the interaction and in more realistic models for the mechanism.[53]

3.3.2 Ensembles

The aim of performing MD calculations, is to get information over the average many-body system called the ensemble average. Therefore molecular dynamic simulations are performed within a thermodynamic ensemble, in which an ensemble is defined as a set of identical systems with the same limitations. An important property of ensembles is that systems have to be ergodic, i.e. the time averaged value of a parameter (which is calculated) is equal to the ensemble average. This postulate implies that thermodynamic properties can be derived from the calculations, if the system is simulated long enough.

Several ensembles exist. For example in the NVT (canonical) ensemble, the number of particles, the volume and the temperature of the system is conserved. Other well known ensembles are the NPT or the NVE (microcanonic) ensemble in which number of particles, pressure and temperature or number of particles, volume and energy are kept fixed, respectively. Standard the NVE ensemble is used in computational methods, but

at industrial reaction conditions it is often more interesting to keep the pressure and temperature constant. Therefore, the NPT and NVT ensemble is used.

In order to keep the temperature constrained a thermostat is applied on the system. The constant temperature is obtained by exchanging energy from the system with a heat bath. The Nosé-Hoover method will be used in this master thesis for the production run. The disadvantage of this method is that the Nosé-Hoover thermostat has the risk of being non-ergodic. On the other hand, the Nosé-Hoover thermostat is easy to implement and time reversible. In order to keep the pressure constant in dynamic simulations the volume of the simulated box is varied (barostat).

3.3.3 Metadynamics

Due to the large system in this master thesis, only a short time (on the order of ps) is simulated during the molecular dynamics which is too short for reactions to proceed. A reaction is thus a rare event and will almost never take place due to its high activation barrier. The probability of sampling a state is proportional to the Boltzmann factor exp(-E/k_BT). States with a higher energy will have a lower probability to be sampled and thus reactions with high barriers on the PES will need a long time to be sampled. To overcome this, the metadynamics methodology is developed to stimulate the occurrence of a reaction.

Before further attention is given to the computational method of metadynamics simulations, the concept of collective variable is introduced. A collective variable is used to describe the different states of a reaction and is determined by e.g. the coordination number (CN) which is defined as follows:

$$CN = \sum_{i,j} \frac{1 - (r_{ij}/r_0)^{nn}}{1 - (r_{ij}/r_0)^{nd}} \tag{3.5}$$

with r_ij the distance between two atoms i and j, r_0 the reference distance. Nn and nd are chosen parameters and are chosen such that the coordination number is equal to 0.5 at the reference distance with typically a value of 6 and 12 for respectively nn and nd.[81]

In the metadynamics approach energy (in the form of Gaussian hills) is added to the free energy surface in function of a limited number of collective variables (CV) in order to overcome the reaction barrier. Based on these Guassian hills the free energy surface van be reconstructed. Mathematically this reconstruction technique is defined as follows:

$$\lim_{t\to\infty} V_G(s,t) \; - F(s)$$

with the sum of the Gaussian potentials V_G defined as:

$$V_G(S(x),t) = w \sum_{t'=\tau_G,2\tau_G,\ldots;t'<t} exp(-(S(x)-s(t'))^2/(2\delta s^2)) \tag{3.6}$$

with F the free energy, s(t') a function of the collective variable at time t' and S(x) a function of the collective variable at time t. τ_G is the time interval between two added Gaussian hills, w the height and δ the width of the added Gaussian hill.
A schematic representation of the technique is shown in Figure 3.4.

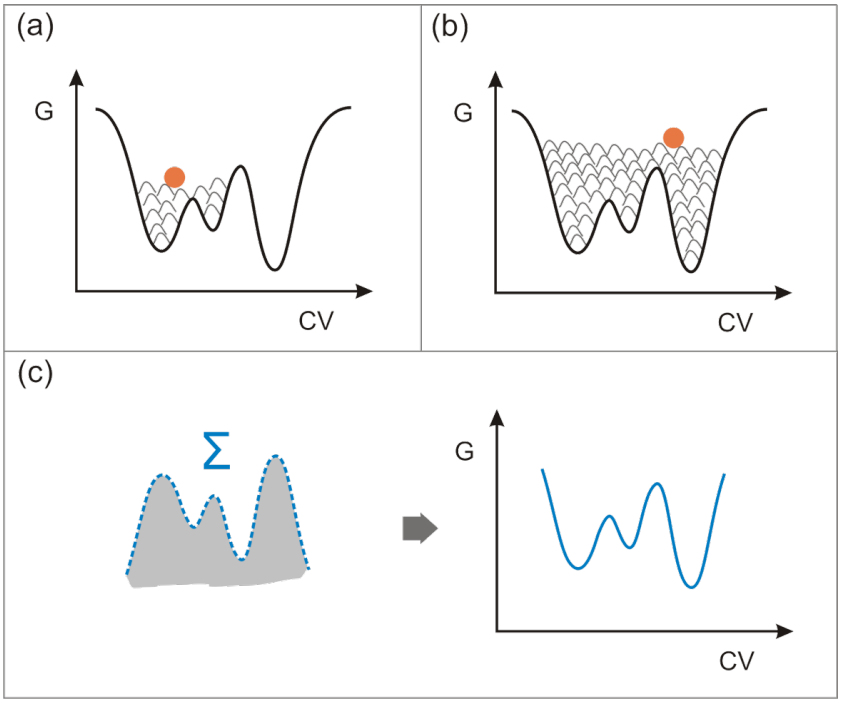

Figure 3.4: Schematic representation of Molecular dynamic techniques. a) Gaussian hills are added to the PES b) in order to overcome the reaction barrier. c) The inverse of the scanned surface reconstructs the free energy profile.[109]

3.4 Methodology used in this masterthesis

This master thesis will focus on the paring mechanism within the MTO mechanism in H-SAPO-34 using molecular dynamic simulations. The molecular dynamic approach is used in order to account for the dynamics of the system. As discussed in the literature review, the topology of the catalyst will be included. Using molecular dynamics in heterogeneous materials, is rather new because of its computationally difficulties. An empty H-SAPO-34 unit cell containing 110 atoms is used for which periodic boundary conditions are applied in order to get a full representation of the catalyst topology. The catalyst is activated by the substitution of two Si substitutional defects, resulting in a

framework with an effective negative charge.

It should be clear that a difference in computational method and reaction conditions is very determining for the results of the simulation. All simulations are performed using CP2K with GTH basis set and pseudopotential. Furthermore, the combined GPW basis set approach is used with the revPBE functional and dispersion interactions are added (Grimme D3 dispersion correction).[112] AIMD simulations are obtained with a timestep of 0.5 fs in the NPT ensemble at 623 K and 1 atm. The system was first equilibrated with the CSVR thermostat and thereafter a 50 ps production run with a chain of five Nosé-Hoover thermostats was obtained. The pressure was controlled by a MTK barostat.

For the metadynamics simulations the same basis set and functionals are used but these simulations are performed in the NVT ensemble at 623 K using a chain of five Nosé-Hoover thermostats. A timestep of 0.5 fs was taken and Gaussian hills of 5.0 kJ/mol were added every 50 steps. The width of the Gaussian hills was set to 0.02.

Chapter 4

Effect of water on the paring mechanism as studied by molecular dynamics simulations

As mentioned in Chapter 2, the hydrocarbon pool mechanism is considered as starting point for this master thesis. Herein, hydrocarbon pool species act as co-catalyst in the MTO mechanism. The HP species can be of aromatic or aliphatic nature resulting in an aromatic or alkene cycle. In this master thesis the aromatic cycle will be studied and more specific, the paring cycle which is characterized by a contraction and expansion of the aromatic intermediate.

An overview of the full paring reaction cycle for the formation of propylene can be found in Figure 2.2 of Chapter 2. As noted by Arstad et al.[65] the propylene formation requires high energy barriers causing questions for the feasibility of the complete route. Therefore, this master thesis focuses on some important reaction steps within this cycle, as shown in Figure 4.1. The first intermediate, i.e. heptamethylbenzenium cation (heptaMB$^+$), is the results of repeatedly methylation of an aromatic species such as toluene. The first step that will be investigated in this master thesis is the contraction reaction of heptaMB$^+$ to the pentamethyl-isopropyl-cyclopentadienyl cation (5-iC_3−CP$^+$). In a second reaction the propylene carbon-carbon bound between the ring atom and isopropyl group is broken and a hydride shift takes place resulting in the formation of propylene and the pentamethylcyclopentadienyl cation (PMCP$^+$). The molecules of interest will be abbreviated in the discussion and are also given in Figure 4.1.

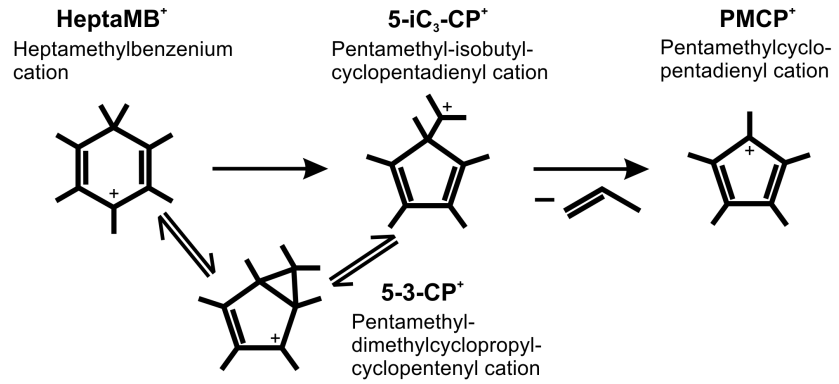

Figure 4.1: Overview of the investigated reactions within the paring cycle in H-SAPO-34.[32]

An objective in the research towards the MTO process is to obtain a better control of the ethylene/propylene ratio. Herein, water can be part of the methanol feed and it is formed as byproduct in the conversion of methanol towards olefins. Therefore, insight in the effect of water can result in a better control of the product distribution and tune the product distribution to lower or higher olefin molecules. To analyze the effect of water on the paring mechanism, cases with different water loadings are considered for all above mentioned intermediates. On all these case studies AIMD simulations have been performed as described in Section 2.5 of Chapter 3.

4.1 Notes on the performed simulations

The four studied cases with different amount of water loading are represented in Figure 4.2. In case 0, one hydrocarbon molecule is placed in one of the two cages. To analyze the direct interaction of the solvent with the aromatic intermediate, the unwanted diffusion of water to a neighboring cage is limited by loading both cages with an intermediate and the exact same water loading. Therefore, case 1 contains in each cage of the unit cell the considered intermediate. This results in the removal of the proton of the framework, because two charged intermediates are present. In case 2 and 3, two respectively four water molecules are added to each cage of the unit cell. The latter two cages representing the low and high water loading. In case of the intermediate pentamethylcyclopentenyl cation (i.e. $PMCP^+$) propylene is placed in the second cage in case 0. This is not in case 1, 2 and 3.

Besides these four cases, an empty H-SAPO-34 unit cell was simulated because it serves as reference for the other simulations.

During simulation of 5-iC_3−CP^+ it was seen that both the bicyclic, 5-3-CP^+ as 5-iC_3−CP^+

are present in the time frame during the simulation of the five-ring specie. 5-iC$_3$−CP$^+$ is found to be in equilibrium with (5-3-CP$^+$) Thus, when the results of the ab initio molecular dynamic simulations of 5-iC$_3$−CP$^+$ are discussed, both five-ring species are actually meant. The bicyclic molecule was also taken into account in research by Wang et al.[62] when proposing their paring mechanism.

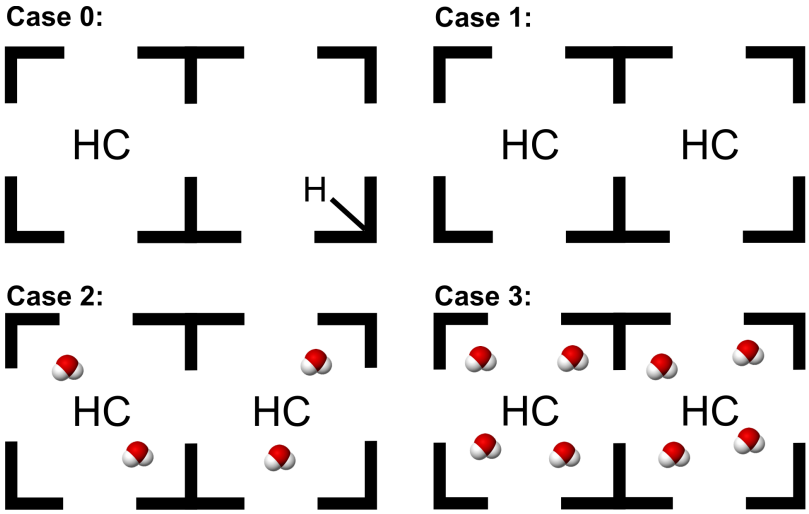

Figure 4.2: Overview of the ab initio simulations for every intermediate with different water loadings.

The effect of water, the behavior and stability of the carbocationic intermediate is studied by performing several analyses on the results of the AIMD simulations for the three considered intermediates of the paring mechanism. First of all, the volume of the framework is studied because this might act as driving force for the contraction step to proceed. Together with the variation of the unit cell volume, the change in the unit cell parameters are analyzed to elucidate possible anisotropy in these variations. The energy profile of the calculations obtained from AIMD calculations is investigated. However, no activation barriers are calculated, the energy profile gives an idea of the driving force for the reaction to proceed. Furthermore, the mobility of the solvent molecules and aromatic HP species within the zeotype framework are studied and visualized in order to see the preferred position of the water molecules. Herein, clustering of the water molecules is of course evaluated. 2D histograms are made to visualize hotspots in the orientation of the intermediate. The position of the aromatic species is than linked to the previous results.

4.2 Framework flexibility

During the MD simulations, the physical movement of a molecular system is followed over time (50 ps), resulting in a movie of the motion of the interacting molecules. First

of all, a lot of information can be obtained visually, giving an idea of interactions, preferential orientations, etc. However, these insights need to be quantified by analyses. At first, the framework flexibility is studied because this might act as driving force for some reaction steps in which the volume of the intermediate also changes. Together with the variation of the unit cell volume, the change in the unit cell parameters in all three directions, indicated on Figure 4.21, are analyzed to elucidate possible anisotropy in these variations. It is noted that the choice of the NPT ensemble makes volume changes possible.

Wragg et al.[119] experimentally investigated the volume variation within H-SAPO-34 by in situ and ex situ XRD under MTO conditions. A volume increase of 0.5 % was measured when adding methanol. On the other hand, a volume decrease of 2 %, with contraction in both the a and c direction, was measured when adding water. The volume increase/decrease of the unit cell was linked by Wragg et al. to the strength of interaction with the framework and size of the adsorbent. They suggested that water molecules are able to coordinate protons from the framework and thereby reduce the unit cell volume (especially in the c direction). Methanol is less attracted to the framework, resulting in a slight expansion.[119,120,121]

In Figure 4.3 the variations of the geometrical unit cell parameters for case 0 are shown for three intermediates studied in this master thesis relative to an empty H-SAPO-34 unit cell. In order to have an equal amount of atoms in each simulation, propylene is also included together with $PMCP^+$. The variation as shown graphically is defined as the difference of the 50 ps average parameter x (with x = a, b, c or volume) and the 50 ps average parameter x of an empty unit cell divided with this 50 ps average parameter of the empty unit cell (see Equation 4.1).

$$\frac{\bar{x} - \bar{x}_{empty}}{\bar{x}_{empty}} \times 100 \tag{4.1}$$

As can be seen in Figure 4.3, adding an aromatic intermediate to the H-SAPO-34 cage leads to an increase of the volume of the unit cell. The volume increase is the strongest for $heptaMB^+$ with an increased volume of 2.1 % compared to an empty H-SAPO-34 unit cell. Remarkable is that the elongation occurs in the b and c direction whereas in the a direction there is almost no elongation (this was also seen by Wragg et al.[121]). The same trend can be seen for $PMCP^+$ with a small contraction of 0.1 % in the a direction. For 5-3-CP^+, the elongation is less anisotropic. The volume increase of 5-3-CP^+ and $PMCP^+$ is respectively 1.8 % and 1.6 %. An explanation for these volume differences can be found in the intermediate molecule. $HeptaMB^+$ covers a higher volume within the framework compared to 5-3-CP^+ and $PMCP^+$ which explains the volume difference. Perhaps the different directions will be made clear by further analyses.

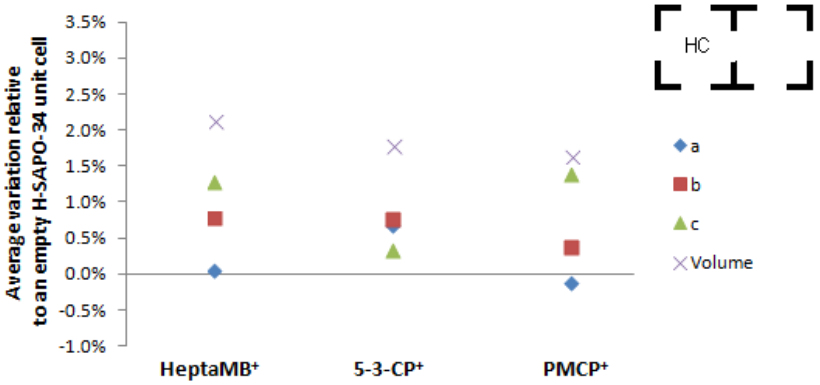

Figure 4.3: Average variation of unit cell parameters and volume relative to an empty H-SAPO-34 unit cell for case 0 at 623 K and 1 atm for three intermediates for a 50 ps MD simulation.

Analogue figures are made for the different water loadings per intermediate. Again, the change of the unit cell parameters are expressed relative to an empty H-SAPO-34 cage. The result for the intermediate heptaMB$^+$ is shown in Figure 4.4. With an increasing water loading, there is an increase in the volume of the unit cell. At the highest loading, a significant volume increase of 2.7 % is found. In earlier research by De Wispelaere et al., the volume was found to first decrease and than increase with an increasing loading of water. However in this master thesis the cages are already filled up enough even at low water loadings to be past this decrease seen in earlier research. In Figure 4.4 it can also be noted that there is a strong anisotropic behavior and the anisotropic behavior decreases with increasing water loading. The elongation is 2.4 %, 2.5 % and 2.0 % in the c direction for case 1, 2 and 3, respectively which is in accordance with research by Wragg et al.[121]

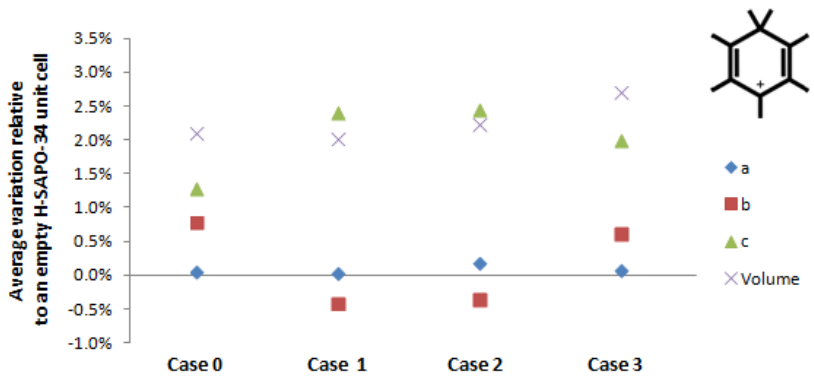

Figure 4.4: Average variation of unit cell parameters and volume relative to an empty H-SAPO-34 unit cell at 623 K and 1 atm of heptaMB$^+$ for a 50 ps MD simulation.

In case of 5-3-CP$^+$ as considered intermediate within the H-SAPO-34 cage, all the unit cell parameter variations are positive (see Figure 4.5). This is not the case for PMCP$^+$ (see Figure 4.6). These two figures show some differences with Figure 4.4 in which the unit cell parameters and volume of heptaMB$^+$ is shown. First of all, the elongation in the c-direction is not present for the bicyclic species, 5-3-CP$^+$. For this intermediate the volume of the unit cell decreases again in case 3 and the elongation is less anisotropic in this case. This event will be discussed in more detail when interpreting the results of the mobility of the water molecules and position of the intermediate (see section 4.4 and 4.5). For PMCP$^+$ the results of case 2 are rather different from the other cases with a large increase in the a-direction and a decrease in the b-direction. This cannot be explained yet at this moment and will be further investigated at the end of this chapter. At this moment it is suggested that the framework feels the loading of the cages and reforms as a consequence of this.

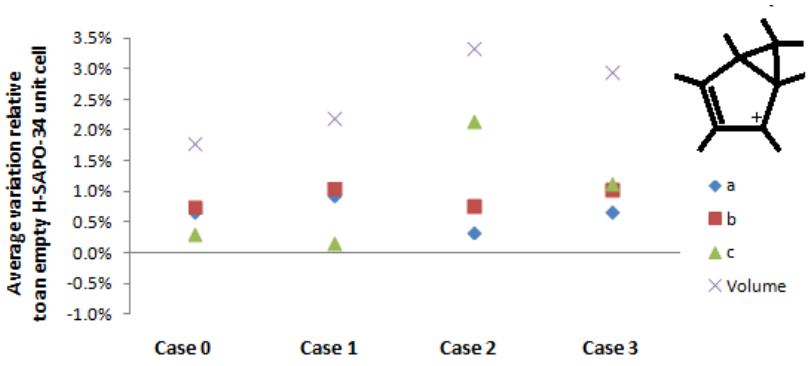

Figure 4.5: Average variation of unit cell parameters and volume relative to an empty H-SAPO-34 unit cell at 623 K and 1 atm of 5-3-CP$^+$ for a 50 ps MD simulation.

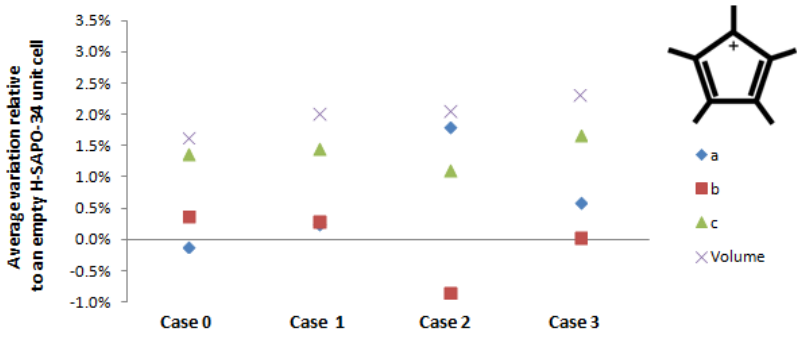

Figure 4.6: Average variation of unit cell parameters and volume relative to an empty H-SAPO-34 unit cell at 623 K and 1 atm of PMCP$^+$ for a 50 ps MD simulation.

In the above figures the change of the unit cell parameters is shown relative to an empty H-SAPO-34 unit cell. However, the unit cell parameters of H-SAPO-34 is not at all constant in the c-direction. This can be shown in Figure 4.7. During the simulation there is a sudden contraction in the c-direction. This problem has also be seen in earlier research at the Center for Molecular Modeling. This is remarkable moreover because these drops does not occur with filled cages. Therefore, it is hard to indicate the accuracy of the obtained results as they are compared to this empty unit cell. In order to get an idea of the accuracy of the simulations for the different intermediates, one shows the evolution of the volume of the unit cell during the simulation. In Appendix A the unit cell parameter variation are shown after 30, 35, 40, 45 and 50 ps simulation. The unit cell parameters variation are calculated relative to a 50 ps empty H-SAPO-34 simulation. This approach is used in order to test the accuracy of the simulations for the different intermediates without consideration of the accuracy of the empty H-SAPO-34 unit cell. For most simulations a steady state regime is obtained with little deviations (0.2 %), however some deviations were quiet large (0.5 %). In order to improve these result, one can simulate longer.

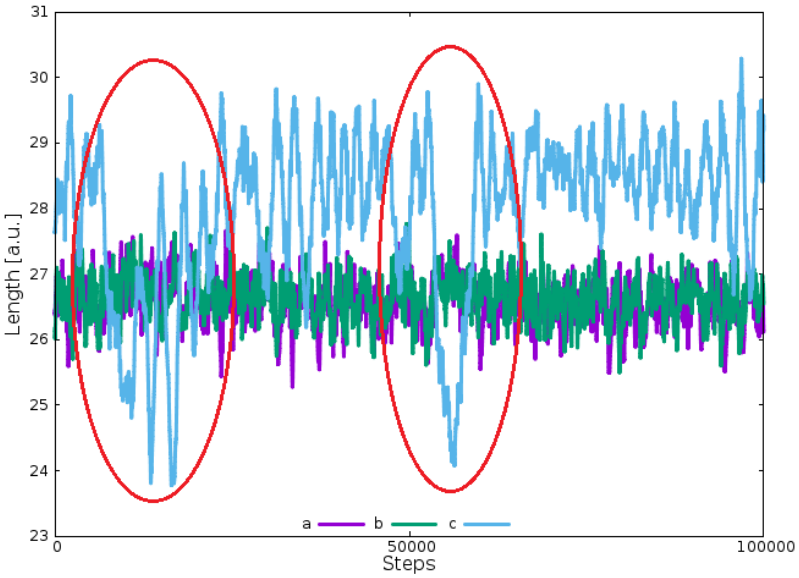

Figure 4.7: Unit cell parameters of an empty H-SAPO-34 unit cell at 623 K and 1 atm during an MD simulation. During this simulations two drops in the c-direction are observed as indicated in red.

From this analysis of the framework flexibility, it can be concluded that the unit cell variation are very anisotropic. When considering the intermediate heptaMB$^+$, elongation is strongly present in the c-direction and contraction is noticed in the a-direction in case 1 and 2. The elongations are more fluctuating for the other investigated intermediates.

Furthermore, a more compact intermediate (such as the five-ring species) results in a volume decrease of the framework compared to heptaMB$^+$. Apparently both the water loading and the intermediate influence the behavior of the unit cell in different directions for different intermediates and further analyses of these characteristics is needed to understand the behavior seen here.

4.3 Energy profile for the paring cycle

Secondly, the average potential (U) and total energy (E=U+K) per simulation are calculated and compared to a reference (in this case heptaMB$^+$ will be used as reference). The energy profile gives an idea of the difficulty of the step and is a measure for the driving force of the overall mechanism (although no transition state energies are calculated). For energy calculations it is of course necessary to compare simulations with an equal amount of atoms. In case 0, propylene is placed in the cage adjacent to the one filled with the carbocationic intermediate and thus an equal amount of atoms is obtained for the three intermediates. Placement of propylene in the same cage leads to reaction between the two molecules which is unwanted. In Appendix E this unwanted result is shown. The formation of the bicyclic specie hints that PMCP$^+$ is a rather unstable specie but will be further discussed in the next paragraph. In case 1-3 this methodology is not possible since both cages contain an aromatic intermediate (and the placement of the intermediate anticipates on the unwanted diffusion of water molecules). Therefore, these simulations of PMCP$^+$ cannot be compared to one another.

In Figure 4.8 the results are shown for case 0, in Figure 4.9 the results are shown for case 1-3 for heptaMB$^+$ and 5-3-CP$^+$. From Figure 4.8 it is concluded that the paring cycle has an increasing energy level which is opposite to the volume of the unit cell as discussed before. PMCP$^+$ already has an energy 133 kJ/mol higher compared to heptaMB$^+$ which suggests a low driving force for this route. The anti-aromatic nature of PMCP$^+$ is presumed to be the cause of this. However when looking at Figure 4.9, the energy difference between heptaMB$^+$ and 5-3-CP$^+$ increases at first (when two water molecules are added in each cage) but this difference diminishes when four water molecules are added in each cage. Thus, it can concluded that the energy level first increases, but at high water loadings (case 3) this result in the same energy level as in case 0. Perhaps water stabilizes the intermediate within the framework resulting in lower energy barriers. Thus, from these, it can be concluded that there certainly is an effect of water on the energy profile. Moreover, this effect is quiet outspoken but at high water loadings the effect completely cancels out again. A more detailed study of the energy profile of PMCP$^+$ can give a better understanding.

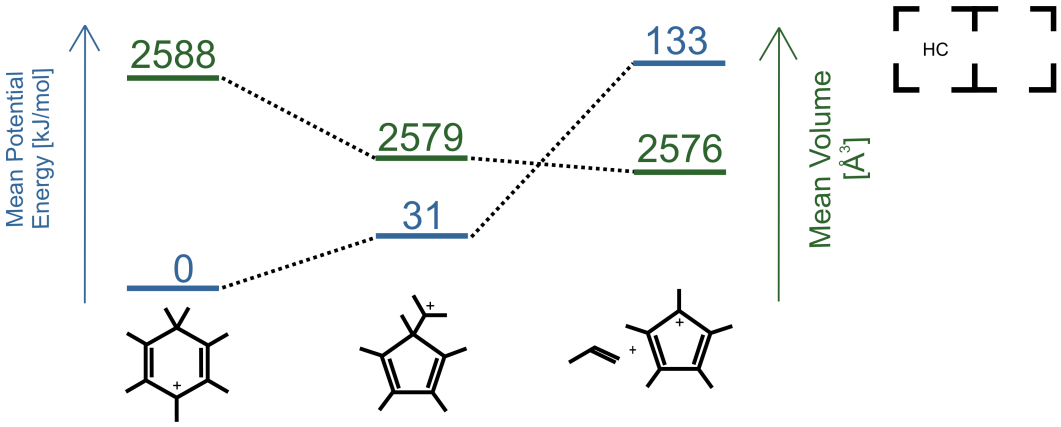

Figure 4.8: Energy profile of case 0 for the different molecules relative to heptaMB$^+$ at 623 K and 1 atm during a 50 ps MD simulation

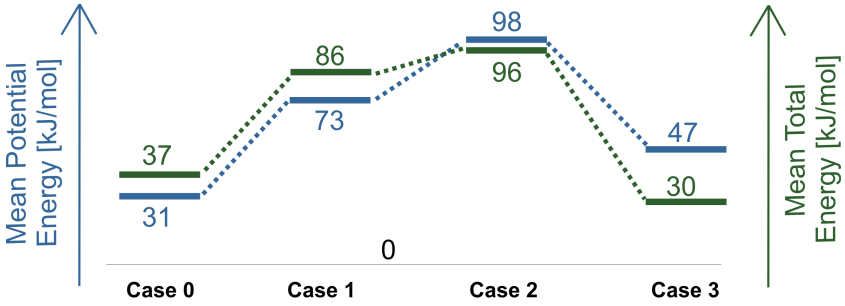

Figure 4.9: Energy profile for the different cases of 5-3-CP$^+$ relative to heptaMB$^+$ at 623 K and 1 atm during a 50 ps MD simulation. Note that the relative energy state is different for each case.

Again, the mean potential energy of 5-3-CP$^+$ compared to heptaMB$^+$ is given but this time the variations over simulated time is analyzed. In Figure 4.10 the thermodynamic profile is shown after 30, 35, 40 and 45 ps for heptaMB$^+$ (the thermodynamic variation profile for 5-3-CP$^+$ is shown in Appendix B) in order to get an idea of the convergence of the simulation. It can be concluded that the relative energy difference varies quiet largely (-8 - 20 kJ/mol). A simulation of 50 ps is rather short to do accurate energy calculations because of the rather large energy deviations over time. Therefore, to increase the accuracy of the energy calculations, one can simulate longer. However this will require more time and is not done in this master thesis.

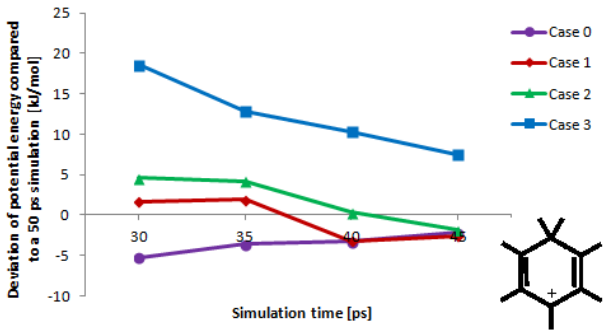

(a)

Figure 4.10: Potential energy difference at 623 K and 1 atm between the energy calculated at 30, 35, 40 and 45 ps and the energy calculated after 50 ps for heptaMB$^+$.

4.4 Mobility of the water molecules

In this master thesis only water is considered as solvent molecule because it is aimed to investigate the effect of water on the paring cycle. In case 2, there are in total four water molecules to visualize, in case 3 this amounts up to eight water molecules per unit cell. In the analysis hereof, its position along the MD simulation is plotted for each water molecule separately (which is done for the clarity of the figures) while all the other molecules are kept fixed. However, this results in four figures in case 2 and eight figures in case 3. Because of the high amount of plots, only two plots will be shown here (most extreme cases). The plots for the non-discussed water molecules are given in Appendix D. The aim of this type of analysis is to give an idea of the mobility of the water molecule during the MD simulation in one plot. For 50 ps, the location of the water molecule is plotted every 100 steps.

At the start of the simulation the water molecules were equally spaced in both cages of the unit cell. However, after the system is equilibrated, it was found that the water molecules are positioned in several places: the water molecules could be positioned in between the two cages, around the intermediate or in the empty cage that is a result of periodic extension. The origin of the so called empty cage is graphically shown in Figure 4.11. Although, the unit cell is filled up with an intermediate in both cages of the unit cell, an extra cage containing no intermediate molecules is made.

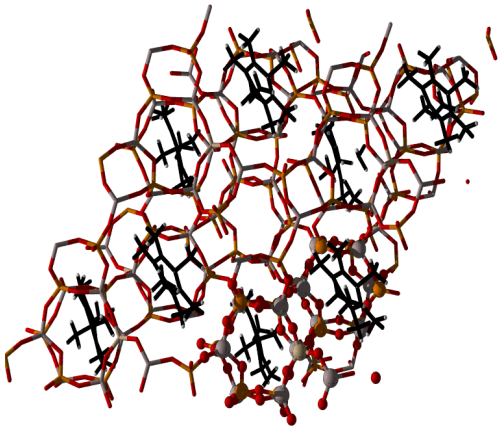

(a)

Figure 4.11: The unit cell is highlighted and shows by periodic extension the origin of the empty unit cell.

Together with the visual way of representing the position of the water molecules other quantitative results will be shown here such as the amount of clustering of water molecules and histograms of the measured distance between oxygen of the water molecules and the framework, the intermediate and each other. Our interest will be focused on the shortest distances between the considered atoms.

4.4.1 HeptaMB$^+$

At first, the simulations with heptaMB$^+$ as HP species is considered with both types of water loading. Herein, most water molecules are located in between the cages filled with the intermediate (i.e. the empty cage) as shown in Figure 4.12a and Figure 4.13a. In case 3, six of eight water molecules are placed in the empty cage. Herein, the water molecules have a lot of space and form clusters with each other. The driving force for this movement can be linked to the fact that the water molecules are less restricted to any position. However, the space available in the intermediate containing cages is large enough, water molecules clearly prefer the empty cage. The water molecules seem to have only a low interaction with the Si position as the water molecules do not have a specific orientation towards the active site in the empty cage. The two other water molecules in case 3 do have preferred positions (see Figure 4.13b), also in case 2 a water molecule is placed close to the considered intermediate (see Figure 4.12b). When looking back at the unit cell parameters and volume of heptaMB$^+$, case 2 and 3 were quiet similar. The small increase in volume can be explained by the increased water loading. For case 3 however, the total volume did increase but the elongations were more isotropic. Can the position of the water molecules explain this behavior and the energy profile as discussed in Section 4.3? On a first sight, no difference is noticed between case 2 and 3. The position

of the water molecules are rather similar. Therefore, some other analyses are considered.

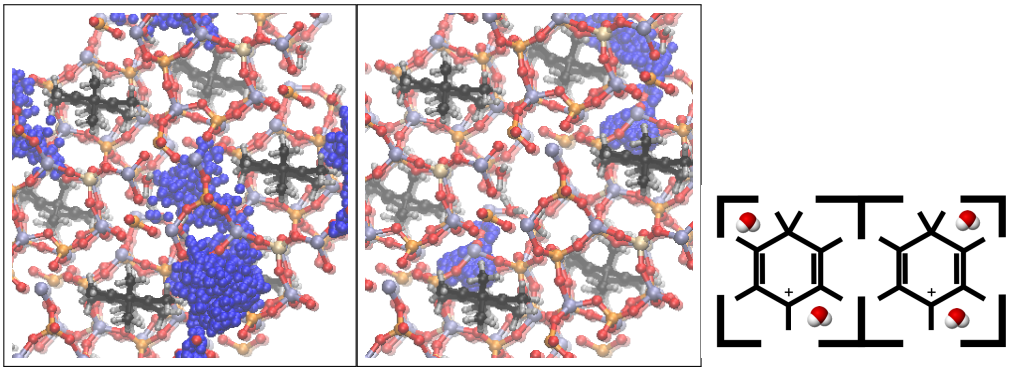

(a) **(b)**

Figure 4.12: MD visualization of the different positions that an oxygen atom of a water molecules has in a 50 ps MD simulation in H-SAPO-34 in case 2 with heptaMB$^+$ at 623 K and 1 atm for two different water molecules (a and b). a) water molecule is positioned in the empty cage b) water molecule is positioned near the intermediate.

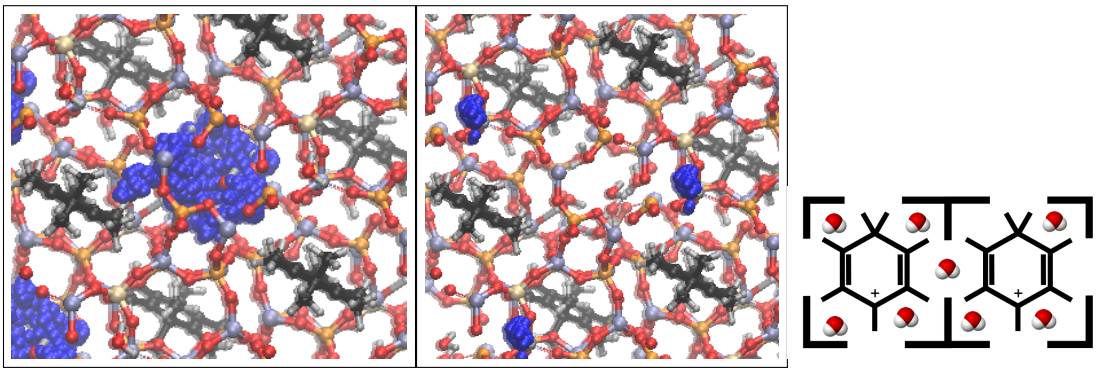

(a) **(b)**

Figure 4.13: MD visualization of the different positions that an oxygen atom of a water molecules has in a 50 ps MD simulation in H-SAPO-34 in case 3 with heptaMB$^+$ at 623 K and 1 atm for two different water molecules (a and b). a) water molecule is positioned in the empty cage b) water molecule is positioned near the intermediate.

When evaluating the effect of water on the paring mechanism, it is of course interesting to evaluate the amount of clustering of water. In this master thesis clustering is considered if the distance between two water oxygen atoms is less than 3.5 Å. In case 2, 50 % of the water molecules does not form a cluster, 30 % forms dimers and 20 % trimers. These values shift with higher loadings (in case 3): all water molecules cluster. Herein,

68 % forms a dimer, 15 % trimers, 11 % tetramers and 6 % pentamers. A clear trend to higher cluster formation is seen with high water loading which should not be surprising.

4.4.2 5-3-CP$^+$

For the bicyclic 5-3-CP$^+$ species, more water molecules are constrained to their position compared to heptaMB$^+$. Figure 4.14a shows a water molecule placed in the empty cage. Figure 4.14b shows a water molecule placed close to the intermediate. When looking back at the unit cell parameters and volume of 5-3-CP$^+$ for the different cases, there was no trend visual. Case 2 was quiet different from the other cases. From the analysis of the position of the water molecule, it can be concluded that in case 2, three of the four water molecules are positioned around the intermediate which causes an increase in the volume. In case 3, also three (of eight) water molecules are positioned close to the intermediate. Furthermore, in case 2 the clustering consists only of dimers (72 %). 28 % does not form any cluster. In case 3, 66 % of the water molecules forms dimers, 20 % trimers, 9 % tetramers and 4 % pentamers. Again, the amount of clustering increases with increasing water loading. There is a big effect on the energy barriers so it should be clear that the effect of water on the paring mechanism is not at all negligible.

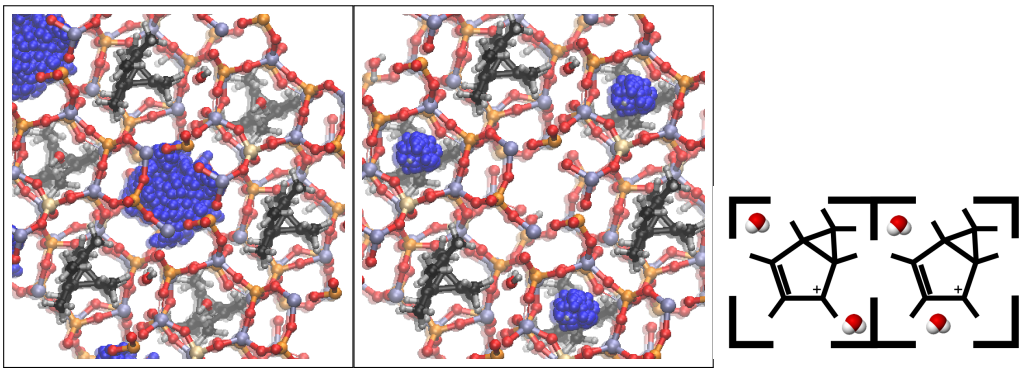

(a) **(b)**

Figure 4.14: MD visualization of the different positions that an oxygen atom of a water molecules has in a 50 ps MD simulation in H-SAPO-34 in case 2 with 5-3-CP$^+$ at 623 K and 1 atm for two different water molecules (a and b). a) water molecule is positioned in the empty cage b) water molecule is positioned near the intermediate.

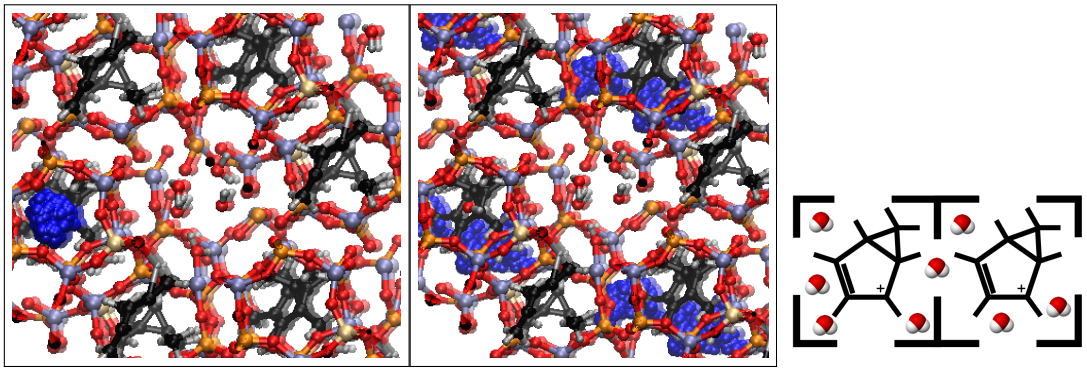

(a) **(b)**

Figure 4.15: MD visualization of the different positions that an oxygen atom of a water molecules has in a 50 ps MD simulation in H-SAPO-34 in case 3 with 5-3-CP^+ at 623 K and 1 atm for two different water molecules (a and b). a) water molecule is positioned in the empty cage b) water molecule is positioned near the intermediate.

4.4.3 $PMCP^+$

The last evaluated intermediate is $PMCP^+$. In case 2, all the water molecules surround the intermediate (see Figure 4.16). This resulted in a contraction in the b-direction and the largest elongation in the a-direction. The position of the water molecules in case 3 is given in Figure 4.17. Furthermore, there is a 93 % probability to find water dimers and only 7 % remains unclustered. When in case 3 more water molecules are added, all water molecules are clustered with a distribution of 52 % dimers, 24 % trimers, 17 % tetramers and 7 % pentamers.

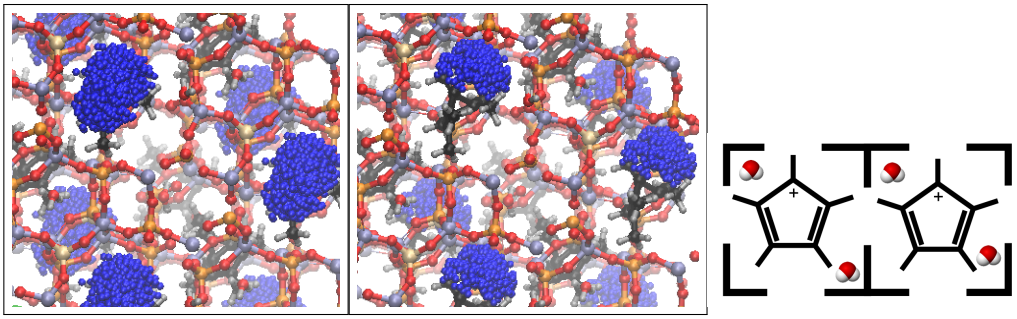

(a) **(b)**

Figure 4.16: MD visualization of the different positions that an oxygen atom of a water molecules has in a 50 ps MD simulation in H-SAPO-34 in case 2 with $PMCP^+$ at 623 K and 1 atm for two different water molecules (a and b). Both a and b are positioned close to the intermediate.

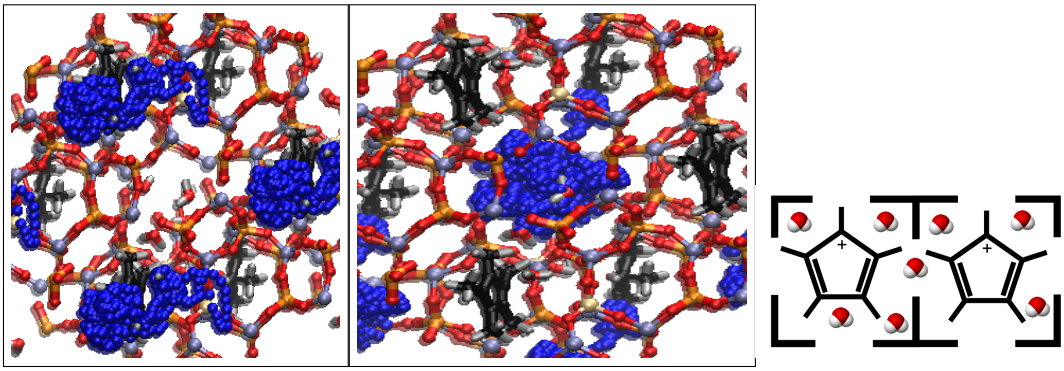

(a) **(b)**

Figure 4.17: MD visualization of the different positions that an oxygen atom of a water molecules has in a 50 ps MD simulation in H-SAPO-34 in case 3 with $PMCP^+$ at 623 K and 1 atm for two different water molecules (a and b). a) water molecule is positioned in the empty cage b) water molecule is positioned near the intermediate.

4.4.4 Location of the water molecules by investigating distances

At last, the location of the water molecules is further investigated by calculating the shortest distance at any time of a water molecule and the other water molecules, the intermediate and the framework atoms. By doing so, the visualizations herefore are quantified. The graphs are obtained by calculated at every time step the distance between an oxygen of a water molecule and the target atoms. From all these distances, the shortest distance is taken and this is done at every time step resulting in the shortest distance probability distribution. The first calculated distance is the distance between an oxygen of a water molecule and the carbon atoms of the hydrocarbon. In Figure 4.18a the result is shown for case 2. Besides a variation in the broadness of the molecules no shift is seen here. This differs in case 3 (see Figure 4.18b) were the $PMCP^+$ has a complete different behavior than the two other molecules where water molecules atoms approach the intermediate quiet closely.

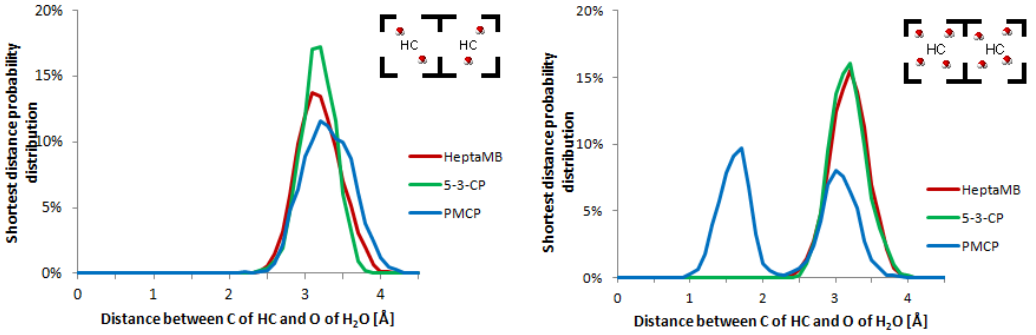

(a) **(b)**

Figure 4.18: Distribution of the shortest distance between oxygen atom of H_2O and carbon atom of the considered intermediates in case 2 for a 50 ps MD simulation at 623 K and 1 atm.

In Figure 4.19 the clustering is shown in forms of the shortest distance probability distribution. First of all, between Figure 4.19a and Figure 4.19b, there is a shift to the left to smaller distances which is caused by the increased water loadings. For case 2, again and more outspoken, the distribution becomes smaller for $PMCP^+$ compared to 5-3-CP^+, which is again smaller than $heptaMB^+$. In Figure 4.19b $PMCP^+$ again shows two peaks. The nature hereof, was found by observation of the motion. During the simulation a water molecule approach the neighboring oxygen atom of the Si-atom and forms a covalent bond. Resulting in the formation of OH^-. Although, it is expected that this situation is highly unstable, it is seen during a significant time and this will probably be an artifact of the performed simulation.

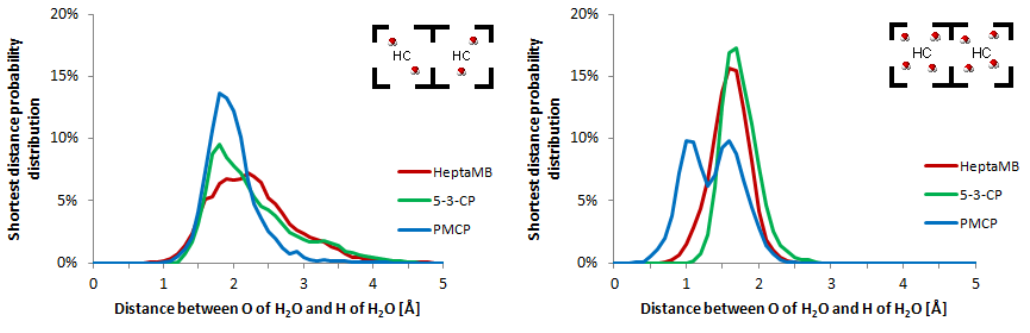

(a) **(b)**

Figure 4.19: Distribution of the shortest distance between oxygen atom of H_2O and hydrogen atoms of other water molecules of the considered intermediate for a 50 ps MD simulation at 623 K and 1 atm.

At last, the distance between the water molecules and the framework is considered and

shown in Figure 4.20. In Figure 4.20a the distribution is shown for low water loading for the three considered intermediates. It is seen that $PMCP^+$ is shifted to the right compared with the distributions of the two other intermediates. Compared with Figure 4.18a $PMCP^+$ is equally attracted towards the intermediate as the framework. For the other two intermediates it can be concluded that water molecules prefer interaction with the framework.

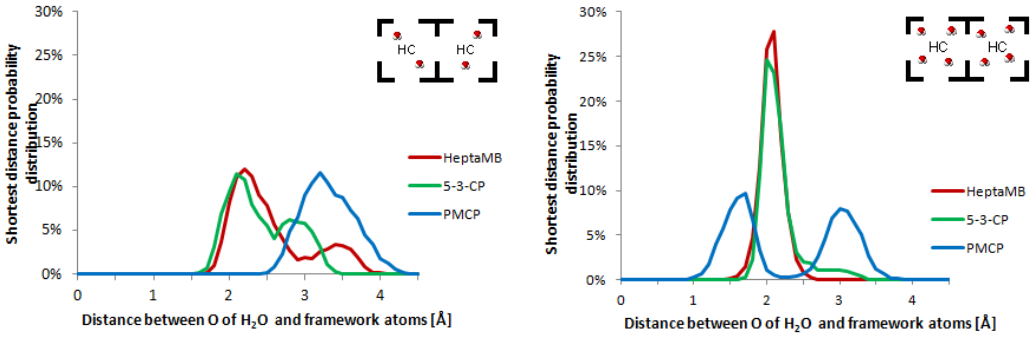

Figure 4.20: Distribution of the shortest distance between oxygen atom of H_2O and Si/Al/P atoms of the framework for the considered intermediate for a 50 ps MD simulation at 623 K and 1 atm.

4.5 Mobility of the carbocationic intermediates

One of the questions that rises within the MD analysis of the paring mechanism is how the hydrocarbons orientate in the zeotype framework. This information can be valuable to see whether or not there is a preferential direction, which can give further insight on the volume of the framework and the energy calculations in Section 4.2 and Section 4.3. Two angles, further denoted as α and β, are defined in Figure 4.21 to analyze the orientation of the intermediates. α is the angle between the plane spanned by the ring carbon atoms of the hydrocarbons and the vector spanned by six of the T-atoms of the framework. β is the angle defined between the ring carbon atoms of the hydrocarbons and the vector spanned by four of the T-atoms of the framework that are perpendicular to the previous framework atoms. Due to symmetry reasons α en β will be in the range between 0°and 90°. As there are two simulated cages they will be considered as one 100 ps simulation. Figure 4.22 visualizes the boundaries of the range (α, β).

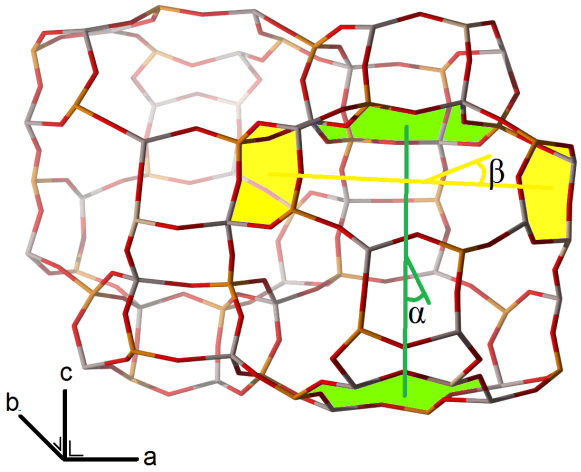

Figure 4.21: Visualization of the defined angles α and β within the H-SAPO-34 cage.

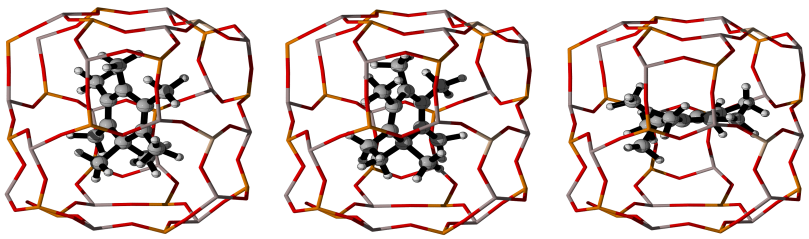

(a) **(b)** **(c)**

Figure 4.22: Snapshots at the boundaries of the accessible (α, β) area represented here for heptaMB$^+$. a) (0°, 0°), b)(0°, 90°), (90°, 0°)

4.5.1 HeptaMB

Case 1

The analysis is started with intermediate heptaMB$^+$. To recapitulate, from the framework analysis it was concluded that there was an elongation in the c-direction even if no water molecules were present (as in case 1). In Figure 4.23a the position of the intermediate is shown for both cages. First of all, the position of the intermediate in both cages is quiet alike. This orientation corresponds to a vertical orientation (in the c direction) of the intermediate within the H-SAPO-34 framework. Its orientation is therefore linked to the framework flexibility. From the 50 ps movie of the simulation it was seen that the molecule did move but according to Figure 4.23a the area is relative small. As no water loading is present the intermediate appears to have a preferential orientation along the c-direction. In Figure 4.23b a snapshot is shown of a highly favored orientation (hotspot) in order to create a better understanding of the 2D-histograms.

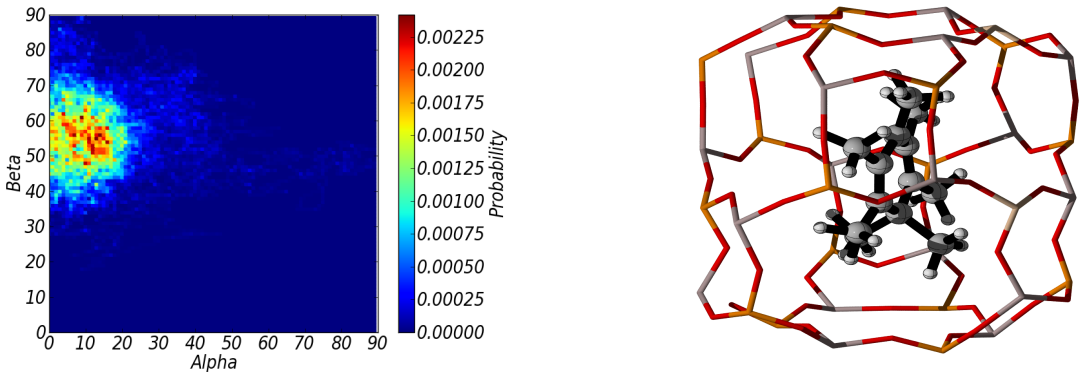

(a) **(b)**

Figure 4.23: a) Probability density distribution of the position of heptaMB$^+$, b) snapshot of the most favorable position of heptaMB$^+$ ($\alpha = 8°$, $\beta = 59°$) in case 1 in H-SAPO-34 in a 100 ps MD simulations at 623 K and 1 atm.

Case 2

The result of case 2, when two water molecules are added to each cage, is shown in Figure 4.24a. This result looks similar to the previous result, when no water molecules were present but is more constrained. The similarities between case 1 and case 2 were also found in Section 4.2 were the framework flexibility was investigated. Figure 4.24b shows a snapshot of the preferred position. At this snapshot there was one water molecule present in the cage as is also shown in Figure 4.24b but its location was more closely to the framework than the intermediate molecule.

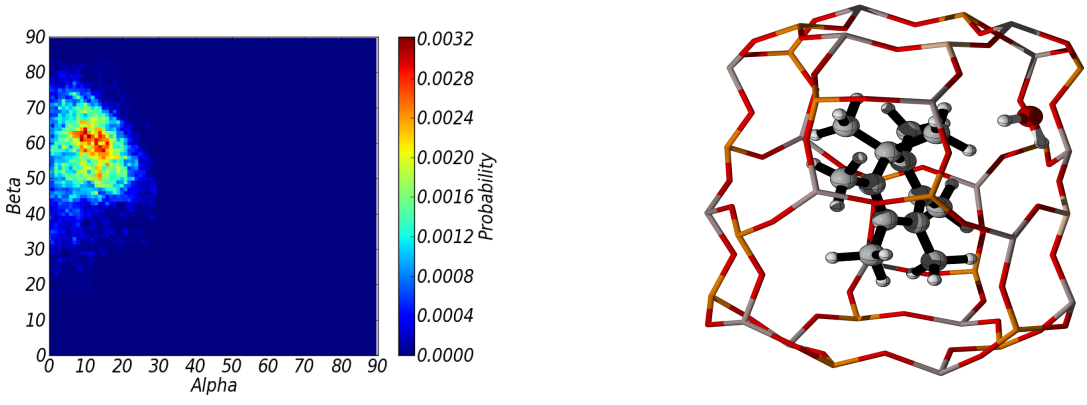

(a) **(b)**

Figure 4.24: a) Probability density distribution of the position of heptaMB$^+$, b) snapshot of the most favorable position of heptaMB$^+$ ($\alpha = 9°$, $\beta = 61°$) in case 2 in H-SAPO-34 in a 100 ps MD simulations at 623 K and 1 atm.

Case 3

The result of case 3, when four water molecules are added to each cage, is shown in Figure 4.25. The 2D histogram shows two favorable orientations of the intermediate each corresponding to one cage with a difference in β. This can be due to the sensitiveness of the MD simulation of the intermediate on its the initial position. Furthermore, the position of the water molecules can withhold the intermediate of a certain position as is shown in Figure 4.24b. As it was seen that there were more water molecules surrounding the intermediate in one of the two cages (as shown in Figure 4.25b where the position in the β is equal to 45°is shown) and this tilts the intermediate.

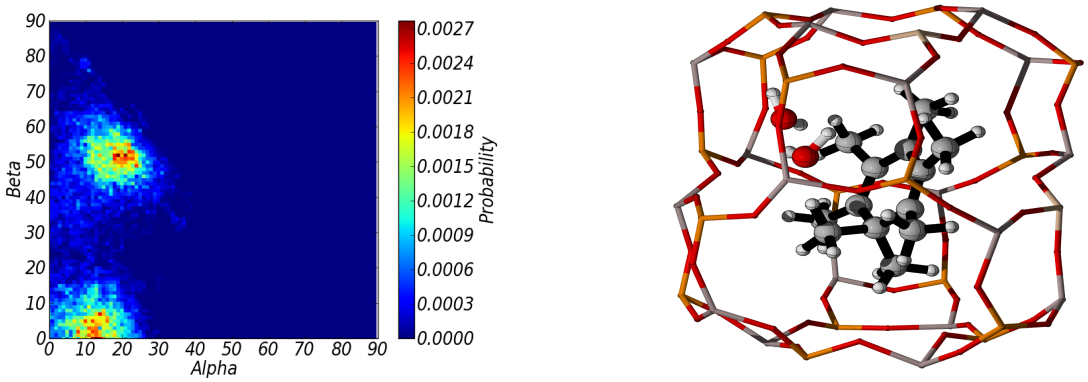

(a) **(b)**

Figure 4.25: a) Probability density distribution of the position of heptaMB$^+$, b) snapshot of the most favorable position of heptaMB$^+$ ($\alpha = 21°$, $\beta = 45°$) in case 3 in H-SAPO-34 in a 100 ps MD simulations at 623 K and 1 atm.

The analysis of the variation of the unit cell parameters discussed in Paragraph 4.2 showed an increase in the b-direction and an increase in the a-direction. Furthermore, when investigating the shortest distance between one of the carbon atoms of heptaMB$^+$ and the Si-atom of the framework, as shown in Figure 4.26 not a lot of differences is seen except from case 3 where there is a small time frame in which the intermediate is closely positioned to the framework. These distances are not of the order of a chemical bond but can be considered as the result of elektrostatic and van der Waals interaction.

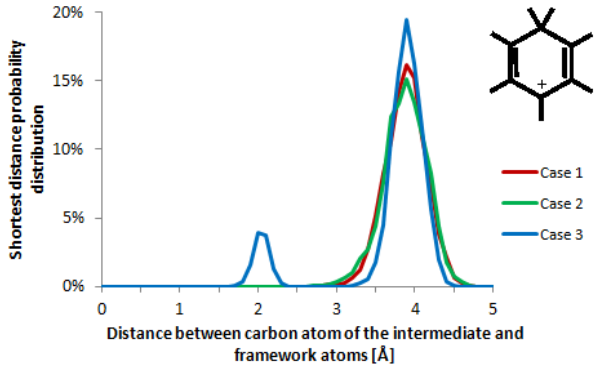

Figure 4.26: Probability distribution of the distance between Si of the framework and carbon atoms of heptaMB$^+$ in H-SAPO-34 in a 50 ps MD simulations at 623 K and 1 atm for the three cases.

It can be concluded that adding water molecules to the framework results in competition between water molecules and heptaMB$^+$ for interaction with the acid site. This results in a different orientation of the intermediate within the framework and thereby results in a less anisotropic behavior of the framework with increased water loading. Furthermore, with increasing water loading the intermediate is more constrained to its position.

4.5.2 5-3-CP$^+$

Case 1

The elongation of the catalyst framework in the c-direction is less pronounced when introducing 5-3-CP$^+$ in the H-SAPO-34 pores compared to heptaMB$^+$ as was discussed in Paragraph 4.2. This can also be seen in Figure 4.27a were the angle α represents the deviation form the c-direction and this is larger than in the previous cases (see Figure 4.27b for a snapshot with α equal to 27°and β equal to 43°). The results found for framework flexibility thus corresponds to the results found for intermediate orientation. In this case no water molecules are present to stabilize the stability of the intermediate and as shown in Paragraph 4.3 it was seen that PMCP$^+$ is 86 kJ/mol higher in energy than heptaMB$^+$.

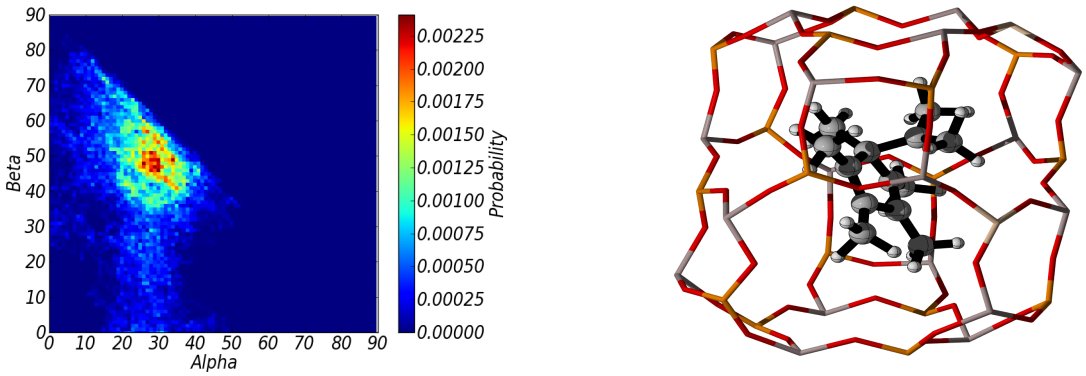

(a) **(b)**

Figure 4.27: a) Probability density distribution of the position of 5-3-CP$^+$, b) snapshot of the most favorable position of 5-3-CP$^+$ ($\alpha = 27°$, $\beta = 43°$) in case 1 in H-SAPO-34 in a 100 ps MD simulations at 623 K and 1 atm.

Case 2

In case 2, the elongation of the framework flexibility of 5-3-CP$^+$ was much more present than in case 1 with the largest increase in the c-direction. When comparing 4.27a and 4.28a a shift towards lower α angles is seen which can explain the elongation in the c-direction. The narrow distribution for Figure 4.28a is remarkable and can be explained by the surrounding of the water molecules limiting the movement of the cation, as seen in 4.28b. Again, an increase in energy was seen for case 2 compared to case 1 as seen in Figure 4.9. Apparently, the addition of water molecules destabilize the system.

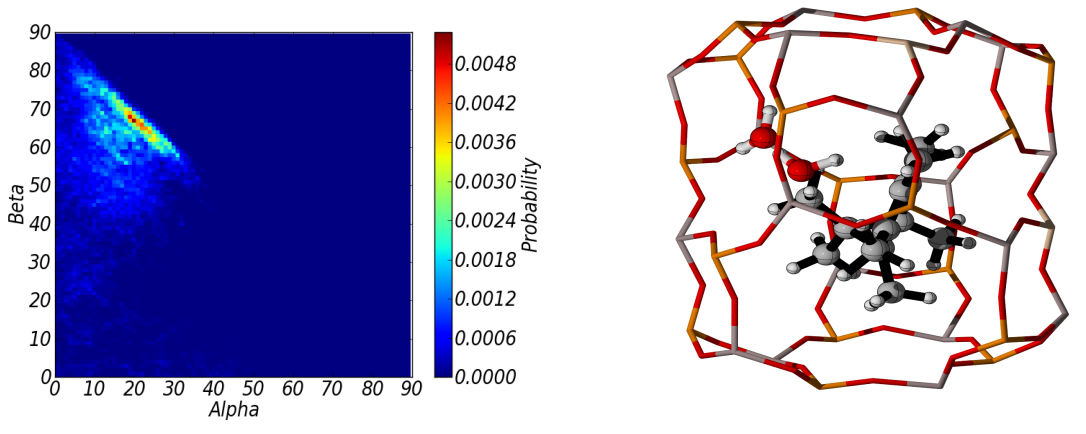

(a) **(b)**

Figure 4.28: a) Probability density distribution of the position of 5-3-CP$^+$, b) snapshot of the most favorable position of 5-3-CP$^+$ ($\alpha = 20°$, $\beta = 69°$) in case 2 in H-SAPO-34 in a 100 ps MD simulations at 623 K and 1 atm.

Case 3

In case 3, the framework expansion was again far less anisotropic than case 1 and 2 as shown in Figure 4.5. The 2D-histogram of the position of the intermediate is shown in Figure 4.29a. The two areas again corresponds to the position of the intermediate in the two cages which differ in the β orientation. The intermediate is not stringent by the water molecules and thus can move in a large area which can result in the more isotropic behavior. Again, in Figure 4.29b a snapshot is shown of the most favorable position whereas the water molecules are located close to the framework. The shortest distance distribution is given in Figure 4.30. There is a small shift in case 1 to smaller distances compared with case 2 and 3. It can be concluded that at high water loadings there is concurrence between water molecules and the intermediate to position close to the active site. The energy profile as shown in Figure 4.9 showed a strong decrease in energy when adding water molecules. Although, the water molecules does not get closer to the intermediate, th water molecules did position itself closer to the framework as shown in Figure 4.20. This result in concurrence between the water molecules and the intermediate to interact with the framework resulying in a lower energy level.

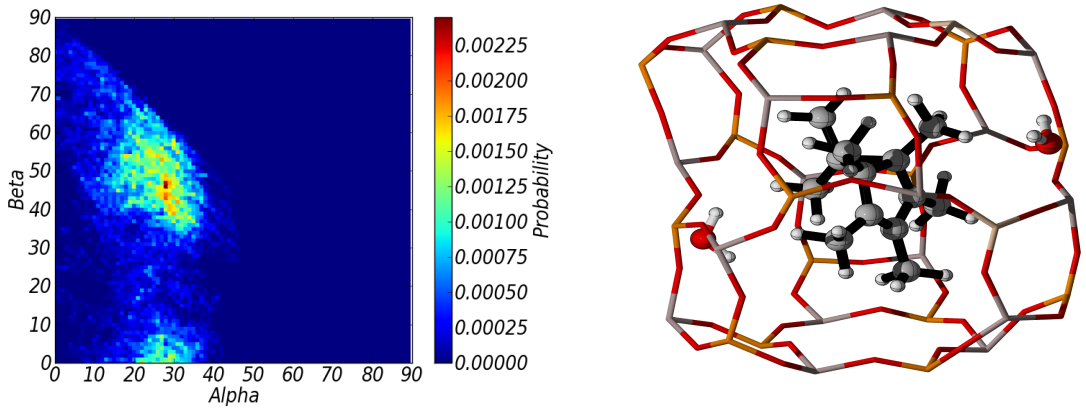

(a) **(b)**

Figure 4.29: a) Probability density distribution of the position of 5-3-CP$^+$, b) snapshot of the most favorable position of 5-3-CP$^+$ ($\alpha = 25°$, $\beta = 44°$) in case 3 in H-SAPO-34 in a 100 ps MD simulations at 623 K and 1 atm.

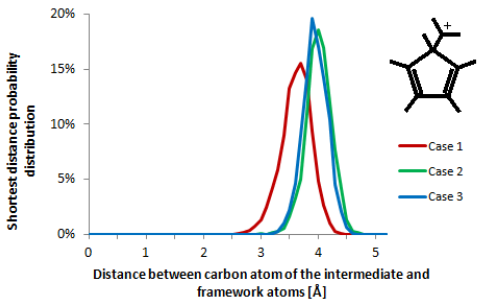

Figure 4.30: Probability distribution of the distance between Si of the framework and carbon atoms of heptaMB$^+$ in H-SAPO-34 in a 50 ps MD simulations at 623 K and 1 atm for the three cases.

4.5.3 PMCP$^+$

Case 1

The last intermediate, PMCP$^+$, is widely distributed within the framework for case 1 and 3, as shown in Figure 4.31a and 4.33a. This is also reflected in Figure 4.34 where the position of the intermediate is more widely distributed compared with the Si atom of the framework.

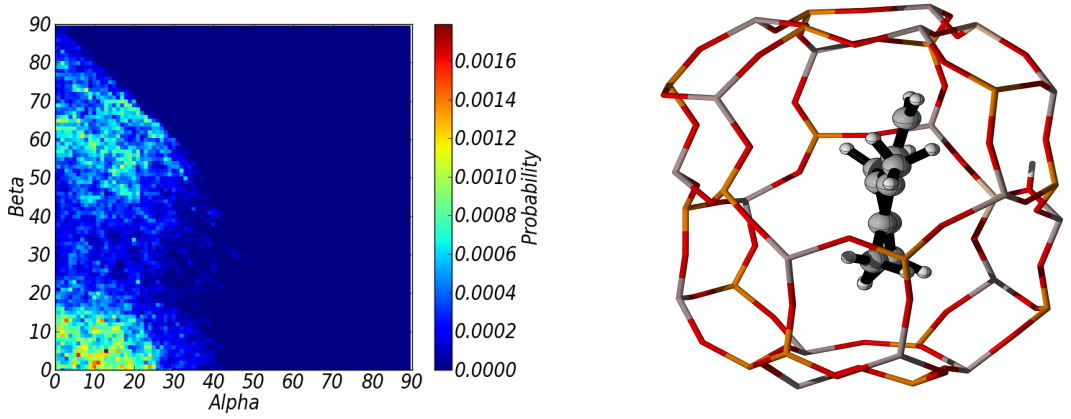

(a) **(b)**

Figure 4.31: a) Probability density distribution of the position of PMCP$^+$, b) snapshot of the position of PMCP$^+$ ($\alpha = 5°$, $\beta = 35°$) in case 1 in H-SAPO-34 in a 100 ps MD simulations at 623 K and 1 atm.

Case 2

In the second case, no exchange between hydrogens took place, resulting in a smaller distribution of the shortest distance between the intermediate and the framework (see

Figure 4.34). The elongation of the unit cell parameter a is graphically seen in Figure 4.32b and again the position of the intermediate is linked to the framework flexibility. In Figure 4.33a again β variates widely as was also noticed in the previous case.

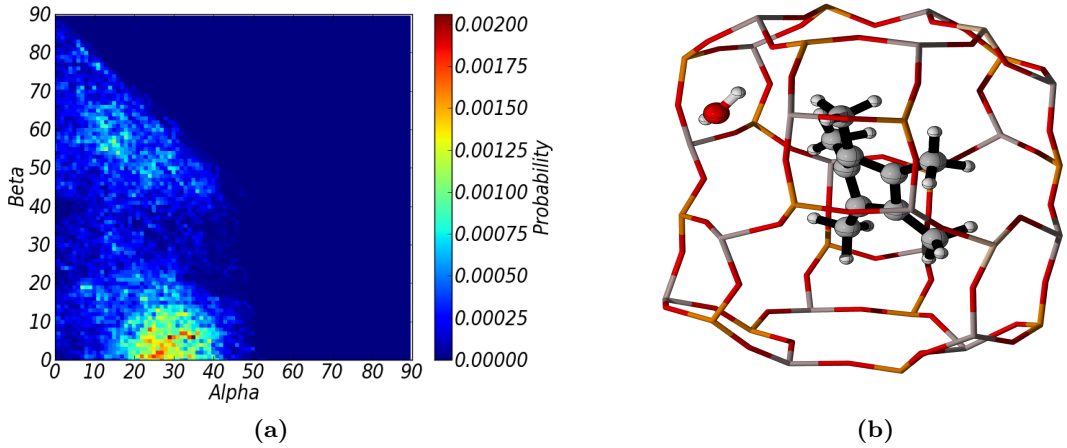

(a) **(b)**

Figure 4.32: a) Probability density distribution of the position of $PMCP^+$, b) snapshot of the position of $PMCP^+$ ($\alpha = 25°$, $\beta = 8°$) in case 2 in H-SAPO-34 in a 100 ps MD simulations at 623 K and 1 atm.

Case 3

At last, in Figure 4.33 the 2D histogram is shown for a high water loading. The intermediate position shows some similarities with case 1 (see 4.29). Visually it was seen that there is an interaction between the water molecules and the framework. This results in the repositioning of the intermediate further away from the Si-atom resulting in a broader distribution of the shortest distance (Figure 4.34).

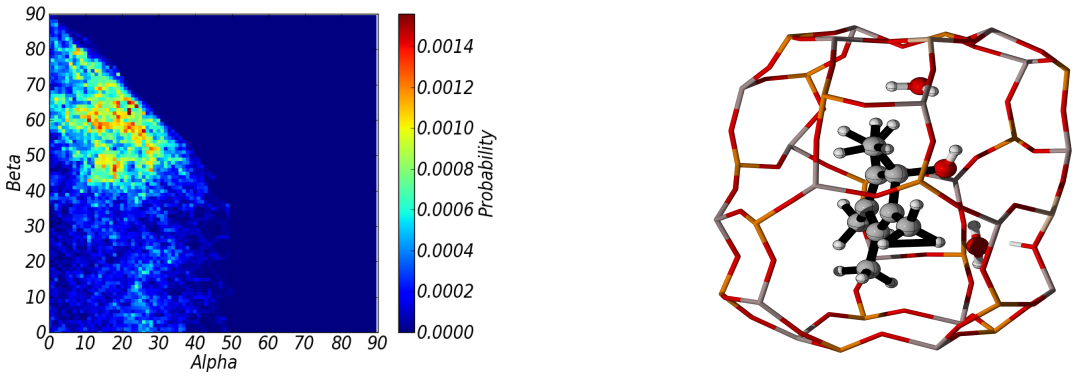

(a) **(b)**

Figure 4.33: a) Probability density distribution of the position of $PMCP^+$, b) snapshot of the position of $PMCP^+$ ($\alpha = 13°$, $\beta = 58°$) in case 3 in H-SAPO-34 in a 100 ps MD simulations at 623 K and 1 atm.

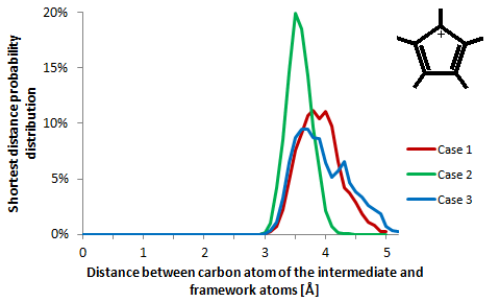

Figure 4.34: Probability distribution of the distance between Si of the framework and carbon atoms of $heptaMB^+$ in H-SAPO-34 in a 50 ps MD simulations at 623 K and 1 atm for the three cases.

To conclude this chapter, addition of a high loading of water increases the driving force for the considered reactions of the paring mechanism. However, at short distances, water destabilizes the intermediate molecule. Taking into account the increased amount of clustering upon increasing water loadings, it can be assumed that due to the clustering there is less competition between the water molecules and the carbon atoms to interact with the framework stabilizing the system.

Chapter 5

Evaluation of the paring mechanism by metadynamics simulations

As mentioned earlier, the HP mechanism is the starting point of this master thesis as it is the generally accepted mechanism to describe the MTO process nowadays. In the archetypal H-SAPO-34 catalyst, polymethylbenzenes are identified as the major HP species. Therefore, with the focus on the paring mechanism, the hexaMB is considered as HP species.[32,49,50] In earlier research already a complete energetic description of the paring route was given by static calculations based on hexaMB as HP species[65] and in the previous chapter it was found that in some cases there was a low driving force for the paring route to proceed. Therefore, in this master thesis some well defined reaction steps based on hexaMB as HP species are recalculated using metadynamics calculations to evaluate the kinetic driving force of the paring cycle at realistic operating conditions.

In the previous chapter AIMD simulations were performed in the NPT ensemble. However with these large systems (around 176 atoms dependent on the considered intermediate and solvent molecule) and the required level of theory, only a short simulation time (50 ps) is possible. These simulation times are too short for reactions to occur as chemical reactions are rare events. Therefore, metadynamics is an important technique to model chemical reactions. Based on the added Gaussian potentials, the free energy surface (FES) can be reconstructed. For more details on the computational method, I refer to 3.4. The two reactions that are considered are given in Figure 4.1.

The equilibrated systems obtained from the AIMD simulations are taken as starting point for the metadynamics simulations. Hereby, the time-averaged volume and unit cell dimensions is taken and will be kept constant in the MTD simulations.

5.1 Contraction reaction of heptaMB$^+$ to 5-iC$_3$−CP$^+$/ 5-3-CP$^+$

To recapitulate, the first reaction that will be considered in the metadynamics simulations is the contraction reaction of heptaMB$^+$ to 5-iC$_3$−CP$^+$. The latter species was found to be in equilibrium with the bicyclic molecule 5-3-CP$^+$ in the AIMD simulations. It will be investigated if this phenomena also occurs during metadynamics simulations. Two CVs are defined to describe the contraction reaction and are indicated in Figure 5.1. The first CV is a coordination number between C2 and C6 in order to simulate the formation of this bond. The second CV is defined as the coordination number between C1 on the one hand and C2 and C6 on the other hand. This coordination number ensures the breaking of the bond C1-C2 or C1-C6. Previous simulations have shown that the formed isopropyl group is very mobile.[65] Therefore, to avoid a ring walk of the isopropyl group, a wall is added between C1 and C3, C4 and C5.

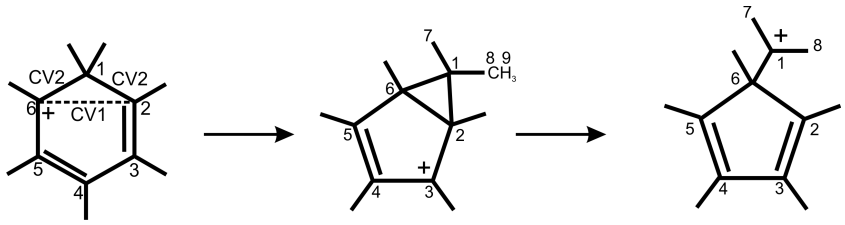

Figure 5.1: Atomic labeling of heptaMB$^+$ together with a visualization of the two defined CV for the contraction reaction of heptaMB$^+$.

The 2D free energy surface of the contraction reaction is given in Figure 5.2. The two regions corresponding with 5-iC$_3$−CP$^+$ and 5-3-CP$^+$ are both visualized. heptaMB$^+$ is more stable than the five-ring molecules.

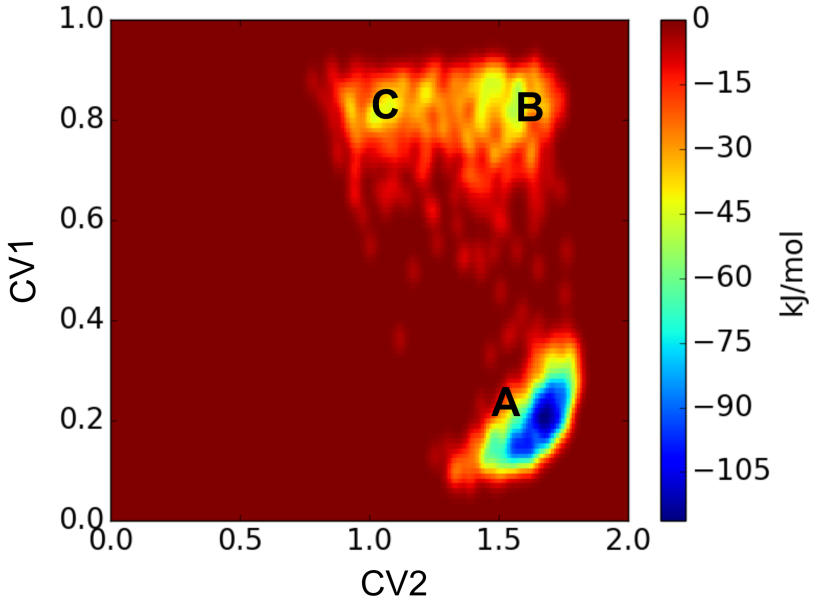

Figure 5.2: 2D FES obtained from the metadynamics simulation of the ring contraction of heptaMB$^+$ at 623 K and 1 atm in case 0.

The different states of the molecule are visualized in Figure 5.3. Whereas the transition in the collective variables is shown in Figure 5.4.

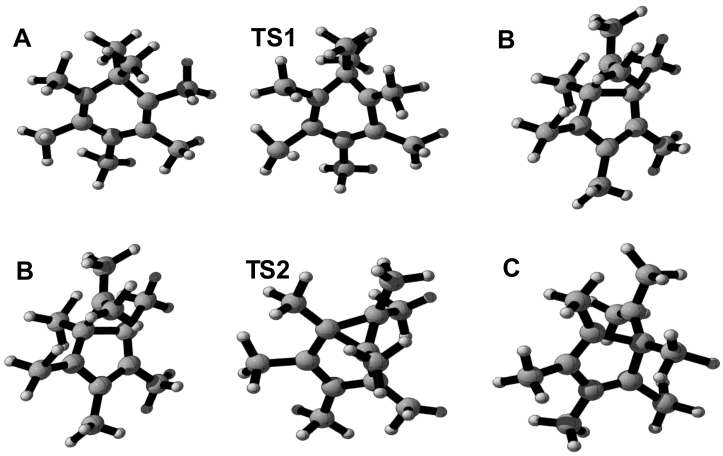

Figure 5.3: Visualization of the different states for the ring contraction of heptaMB$^+$.

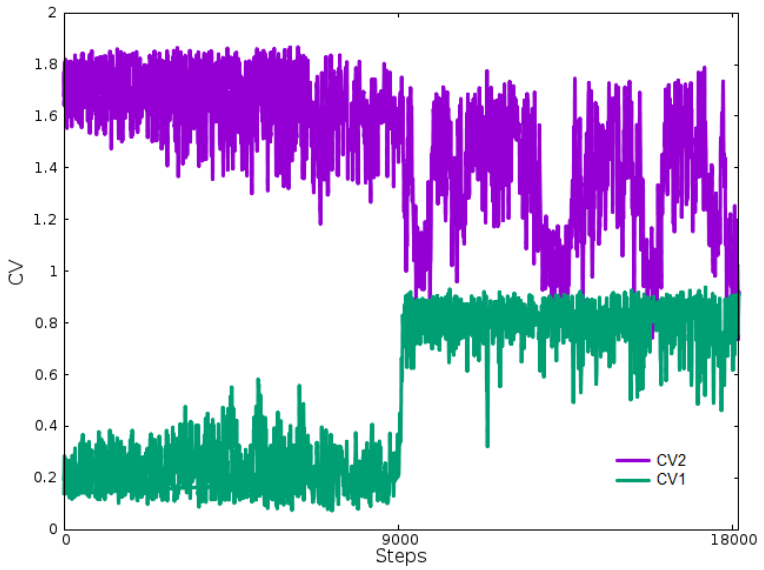

Figure 5.4: Visualization of the transition in collective variables.

5.2 Propylene formation of 5-3-CP$^+$

In the second investigated reaction the carbon-carbon bound of the ring and isopropyl group is broken and a hydride shift takes place resulting in the formation of propylene and PMCP$^+$. For the second reaction again two CVs are defined which are indicated in Figure 5.5. The first CV is defined as the coordination number between C6 on the one hand and C1 and C5 in order to stimulate the breaking of the carbon-carbon bond. The second CV is taken as the difference between two CVs, namely the coordination number between H9 and C8 and the coordination number between H9 and C6. This coordination number simulates the hydride shift.

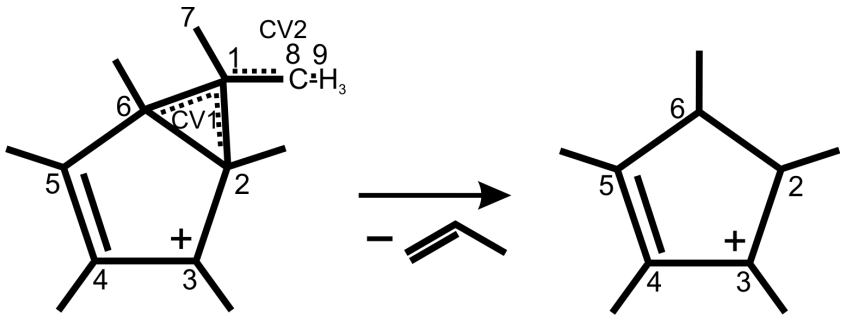

Figure 5.5: Visualization of the two defined CV for the formation of propylene.

In the second investigated reaction, C1 must split from both C6 and C2. When adding energy it will soon result in the breakage of one of the carbon-carbon bonds but a rather large energy barrier is needed to result in the full breakage of propylene. The incomplete

obtained 2D free energy profile is shown in Figure 5.6 with its lowest energy around -90 kJ/mol. However the result is incomplete, it can be stated that the results are in accordance with the results obtained in 4.3.

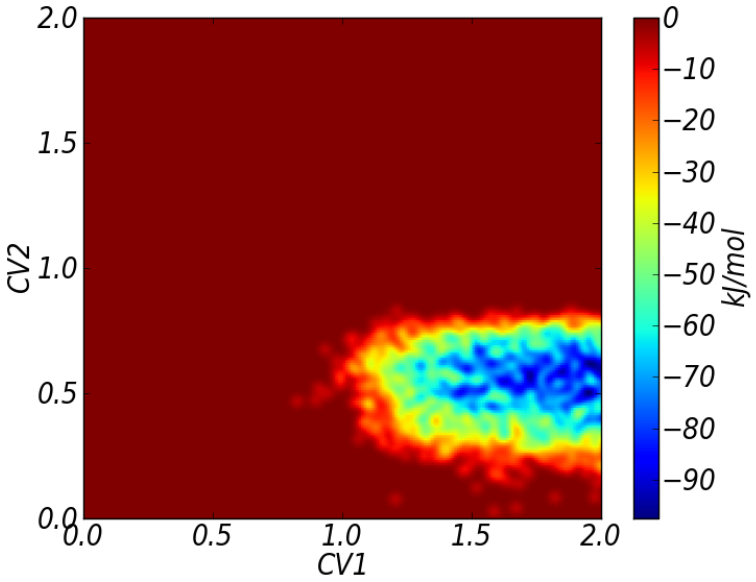

Figure 5.6: 2D FES obtained from the metadynamics simulation of the propylene formation of 5-3-CP^+ at 623 K and 1 atm in case 0.

Chapter 6

Conclusion

The Methanol-to-Olefins process is a complex process. Even today, the mechanism is not fully unraveled and it is still under investigation, but the hydrocarbon pool mechanism is nowadays generally accepted.[32] In the light of H-SAPO-34, polymethylbenzenes are identified as the major HP species wherefore the side-chain and the paring mechanism has been proposed. The paring mechanism, which is characterized by subsequent ring contraction and expansion reactions of the aromatic HP molecules, was proposed to explain the scrambling that was experimentally seen.[60]

This work is an investigation of the paring mechanism to test its viability and to see what the effect of water is on this mechanism. The experimental studies on the paring mechanism are limited and the stability of $PMCP^+$ within the reaction mechanism is unclear.[50] Therefore, in this work, the paring mechanism is studied and moreover, the effect of water on the paring mechanism. Insight of the effect of water on the molecular level is studied because it is aimed to obtain a better control of the ethylene/propylene ratio.

AIMD simulation were performed for the three considered intermediates: $heptaMB^+$, $5\text{-}3\text{-}CP^+$ and $PMCP^+$. Two types of water loading are considered: low water loading (with 2 water molecules to each cage of the unit cell) and high water loading (with 4 water molecules to each cage of the unit cell). These are compared with the results were no water molecules were added. Analysis of the framework flexibility, the energy profile and mobility of the water molecules and carbocationic intermediate were discussed and linked to each other. Finally, metadynamics simulations were performed to calculate the free energy barriers between the different intermediates.

It was found that during an AIMD simulation of $heptaMB^+$, the unit cell is elongated in the direction of the elongation of the carbocationic intermediate for all studied cases. Furthermore, it was seen that the position of $heptaMB^+$ is not much restricted by the

solvent molecules at low water content due to the diffusion of the solvent to the empty cage where no intermediate was located. However with an increased water loading it was found that more solvent molecules are positioned close to heptaMB$^+$. It is concluded that adding water molecules to the framework results in competition between water molecules and HeptaMB$^+$ with the active site of framework. This results in a different orientation of the intermediate within the framework and thereby results in a less anisotropic deformation of the framework. It is stated that the position of the solvent molecules influences the position of the intermediate which again effects the framework flexibility.

During an AIMD simulation of 5-3-CP$^+$ in the H-SAPO-34 unit cell there was a less outspoken preferred direction of the carbocationic intermediate to locate itself. Investigation of the shortest distances of the intermediate to the framework resulted in the conclusion that no differences are noticed between heptaMB$^+$ and 5-3-CP$^+$. Furthermore, the shortest distance of the water molecules towards the framework and the intermediate does not differ much. However, it was seen that more water molecules are constrained to the intermediate 5-3-CP$^+$ than this was the case for heptaMB$^+$. This explains the different behavior of the framework flexibility and location of the intermediate within this framework. Thus it is concluded that for 5-3-CP$^+$, the effect of water increases which is reflected in the position of the 5-3-CP$^+$ and hence effect the framework flexibility.

From these two intermediates an energy profile was made for all four cases where the energy level of 5-3-CP$^+$ was expressed relative to heptaMB$^+$. Although, this energy profile does not include transition state energies it is a measure for the driving force of the reaction step. The energy difference between heptaMB$^+$ and 5-3-CP$^+$ increases at first (when two water molecules are added in each cage) but this difference diminishes when four water molecules are added in each cage. The effect of water on the energy profile is thus quiet outspoken but at high water loadings the effect completely cancels out again. It should be noted that a simulation of 50 ps is rather short to do accurate energy calculations because of the rather large energy deviations over time. When no water molecules were present, it is concluded that the paring cycle has a low overall driving force. PMCP$^+$ lies already 133 kJ/mol higher in energy compared to HeptaMB$^+$ which suggests a low driving force for this route. The anti-aromatic nature of PMCP$^+$ is presumed to be the cause of this.

The last evaluated intermediate is PMCP$^+$. Interaction between the water molecules and the intermediate as well as with the framework is more strongly present than for the other two considered intermediates. Furthermore, the amount of clustering is higher compared with the clustering for the other two considered intermediates. This finally, lead to the global conclusion that the presence of water stabilizes the intermediate. Com-

petition between the water molecules and the intermediate to locate itself towards the Si-atom result in a decrease of the energy level as was seen in the results of 5-3-CP^+.

At last, some metadynamics simulations were performed. The first step, in which the ring contraction proceeds requires a high energy barrier which is not at all realistic to proceed. Furthermore, the propylene formation reaction was investigated. The incomplete obtained 2D free energy profile shows its lowest energy around -90 kJ/mol.

To conclude, there are some indications to doubt the paring mechanism as nowadays proposed. But the effect of water at high water loadings is positive for the driving force of the reaction to proceed. Taking into account the increased amount of clustering upon increasing water loadings, it can be assumed that due to the clustering there is less competition between the water molecules and the carbon atoms to interact with the framework stabilizing the system. Thus, it is suggested that the overall effect of water on the paring cycle is that it can help the formation of propylene at high water loading, in order to overcome the large energy barriers of this route. Further analysis of the free energy profile is needed to calculate the full paring mechanism. Further analysis on the free energy profile should be made in order to obtain a more accurate free energy profile. Furthermore, the expansion of the 5-ring back to the 6-ring should be investigated. An alternative mechanism in which first expansion proceeds before contraction take place seems promising and could be interesting for future work.

Appendix A

Unit cell parameter variation after 30, 35, 40, 45 and 50 ps

In this appendix the unit cell parameters are shown for each simulation after 30, 35, 40, 45 and 50 ps of the 50 ps MD simulation. This to give an idea of the accuracy of the performed simulations.
The variation in a unit cell parameter x (x = a, b, c or volume) is defined as given in Equation A.1.

$$\frac{\bar{x}^{\#ps} - \bar{x}^{50ps}_{empty}}{\bar{x}^{50ps}_{empty}} \tag{A.1}$$

A.1 HeptaMB$^+$

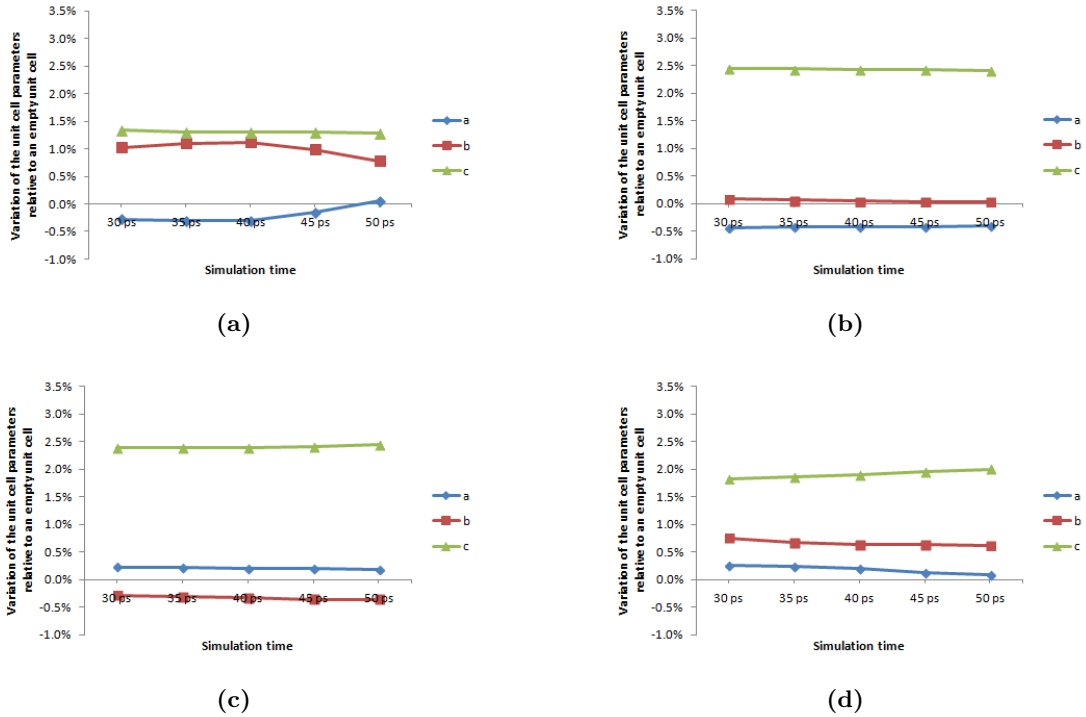

Figure A.1: Average variation of unit cell parameters relative to an empty H-SAPO-34 unit cell at 623 K and 1 atm at 30, 35, 40, 45 and 50 ps of a 50 ps MD simulation of heptaMB$^+$ for a) case 0, b) case 1, c) case 2 and d) case 3.

A.2 5-3-CP$^+$

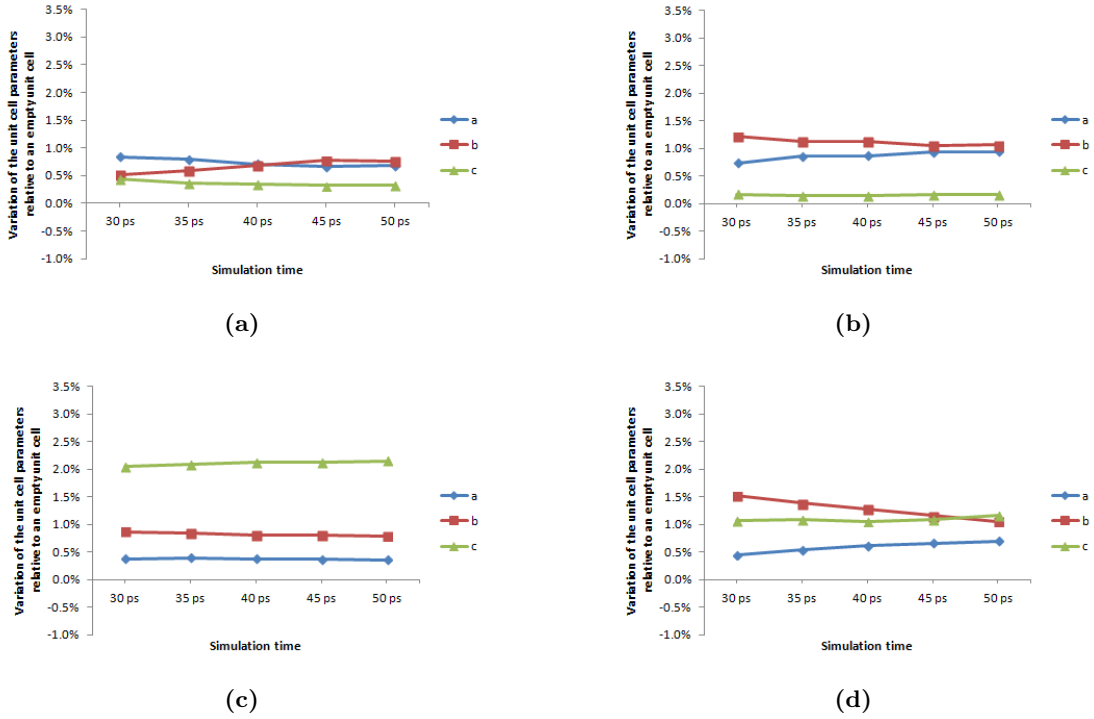

Figure A.2: Average variation of unit cell parameters relative to an empty H-SAPO-34 unit cell at 623 K and 1 atm at 30, 35, 40, 45 and 50 ps of a 50 ps MD simulation of 5-3-CP$^+$ for a) case 0, b) case 1, c) case 2 and d) case 3.

A.3 $PMCP^+$

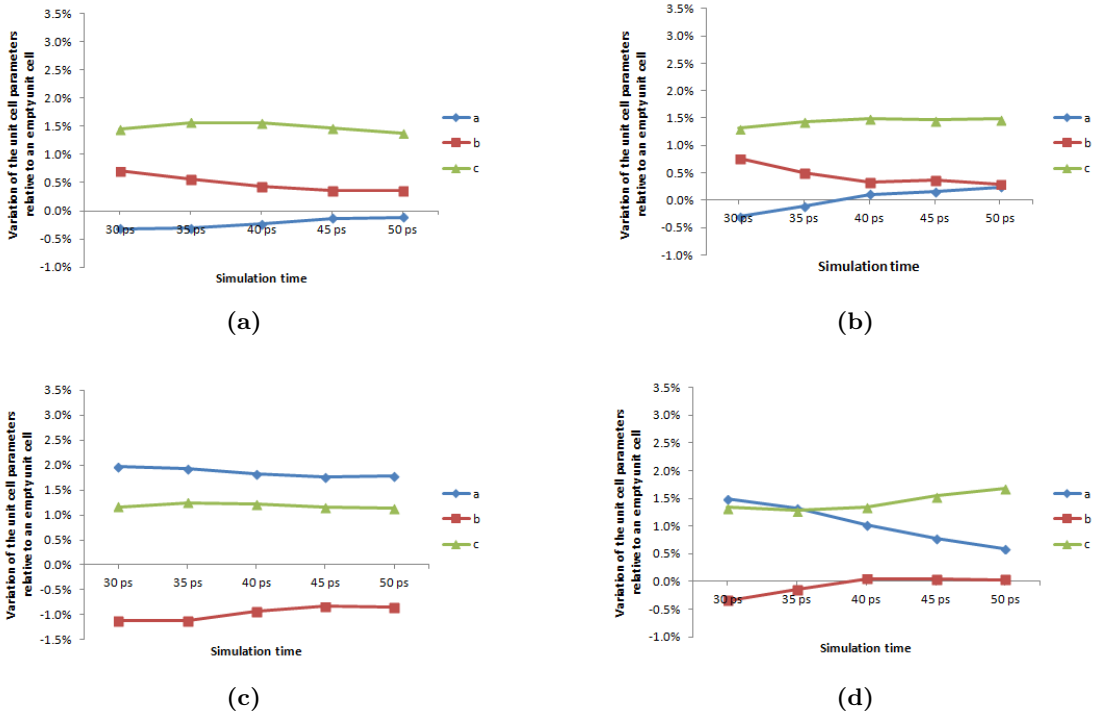

Figure A.3: Average variation of unit cell parameters relative to an empty H-SAPO-34 unit cell at 623 K and 1 atm at 30, 35, 40, 45 and 50 ps of a 50 ps MD simulation of $PMCP^+$ for a) case 0, b) case 1, c) case 2 and d) case 3.

Appendix B

Variation of the unit cell volume after 30, 35, 40, 45 and 50 ps

In this appendix the volume is shown for each simulation after 30, 35, 40, 45 and 50 ps of the 50 ps MD simulation. This to give an idea of the accuracy of the performed simulations.

B.1 HeptaMB$^+$

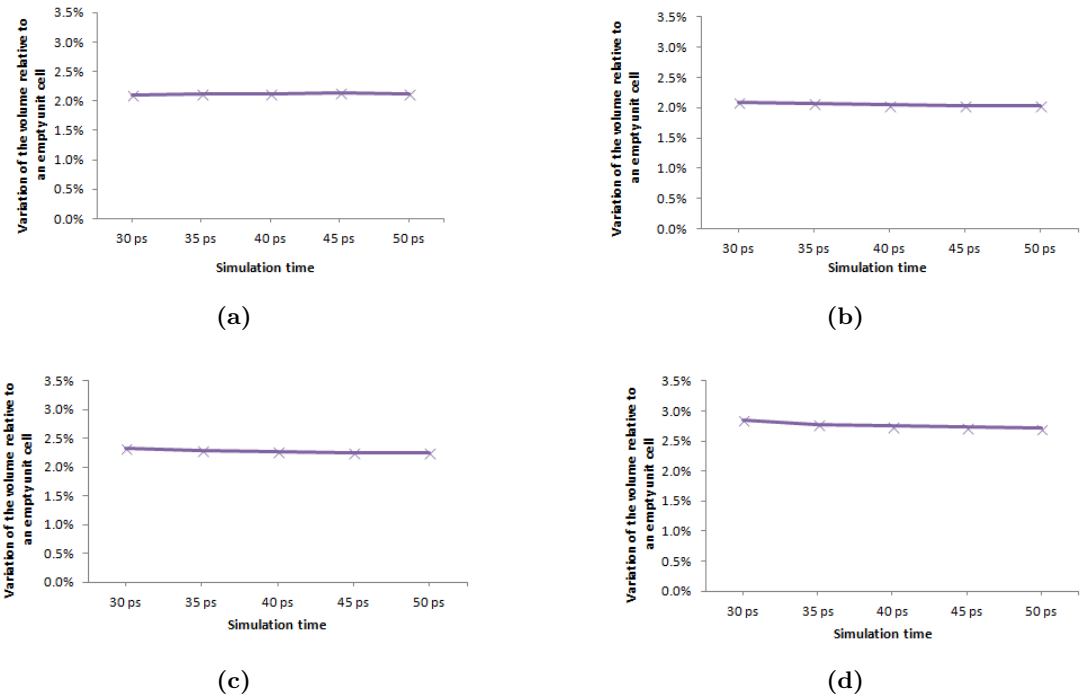

Figure B.1: Average variation of the volume relative to an empty H-SAPO-34 unit cell at 623 K and 1 atm at 30, 35, 40, 45 and 50 ps of a 50 ps MD simulation of heptaMB$^+$ for a) case 0, b) case 1, c) case 2 and d) case 3.

B.2 5-3-CP$^+$

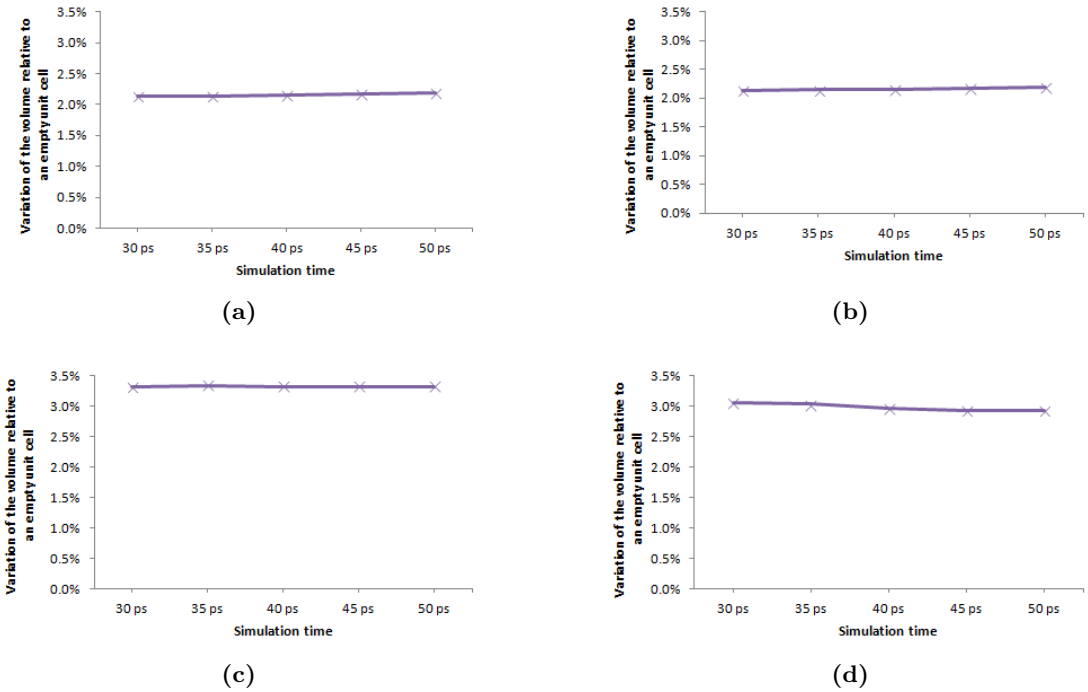

Figure B.2: Average variation of the volume relative to an empty H-SAPO-34 unit cell at 623 K and 1 atm at 30, 35, 40, 45 and 50 ps of a 50 ps MD simulation of 5-3-CP$^+$ for a) case 0, b) case 1, c) case 2 and d) case 3.

B.3 $PMCP^+$

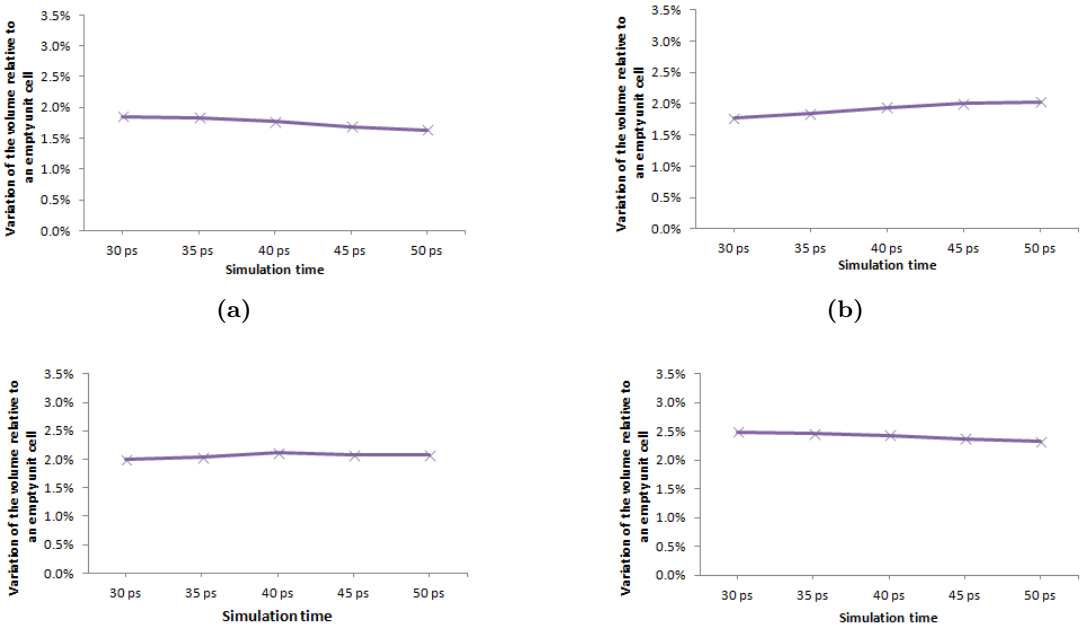

Figure B.3: Average variation of the volume relative to an empty H-SAPO-34 unit cell at 623 K and 1 atm at 30, 35, 40, 45 and 50 ps of a 50 ps MD simulation of $PMCP^+$ for a) case 0, b) case 1, c) case 2 and d) case 3.

Appendix C

Energy deviation after 30, 35, 40, 45 and 50 ps

In this appendix the energy deviation is shown for after 30, 35, 40, and 45 ps of the 50 ps MD simulation. This to give an idea of the accuracy of the performed simulations. The deviation is defined as the energy difference between the energy calculated at 30, 35, 40 and 45 ps and the energy calculated at 50 ps.

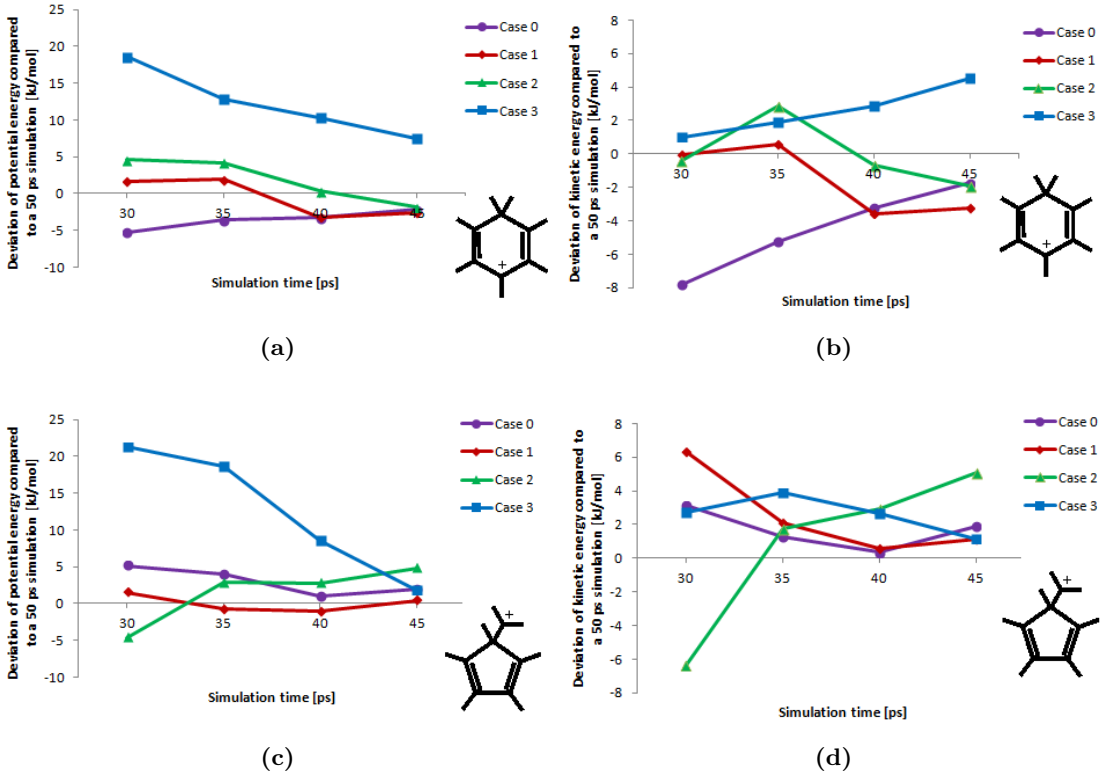

Figure C.1: Energy difference between the energy calculated at 30, 35, 40 and 45 ps and the energy calculated after 50 ps for a) and b) heptaMB$^+$ and c) and d) 5-3-CP$^+$.

Appendix D

Mobility of the solvent molecule

D.1 HeptaMB$^+$

D.1.1 Case 1

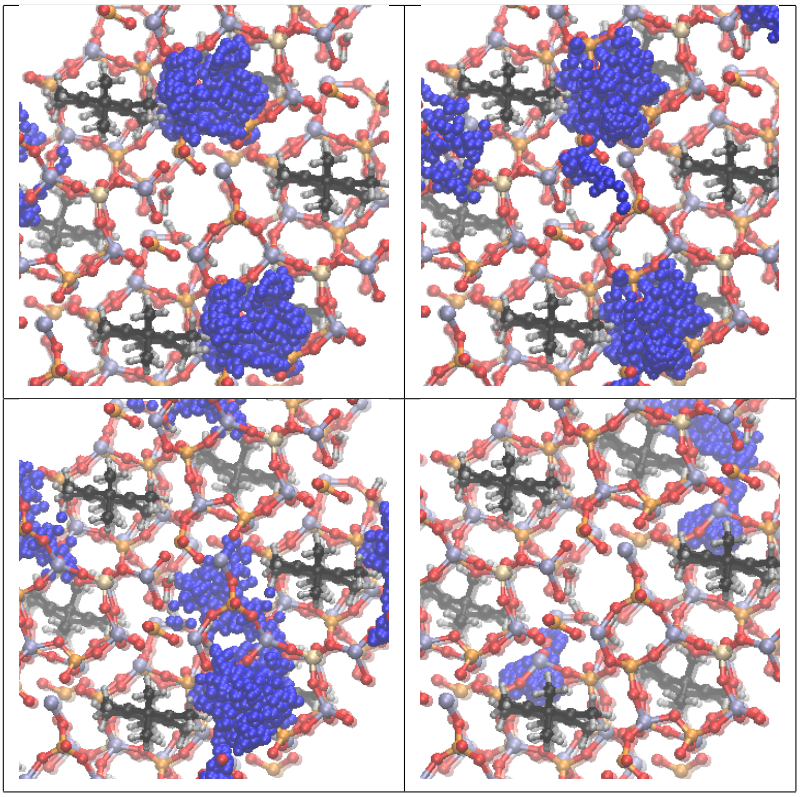

Table D.1: MD visualization of the different positions that an oxygen atom of water molecules has in a 50 ps MD simulation in H-SAPO-34 in case 1 with heptaMB$^+$ at 623 K and 1 atm.

D.1.2 Case 2

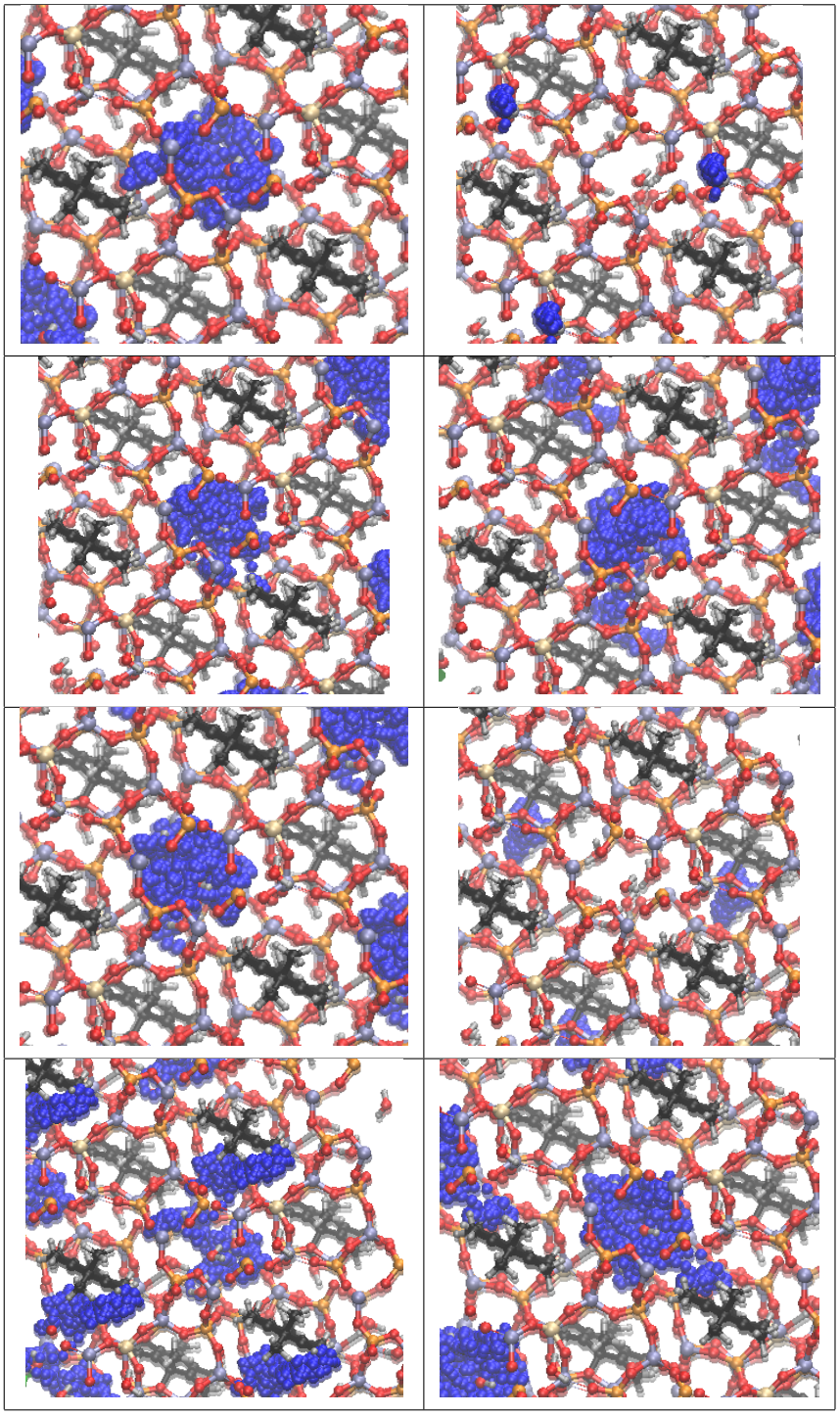

Table D.2: MD visualization of the different positions that an oxygen atom of water molecules has in a 50 ps MD simulation in H-SAPO-34 in case 2 with heptaMB$^+$ at 623 K and 1 atm.

D.2 5-3-CP$^+$

D.2.1 Case 1

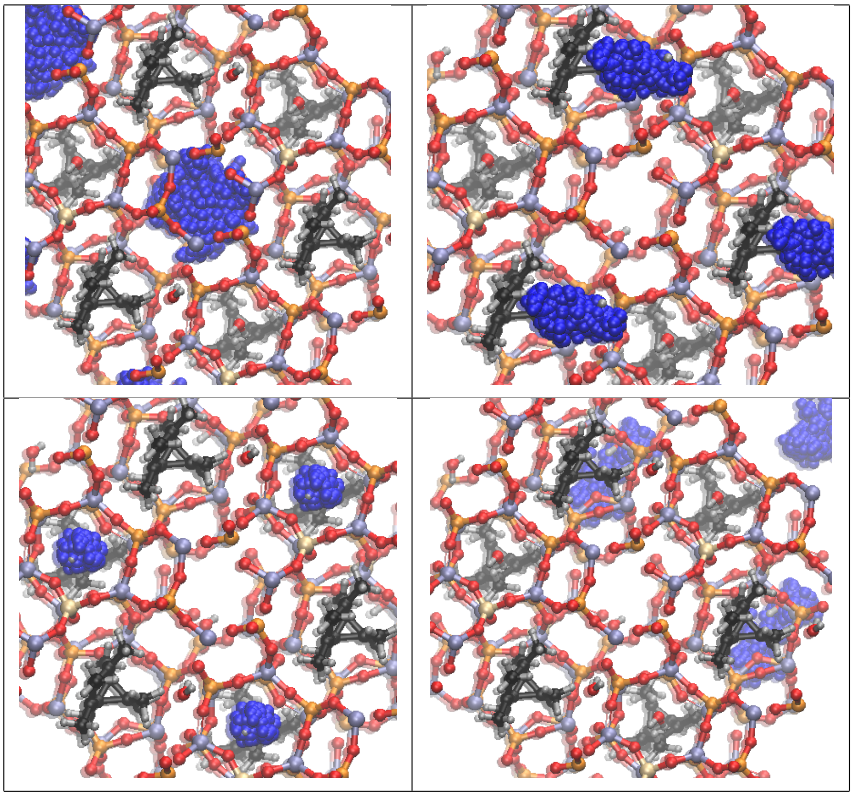

Table D.3: MD visualization of the different positions that an oxygen atom of water molecules has in a 50 ps MD simulation in H-SAPO-34 in case 1 with 5-3-CP$^+$ at 623 K and 1 atm.

D.2.2 Case 2

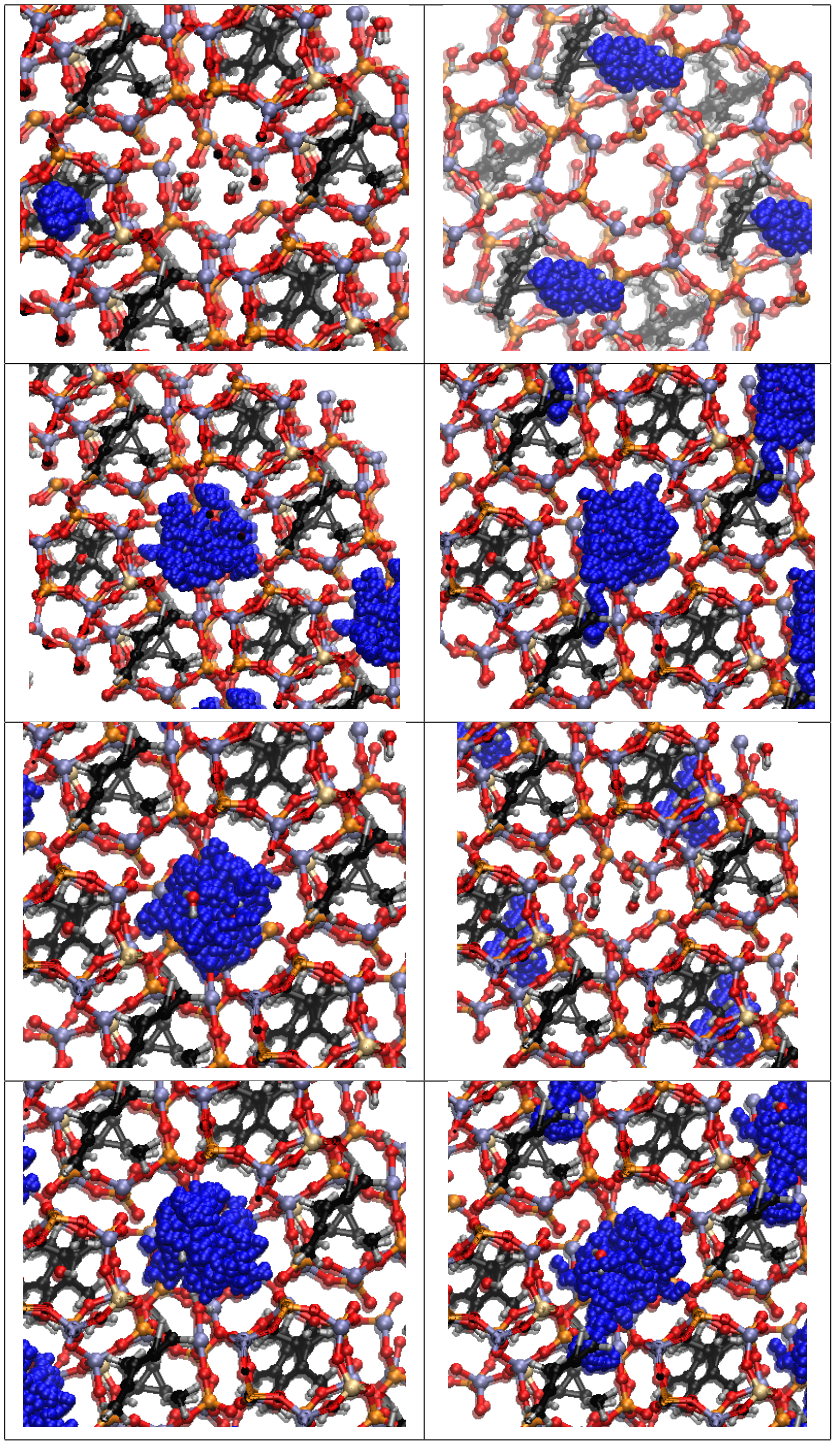

Table D.4: MD visualization of the different positions that an oxygen atom of water molecules has in a 50 ps MD simulation in H-SAPO-34 in case 2 with 5-3-CP$^+$ at 623 K and 1 atm.

D.3 $PMCP^+$

D.3.1 Case 1

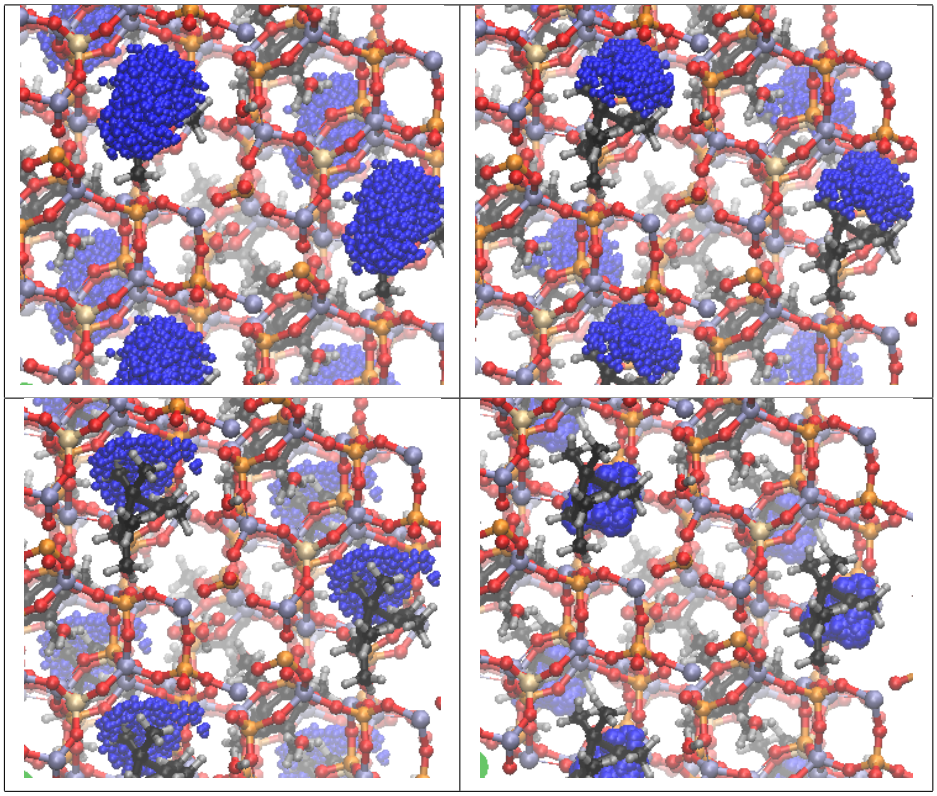

Table D.5: MD visualization of the different positions that an oxygen atom of water molecules has in a 50 ps MD simulation in H-SAPO-34 in case 1 with $PMCP^+$ at 623 K and 1 atm.

D.3.2 Case 2

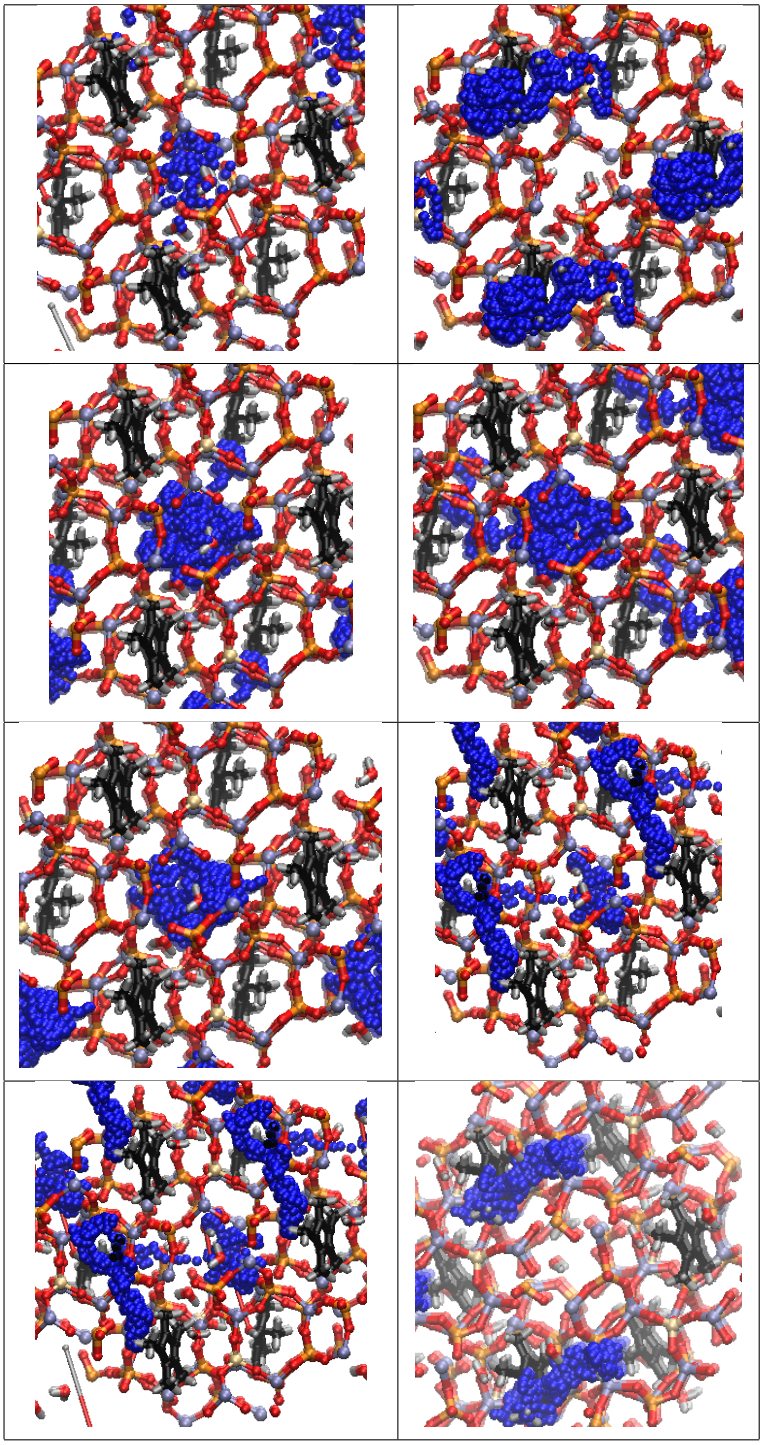

Table D.6: MD visualization of the different positions that an oxygen atom of water molecules has in a 50 ps MD simulation in H-SAPO-34 in case 2 with $PMCP^+$ at 623 K and 1 atm.

Appendix E

Notes on the AIMD simulation of $PMCP^+$ in case 0

During AIMD simulation of $PMCP^+$ and propylene, the bicyclic molecule as shown in Figure E.1 was formed. During these simulations propylene and $PMCP^+$ were placed in the same case of a H-SAPO-34 unit cell. Although it was tried to place propylene in a unfavorable position for reaction, the bicyclic molecule was formed. The result is shown because it confirms the hypothesis of the unstable $PMCP^+$ molecule.

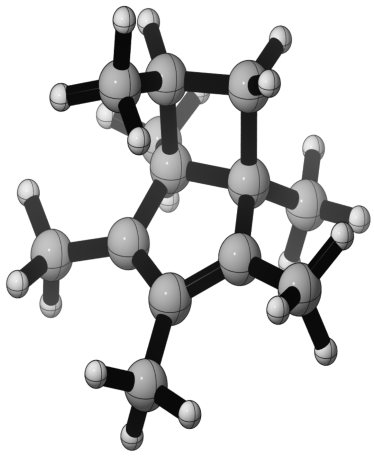

Figure E.1: Bicyclic molecule found during AIMD simulation of $PMCP^+$ and propylene.

Appendix F

Summary of the extra computational details of the metadynamics simulations

F.1 Contraction reaction of heptaMB$^+$ to 5-iC$_3$−CP$^+$/ 5-3-CP$^+$

Table F.1: Collective variables and the quadratic walls applied to them in the MTD simulations of the contraction reaction of heptaMB$^+$, discussed in Section 5.1

CV	r_0 **[Å]**	**Position**	K^α **[kJ/mol]**	Direction	hills
CV1	2.0	-	-	attractive	yes
CV2	2.0	-	-	attractive	yes
CV	2.0	0.55	262550	attractive	no

Table F.2: Unit cell dimensions used during the metadynamics simulations of the contraction reaction of heptaMB$^+$, discussed in Section 5.1

a [Å]	**a [Å]**	**a [Å]**	α [°]	α [°]	α [°]
14.0556	14.0268	15.1532	90	90	120

F.2 Propylene formation of 5-3-CP$^+$

Table F.3: Collective variables and the quadratic walls applied to them in the MTD simulations of propylene formation of 5-3-CP$^+$, discussed in Section 5.2

CV	r_0 **[Å]**	**Position**	K^α **[kJ/mol]**	Direction	hills
CV1	2.0	0.05	262550	repulsive	yes
CV2a	1.2	-	-	attractive	yes
CV2b	1.2	-	-	attractive	yes

Table F.4: Unit cell dimensions used during the metadynamics simulations of the contraction reaction of propylene formation of 5-3-CP$^+$, discussed in Section 5.2

a [Å]	**a [Å]**	**a [Å]**	α [°]	α [°]	α [°]
13.9080	13.8796	14.9941	90	90	120

Appendix G

Poster NCCC

This appendix contains the poster which was presented on March 7 2015 at the 17th Netherlands' Catalysis and Chemistry Conference (NCCC), Noordwijkerhout (NL), as KNCV selected student.

Impact of a mixed water methanol feed on olefin formation during the MTO process

Yentl Pauwels, Kristof De Wispelaere, Simon Bailleul and Veronique Van Speybroeck

Center for Molecular Modeling, Ghent University, Technologiepark 903, 9052 Zwijnaarde, Belgium

The Methanol-to-Olefins (MTO) process

Depletion of oil reserves initiated the quest for alternative processes to produce hydrocarbons.
Within this respect the MTO process is developed in which a methanol source originating from a carbon feedstock can be converted into hydrocarbons using **zeolite catalysts**.[1]

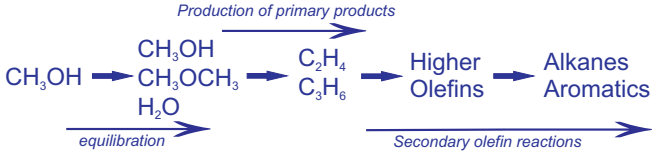

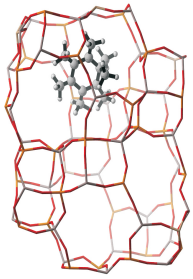

H-SAPO-34[2]

- Silicoaluminophosphate catalyst
- 3D-network: Large cages (10.0x6.7 Å²) and small 8-ring windows (3.8x3.8 Å²)
- Large cages promote methylbenzenes as main hydrocarbon pool species
- Narrow 8-ring window restricts diffusion of large molecules ⟶ High selectivity towards light alkenes

Reaction mechanism

Dual cycle mechanism = indirect hydrocarbon pool mechanism with as HP species[3,4]:

- higher olefins or
- polymethylbenzenes

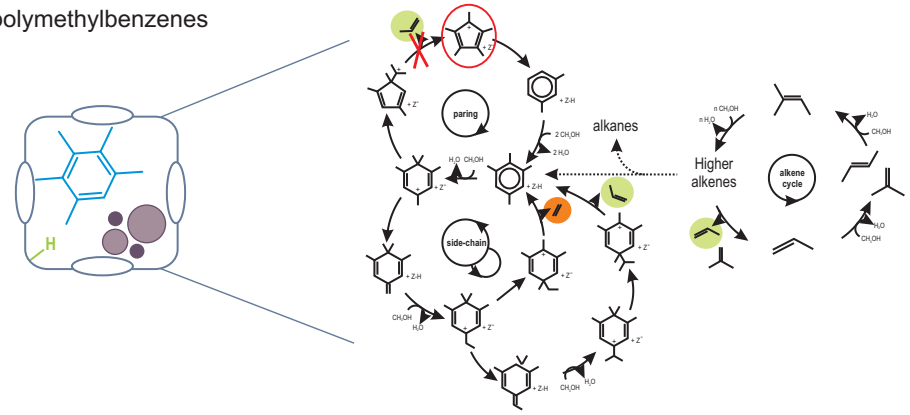

Water is often present in the methanol feed or can be added on purpose to tune the catalyst stability and product selectivity.[5]

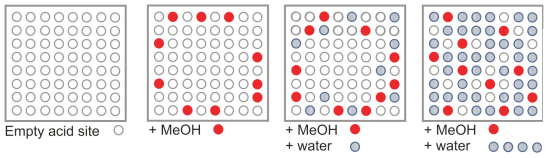

Results

Stability of the intermdiate placed in 1 cage

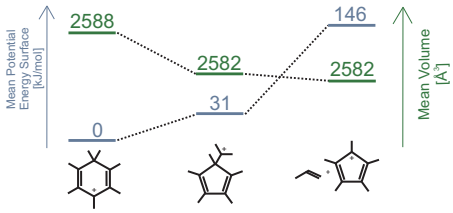

Volume of the unit cell with intermediate in 1 cage

Volume of the unit cell in case 1, 2 and 3

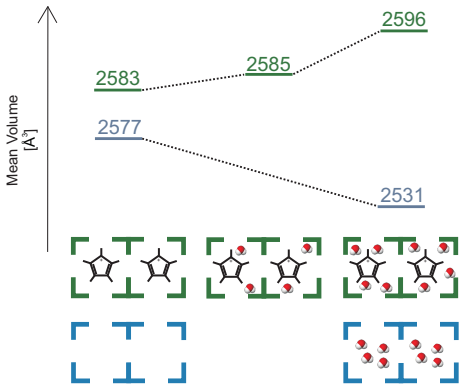

Conclusion and Future work

- Unstable intermediates were found in accordance to literature
- Contraction of the framework can be the driving force for the paring mechanism.
- Contraction of the framework is influenced by the presence of water.[7] In further calculations the influence of water on the reactivity will be examined.

References

[1] Hemelsoet K., Van der Mynsbrugge J., De Wispelaere K., Waroquier M. and Van Speybroeck V., ChemPhysChem 14 (2013) 1526
[2] Lesthaeghe D., Van Speybroeck V., Waroquier M., Stud. Surf. Sci. Catal. 174 (2008) 741-744.
[3] Arstad, B., Nicholas, J. B., Haw, J. F., J. Am. Chem. Soc. 126 (2004) 9, 2991-3001.
[4] Ilias S. and Bhan A., J. Catal. 311 (2014) 6
[5] De Wispelaere K., Wondergem C.S., Ensing B., Hemelsoet K. et al., ACS Catal. (2016)
[6] Grimme, S., J. Chem. Theory Comput 25.12 (2004) 1463-1473.
[7] De Wispelaere K., Ensing B., Ghysels A., Meijer E. J. and Van Speybroeck V., J. Catal. 21.26 (2015) 9385-9396

Objective

- Analysis of the **paring mechanism** via molecular dynamics in order to determine the bottlenecks of the mechanism.
- Investigation of alternative pathways via molecular dynamics in which the bottleneck is defeated.
- Investigate the **effect of a mixed water methanol feed** on the importance of crucial reaction steps in the MTO process in H-SAPO-34.

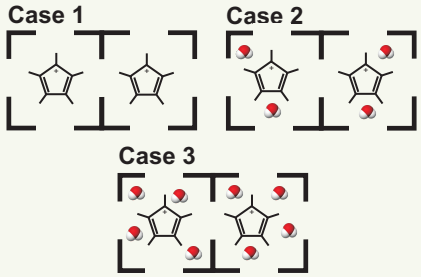

General approach

Molecular dynamics (MD)

⬇

Stability of the intermediate? Dynamic behavior?

⬇

Are there alternative reaction pathways?

MD Methodology[7]

Why MD?

- Simulate reaction steps at MTO reaction conditions: 623 K and 1 atm
- T-effects ⟶ Entropy
- Take into account the effect of high loadings of water

Computational Details:

- Periodic unit cell
- CP2K software
- revPBE-D3 dispersion[6]
- 50 ps simulations

Acknowledgement

List of Figures

List of Tables

Bibliography

[1] S. Sorrell, J. Speirs, R. Bentley, A. Brandt, and R. Miller, "Global oil depletion: A review of the evidence," *Energy Policy*, vol. 38, no. 9, pp. 5290 – 5295, 2010.

[2] C. H. Christensen, J. Rass-Hansen, C. Marsden, E. Taarning, and K. Egeblad, "The renewable chemicals industry," *ChemSusChem*, vol. 1, no. 4, pp. 283–289, 2008.

[3] Transparency Market Research, "Ethylene and propylene market-global industry analysis, size, share, growth, trends, and forecast, 2012-2018," 2012.

[4] G. A. Olah, "Beyond oil and gas: The methanol economy," *Angew. Chem., Int. Ed.*, vol. 44, no. 18, pp. 2636–2639, 2005.

[5] G. W. Huber, S. Iborra, and A. Corma, "Synthesis of transportation fuels from biomass: Chemistry, catalysts, and engineering," *Chem. Rev.*, vol. 106, no. 9, pp. 4044–4098, 2006.

[6] International Business Times, "World energy day 2014: How much oil is left and how long will it last?," 2014.

[7] U.S. Energy Information Administration (EIA), "International energy statistics - crude oil proved reserves," 2015.

[8] K. Bentley, "Global oil and gas depletion: an overview," *Energy Policy*, vol. 30, no. 3, pp. 189 – 205, 2002.

[9] The Guardian, "Opec bid to kill off us shale sends oil price down to 2009 low," 2016.

[10] ihs, "Trading places: Abundant ethane supplies fuel resurgence for north american producers, while middle east faces supply limitations, says ihs," 2015.

[11] C. D. Chang and A. J. Silvestri, "Conversion of methanol and other o-compounds to hydrocarbons over zeolite catalysts," *J. Catal.*, vol. 47, no. 2, pp. 249–259, 1977.

[12] P. Caesar and R. Morrison, "Process for manufacturing ethylene," 1978. U.S. Patent 4,083,889.

[13] L. G. Argauer R.J., "Crystalline zeolite zsm-5 and method of preparing the same," 1972.

[14] M. Dry, "The sasol route to fuels," *Chemtech*, vol. 12, 1982.

[15] T.-c. He, X.-h. Cheng, L. Li, and G.-y. Meng, "Study of methanol-to-gasoline process for production of gasoline from coal," *J. Coal Sci. Eng. (China)*, vol. 15, no. 1, pp. 104–107, 2009.

[16] M. Stocker, "Methanol-to-hydrocarbons: catalytic materials and their behavior," *Microporous Mesoporous Mater.*, vol. 29, no. 1-2, pp. 3–48, 1999.

[17] S. Wilson, B. Lok, and E. Flanigen, "Crystalline metallophosphate compositions," 1982.

[18] F. J. Keil, "Methanol-to-hydrocarbons: process technology," *Microporous Mesoporous Mater.*, vol. 29, no. 1-2, pp. 49–66, 1999.

[19] UOP Honneywell, "Cost effective ethylene production from traditional and non-traditional sources," 2016.

[20] H. Koempel and W. Liebner, *Lurgi's Methanol To Propylene (MTP (R)) Report on a successful commercialisation*, vol. 167, pp. 261–267. 2007.

[21] U. Olsbye, S. Svelle, M. Bjørgen, P. Beato, T. V. W. Janssens, F. Joensen, S. Bordiga, and K. P. Lillerud, "Conversion of methanol to hydrocarbons: How zeolite cavity and pore size controls product selectivity," *Angew. Chem., Int. Ed.*, vol. 51, no. 24, pp. 5810–5831, 2012.

[22] J. Q. Chen, A. Bozzano, B. Glover, T. Fuglerud, and S. Kvisle, "Recent advancements in ethylene and propylene production using the uop/hydro mto process," *Catal. Today*, vol. 106, no. 1-4, pp. 103–107, 2005.

[23] P. Spath and D. Dayton, *Technical and Economic Assessment of Synthesis Gas to Fuels and Chemicals with Emphasis on the Potential for Biomass-Derived Syngas*, pp. 29–57. National Renewable Energy Laboratory, 2003.

[24] K. Aasberg-Petersen, I. Dybkjaer, C. V. Ovesen, N. C. Schjodt, J. Sehested, and S. G. Thomsen, "Natural gas to synthesis gas - catalysts and catalytic processes," *J. Nat. Gas Sci. Eng.*, vol. 3, no. 2, pp. 423–459, 2011.

[25] L. C. Grabow and M. Mavrikakis, "Mechanism of methanol synthesis on cu through co2 and co hydrogenation," *ACS Cat.*, vol. 1, no. 4, pp. 365–384, 2011.

[26] T. Alvaro-Munoz, C. Marquez-Alvarez, and E. Sastre, "Aluminium chloride: A new aluminium source to prepare sapo-34 catalysts with enhanced stability in the mto process," *Appl. Catal., A*, vol. 472, pp. 72–79, 2014.

[27] G. Pop, R. Ganea, D. Ivanescu, G. Ignatescu, R. Boeru, and B. R., "Catalytic process for the preparation of light olefins from methanol in a fluidised bed reactor," 1997. Patent WO2000041986A1.

[28] J. Daviduk and J. Haddad, "Fluid zeolite catalyst conversion of alcohols and oxygenated derivatives to hydrocarbons by controlling exothermic reaction heat," 1979. U.S. Patent 4,328,384.

[29] A. Sapre, "Conversion of methanol to olefins in a tubular reactor with light olefin co-feeding," 1984. U.S. Patent 4,590,320.

[30] P. Tian, Y. X. Wei, M. Ye, and Z. M. Liu, "Methanol to olefins (mto): From fundamentals to commercialization," *ACS Catal.*, vol. 5, no. 3, pp. 1922–1938, 2015.

[31] S. N. Khadzhiev, M. V. Magomedova, and E. G. Peresypkina, "Mechanism of olefin synthesis from methanol and dimethyl ether over zeolite catalysts: A review," *Pet. Chem.*, vol. 54, no. 4, pp. 245–269, 2014.

[32] K. Hemelsoet, J. Van der Mynsbrugge, K. De Wispelaere, M. Waroquier, and V. Van Speybroeck, "Unraveling the reaction mechanisms governing methanol-to-olefins catalysis by theory and experiment," *ChemPhysChem*, vol. 14, no. 8, pp. 1526–1545, 2013.

[33] D. Lesthaeghe, V. Van Speybroeck, G. B. Marin, and M. Waroquier, "What role do oxonium ions and oxonium ylides play in the zsm-5 catalysed methanol-to-olefin process?," *Chem. Phys. Lett.*, vol. 417, no. 4, pp. 309 – 315, 2006.

[34] H. Yamazaki, H. Shima, H. Imai, T. Yokoi, T. Tatsumi, and J. N. Kondo, "Evidence for a 'carbene-like' intermediate during the reaction of methoxy species with light alkenes on h-zsm-5," *Angew. Chem., Int. Ed.*, vol. 50, no. 8, pp. 1853–1856, 2011.

[35] D. Lesthaeghe, V. Van Speybroeck, G. B. Marin, and M. Waroquier, "Understanding the failure of direct c-c coupling in the zeolite-catalyzed methanol-to-olefin process," *Angew. Chem.*, vol. 118, no. 11, pp. 1746–1751, 2006.

[36] R. M. Dessau and R. B. Lapierre, "On the mechanism of methanol conversion to hydrocarbons over h-zsm-5," *J. Catal.*, vol. 78, no. 1, pp. 136–141, 1982.

[37] R. M. Dessau, "On the zsm-5 catalyzed formation of ethylene from methanol or higher olefins," *J. Catal.*, vol. 99, no. 1, pp. 111–116, 1986.

[38] I. M. Dahl and S. Kolboe, "On the reaction mechanism for hydrocarbon formtation from methanol over sapo-34 .1. isotopic labeling studies of the co-reaction of ethene and methanol," *J. Catal.*, vol. 149, no. 2, pp. 458–464, 1994.

[39] C. M. Wang, Y. D. Wang, Y. J. Du, G. Yang, and Z. K. Xie, "Similarities and differences between aromatic-based and olefin-based cycles in h-sapo-34 and h-ssz-13 for methanol-to-olefins conversion: insights from energetic span model," *Catal. Sci. Technol.*, vol. 5, no. 9, pp. 4354–4364, 2015.

[40] S. Svelle, M. Bjørgen, S. Kolboe, D. Kuck, M. Letzel, U. Olsbye, O. Sekiguchi, and E. Uggerud, "Intermediates in the methanol-to-hydrocarbons (mth) reaction: A gas phase study of the unimolecular reactivity of multiply methylated benzenium cations," *Catal. Lett.*, vol. 109, no. 1-2, 2006.

[41] A. J. Jones and E. Iglesia, "Kinetic, spectroscopic, and theoretical assessment of associative and dissociative methanol dehydration routes in zeolites," *Angew. Chem., Int. Ed.*, vol. 53, no. 45, pp. 12177–12181, 2014.

[42] J. F. Haw, W. G. Song, D. M. Marcus, and J. B. Nicholas, "The mechanism of methanol to hydrocarbon catalysis," *Acc. Chem. Res.*, vol. 36, no. 5, pp. 317–326, 2003.

[43] R. Sullivan, C. J. Egan, G. Langlois, and R. P. Sieg, "A new reaction that occurs in the hydrocracking of certain aromatic hydrocarbons," *J. Am. Chem. Soc*, vol. 83, no. 5, pp. 1156–1160, 1961.

[44] T. Mole, G. Bett, and D. Seddon, "Conversion of methanol to hydrocarbons over zsm-5 zeolite: An examination of the role of aromatic hydrocarbons using 13 carbon-and deuterium-labeled feeds," *J. Catal.*, vol. 84, no. 2, pp. 435–445, 1983.

[45] J. F. Haw, J. B. Nicholas, W. G. Song, F. Deng, Z. K. Wang, T. Xu, and C. S. Heneghan, "Roles for cyclopentenyl cations in the synthesis of hydrocarbons from methanol on zeolite catalyst hzsm-5," *J. Am. Chem. Soc.*, vol. 122, no. 19, pp. 4763–4775, 2000.

[46] V. Van Speybroeck, K. De Wispelaere, J. Van der Mynsbrugge, M. Vandichel, K. Hemelsoet, and M. Waroquier, "First principle chemical kinetics in zeolites: the methanol-to-olefin process as a case study," *Chem. Soc. Rev.*, vol. 43, no. 21, pp. 7326–7357, 2014.

[47] D. Lesthaeghe, J. Van der Mynsbrugge, M. Vandichel, M. Waroquier, and V. Van Speybroeck, "Full theoretical cycle for both ethene and propene formation during methanol-to-olefin conversion in h-zsm-5," *ChemCatChem*, vol. 3, no. 1, pp. 208–212, 2011.

[48] S. Svelle, F. Joensen, J. Nerlov, U. Olsbye, K.-P. Lillerud, S. Kolboe, and M. Bjørgen

[49] W. G. Song, H. Fu, and J. F. Haw, "Selective synthesis of methylnaphthalenes in hsapo-34 cages and their function as reaction centers in methanol-to-olefin catalysis," *J Phys Chem B*, vol. 105, no. 51, pp. 12839–12843, 2001.

[50] D. M. McCann, D. Lesthaeghe, P. W. Kletnieks, D. R. Guenther, M. J. Hayman, V. Van Speybroeck, M. Waroquier, and J. F. Haw, "A complete catalytic cycle for supramolecular methanol-to-olefins conversion by linking theory with experiment," *Angew. Chem., Int. Ed.*, vol. 47, no. 28, pp. 5179–5182, 2008.

[51] V. Van Speybroeck, K. Hemelsoet, K. De Wispelaere, Q. Y. Qian, J. Van der Mynsbrugge, B. De Sterck, B. M. Weckhuysen, and M. Waroquier, "Mechanistic studies on chabazite-type methanol-to-olefin catalysts: Insights from time-resolved uv/vis microspectroscopy combined with theoretical simulations," *ChemCatChem*, vol. 5, no. 1, pp. 173–184, 2013.

[52] B. Arstad and S. Kolboe, "The reactivity of molecules trapped within the sapo-34 cavities in the methanol-to-hydrocarbons reaction," *J. Am. Chem. Soc*, vol. 123, no. 33, pp. 8137–8138, 2001.

[53] S. L. C. Moors, K. De Wispelaere, J. Van der Mynsbrugge, M. Waroquier, and V. Van Speybroeck, "Molecular dynamics kinetic study on the zeolite-catalyzed benzene methylation in zsm-5," *ACS Catal.*, vol. 3, no. 11, pp. 2556–2567, 2013.

[54] J. Van der Mynsbrugge, S. L. C. Moors, K. De Wispelaere, and V. Van Speybroeck, "Insight into the formation and reactivity of framework-bound methoxide species in h-zsm-5 from static and dynamic molecular simulations," *ChemCatChem*, vol. 6, no. 7, pp. 1906–1918, 2014.

[55] R. Y. Brogaard, R. Henry, Y. Schuurman, A. J. Medford, P. G. Moses, P. Beato, S. Svelle, J. K. Nørskov, and U. Olsbye, "Methanol-to-hydrocarbons conversion: The alkene methylation pathway," *J. Catal.*, vol. 314, pp. 159 – 169, 2014.

[56] B. Arstad, S. Kolboe, and O. Swang, "A theoretical investigation on the methylation of methylbenzenes on zeolites," *J. Phys. Chem. B*, vol. 106, no. 49, pp. 12722–12726, 2002.

[57] D. Lesthaeghe, A. Horre, M. Waroquier, G. B. Marin, and V. Van Speybroeck, "Theoretical insights on methylbenzene side-chain growth in zsm-5 zeolites for methanol-to-olefin conversion," *Chem. - Eur. J.*, vol. 15, no. 41, pp. 10803–10808, 2009.

[58] K. De Wispelaere, S. Bailleul, and V. Van Speybroeck, "Towards molecular control of elementary reactions in zeolite catalysis by advanced molecular simulations mimicking operating conditions," *Catal. Sci. Technol.*, 2016.

[59] K. De Wispelaere, K. Hemelsoet, M. Waroquier, and V. Van Speybroeck, "Complete low-barrier side-chain route for olefin formation during methanol conversion in h-sapo-34," *J. Catal.*, vol. 305, pp. 76–80, 2013.

[60] M. W. Erichsen, S. Svelle, and U. Olsbye, "H-sapo-5 as methanol-to-olefins (mto) model catalyst: Towards elucidating the effects of acid strength," *J. Catal*, vol. 298, pp. 94 – 101, 2013.

[61] C. Wang, Y. Y. Chu, A. M. Zheng, J. Xu, Q. Wang, P. Gao, G. D. Qi, Y. J. Gong, and F. Deng, "New insight into the hydrocarbon-pool chemistry of the methanol-to-olefins conversion over zeolite h-zsm-5 from gc-ms, solid-state nmr spectroscopy, and dft calculations," *Chem. - Eur. J.*, vol. 20, no. 39, pp. 12432–12443, 2014.

[62] C. M. Wang, Y. D. Wang, H. X. Liu, Z. K. Xie, and Z. P. Liu, "Theoretical insight into the minor role of paring mechanism in the methanol-to-olefins conversion within hsapo-34 catalyst," *Microporous Mesoporous Mater.*, vol. 158, pp. 264–271, 2012.

[63] F. Eder and J. A. Lercher, "Alkane sorption in molecular sieves: The contribution of ordering, intermolecular interactions, and sorption on brønsted acid sites," *Zeolites*, vol. 18, no. 1, pp. 75–81, 1997.

[64] R. Krishna, B. Smit, and S. Calero, "Entropy effects during sorption of alkanes in zeolites," *Chemical Society Reviews*, vol. 31, no. 3, pp. 185–194, 2002.

[65] B. Arstad, S. Kolboe, , and O. Swang, "Theoretical study of the heptamethylbenzenium ion. intramolecular isomerizations and c2, c3, c4 alkene elimination," *J. Phys. Chem. A*, vol. 109, no. 39, pp. 8914–8922, 2005.

[66] B. Arstad, S. Kolboe, and O. Swang, "Theoretical study of protonated xylenes: ethene elimination and h,c-scramling reactions," *J. Phys. Org. Chem.*, vol. 17, no. 11, pp. 1023–1032, 2004.

[67] W. Song, H. Fu, and J. F. Haw, "Supramolecular origins of product selectivity for methanol-to-olefin catalysis on hsapo-34," *J. Am. Chem. Soc*, vol. 123, no. 20, pp. 4749–4754, 2001.

[68] B. Arstad, S. Kolboe, and O. Swang, "Theoretical study of carbon atom scrambling in benzenium ions with ethyl or isopropyl groups," *J. Phys. Org. Chem.*, vol. 19, no. 2, pp. 81–92, 2006.

[69] M. Bjørgen, U. Olsbye, D. Petersen, and S. Kolboe, "The methanol-to-hydrocarbons reaction: insight into the reaction mechanism from c-12 benzene and c-13 methanol coreactions over zeolite h-beta," *J. Catal.*, vol. 221, no. 1, pp. 1–10, 2004.

[70] U. Olsbye, M. Bjørgen, S. Svelle, K.-P. Lillerud, and S. Kolboe, "Mechanistic insight into the methanol-to-hydrocarbons reaction," *Catal. Today*, vol. 106, no. 1, pp. 108–111, 2005.

[71] S. Ilias and A. Bhan, "The mechanism of aromatic dealkylation in methanol-to-hydrocarbons conversion on h-zsm-5: What are the aromatic precursors to light olefins?," *J. Catal.*, vol. 311, pp. 6–16, 2014.

[72] M. Westgård-Erichsen, M. Morten, S. Svelle, O. Sekiguchi, E. Uggerud, and U. Olsbye, "Conclusive evidence for two unimolecular pathways to zeolite-catalyzed dealkylation of the heptamethylbenzenium cation," *ChemCatChem*, 2015.

[73] C. S. Cundy and P. A. Cox, "The hydrothermal synthesis of zeolites: History and development from the earliest days to the present time," *Chem. Rev.*, vol. 103, no. 3, pp. 663–701, 2003.

[74] B. M. Weckhuysen and J. Yu, "Recent advances in zeolite chemistry and catalysis," *Chem. Soc. Rev.*, vol. 44, no. 20, pp. 7022–7024, 2015.

[75] C. Baerlocher and L. McCusker, "Database of zeolite sturctures," 2016. http://www.iza-structure.org/databases/.

[76] A. Corma and J. Martinez-Triguero, "The use of mcm-22 as a cracking zeolitic additive for fcc," *J. Catal.*, vol. 165, no. 1, pp. 102 – 120, 1997.

[77] B. Smit and T. L. M. Maesen, "Molecular simulations of zeolites: Adsorption, diffusion, and shape selectivity," *Chem. Rev.*, vol. 108, no. 10, pp. 4125–4184, 2008.

[78] G. Sastre, D. W. Lewis, and C. R. A. Catlow, "Structure and stability of silica species in sapo molecular sieves," *J. Phys. Chem.*, vol. 100, no. 16, pp. 6722–6730, 1996.

[79] G. Sastre, D. W. Lewis, and C. R. A. Catlow, "Modeling of silicon substitution in sapo-5 and sapo-34 molecular sieves," *J. Phys. Chem. B*, vol. 101, no. 27, pp. 5249–5262, 1997.

[80] B. V. Vora, T. L. Marker, P. T. Barger, H. R. Nilsen, S. Kvisle, and T. Fuglerud, *Economic route for natural gas conversion to ethylene and propylene*, vol. 107 of *Studies in Surface Science and Catalysis*, pp. 87–98. 1997.

[81] J. Van der Mynsbrugge, *Molecular-Level Understanding of Adsorption and Zeolite-Catalyzed Reactions in the Methanol-to-Olefins Process*. University Ghent, 2014.

[82] D. Chen, K. Moljord, and A. Holmen, "A methanol to olefins review: Diffusion, coke formation and deactivation sapo type catalysts," *Microporous Mesoporous Mater.*, vol. 164, pp. 239–250, 2012.

[83] G. Z. Qi, Z. K. Xie, W. M. Yang, S. Q. Zhong, H. X. Liu, C. F. Zhang, and Q. L. Chen, "Behaviors of coke deposition on sapo-34 catalyst during methanol conversion to light olefins," *Fuel Process. Technol.*, vol. 88, no. 5, pp. 437–441, 2007.

[84] J. Weitkamp, "Zeolites and catalysis," *Solid State Ionics*, vol. 131, no. 1, pp. 175–188, 2000.

[85] A. Sassi, M. A. Wildman, H. J. Ahn, P. Prasad, J. B. Nicholas, and J. F. Haw, "Methylbenzene chemistry on zeolite hbeta: Multiple insights into methanol-to-olefin catalysis," *J. Phys. Chem. B*, vol. 106, no. 9, pp. 2294–2303, 2002.

[86] S. Teketel, W. Skistad, S. Benard, U. Olsbye, K. P. Lillerud, P. Beato, and S. Svelle, "Shape selectivity in the conversion of methanol to hydrocarbons: The catalytic performance of one-dimensional 10-ring zeolites: Zsm-22, zsm-23, zsm-48, and eu-1," *ACS Catal.*, vol. 2, no. 1, pp. 26–37, 2012.

[87] J. Z. Li, Y. X. Wei, Y. Qi, P. Tian, B. Li, Y. L. He, F. X. Chang, X. D. Sun, and Z. M. Liu, "Conversion of methanol over h-zsm-22: The reaction mechanism and deactivation," *Catal. Today*, vol. 164, no. 1, pp. 288–292, 2011.

[88] M. Bjørgen, S. Svelle, F. Joensen, J. Nerlov, S. Kolboe, F. Bonino, L. Palumbo, S. Bordiga, and U. Olsbye, "Conversion of methanol to hydrocarbons over zeolite h-zsm-5: On the origin of the olefinic species," *J. Catal.*, vol. 249, no. 2, pp. 195–207, 2007.

[89] J. C. G. Pereira, C. R. A. Catlow, and G. D. Price, "Silica condensation reaction: an ab initio study," *Chem. Commun.*, no. 13, pp. 1387–1388, 1998.

[90] P. McKendry, "Energy production from biomass (part 1): overview of biomass," *Bioresour. Technol.*, vol. 83, no. 1, pp. 37–46, 2002.

[91] F. Wunder, E. Leupold, H. Hachenberg, and H. Schmidt, "Process for the manufacture of lower olefins from methanol/water mixtures," 1981. U.S. Patent 4,296,266.

[92] D. Seddon, T. Mole, and J. Whiteside, "Methanol conversion to hydrocarbons with zeolites and cocatalysts," 1985. U.S. Patent 4,499,314.

[93] L. Miller, S. Miller, and A. Bozzano, "Methanol-water mixtures in olefin production via oxygenate conversion," 2008. U.S. Patent 20,080,039,670.

[94] M. Rothaemel, H. Koempel, B. Ahlers, J. Hofmockel, and M. Wagner, "Method for the production of synthetic fuels from oxygenates," 2006. Patent WO2006076942.

[95] M. Rothaemel, U. Fincke, H. Dropsch, and H. Buchold, "Process and plant for producing synthetic fuels," 2013. U.S. Patent 8,524,970.

[96] J. Senetar, D. Kauff, and A. Bozzano, "Increased conversion of recycled oxygenates in mto," 2015. U.S. Patent 20,150,148,575.

[97] A. T. Najafabadi, S. Fatemi, M. Sohrabi, and M. Salmasi, "Kinetic modeling and optimization of the operating condition of mto process on sapo-34 catalyst," *J. Ind. Eng. Chem.*, vol. 18, no. 1, pp. 29–37, 2012.

[98] A. Marchi and G. Froment, "Catalytic conversion of methanol to light alkenes on sapo molecular sieves," *Appl. Catal.*, vol. 71, no. 1, pp. 139–152, 1991.

[99] W. Wang, A. Buchholz, M. Seiler, and M. Hunger, "Evidence for an initiation of the methanol-to-olefin process by reactive surface methoxy groups on acidic zeolite catalysts," *J. Am. Chem. Soc*, vol. 125, no. 49, pp. 15260–15267, 2003.

[100] D. S. Wragg, M. G. O. Brien, F. L. Bleken, M. Di Michiel, U. Olsbye, and H. Fjellvag, "Watching the methanol-to-olefin process with time- and space-resolved high-energy operando x-ray diffraction," *Angew. Chem., Int. Ed.*, vol. 51, no. 32, pp. 7956–7959, 2012.

[101] K. De Wispelaere, C. S. Wondergem, B. Ensing, K. Hemelsoet, E. J. Meijer, B. M. Weckhuysen, V. Van Speybroeck, and J. Ruiz-Martınez, "Insight into the effect of water on the methanol-to-olefins conversion in h-sapo-34 from molecular simulations and in situ microspectroscopy," *ACS Catal.*, vol. 6, no. 3, pp. 1991–2002, 2016.

[102] K. De Wispelaere, *Advanced molecular simulations of reaction mechanisms and complex reaction environments in the methanol to olefins process.* PhD thesis, 2015.

[103] X. Wu and R. Anthony, "Effect of feed composition on methanol conversion to light olefins over sapo-34," *Appl. Catal., A*, vol. 218, no. 1, pp. 241–250, 2001.

[104] A. G. Gayubo, A. T. Aguayo, A. Atutxa, R. Prieto, and J. Bilbao, "Role of reaction-medium water on the acidity deterioration of a hzsm-5 zeolite," *Ind. Eng. Chem. Res.*, vol. 43, no. 17, pp. 5042–5048, 2004.

[105] Y.-K. Park, S.-W. Baek, and S.-K. Ihm, "Effect of reaction conditions and catalytic properties on methanol conversion over sapo-34," *J. Ind. Eng. Chem.*, vol. 7, no. 3, pp. 167–172, 2001.

[106] R. G. Herman, *Catalytic conversions of synthesis gas and alcohols to chemicals*. Springer Science and Business Media, 2012.

[107] M. Shahda, Y. Dengchao, and W. Huixin, "Methanol conversion to hydrocarbons over a sapo-34 catalyst in a pulse micro reactor," *Pet. Sci. Technol.*, vol. 26, no. 16, pp. 1893–1903, 2008.

[108] K. McLaughlin, M. Matthews, E. Vera-Castaneda, and R. Anthony, "Mechanisms and calculated hydrocarbon distributions for methanol conversion to low molecular weight hydrocarbons," *Prepr. - Am. Chem. Soc., Div. Pet. Chem.*, vol. 29, no. 2, 1984.

[109] V. Van Speybroeck, *Moleculaire Modellering van IndustriÃ≪le processen*. University Ghent, 2015.

[110] A. J. Cohen, P. Mori-Sánchez, and W. Yang, "Insights into current limitations of density functional theory," *Science*, vol. 321, no. 5890, pp. 792–794, 2008.

[111] J. P. Perdew, A. Ruzsinszky, J. Tao, V. N. Staroverov, G. E. Scuseria, and G. I. Csonka, "Prescription for the design and selection of density functional approximations: More constraint satisfaction with fewer fits," *J. Chem. Phys.*, vol. 123, no. 6, p. 062201, 2005.

[112] S. Grimme, "Accurate description of van der waals complexes by density functional theory including empirical corrections," *J. Comput. Chem.*, vol. 25, no. 12, pp. 1463–1473, 2004.

[113] S. Grimme, "Density functional theory with london dispersion corrections," *Wiley Interdiscip. Rev.: Comput. Mol. Sci.*, vol. 1, no. 2, pp. 211–228, 2011.

[114] B. G. Lippert, J. H. Parrinello, and Michele, "A hybrid gaussian and plane wave density functional scheme," *Molecular Physics*, vol. 92, no. 3, pp. 477–488, 1997.

[115] J. Hutter, M. Iannuzzi, F. Schiffmann, and J. VandeVondele, "cp2k: atomistic simulations of condensed matter systems," *Wiley Interdiscip. Rev.: Comput. Mol. Sci.*, vol. 4, no. 1, pp. 15–25, 2014.

[116] J. VandeVondele, M. Krack, F. Mohamed, M. Parrinello, T. Chassaing, and J. Hutter, "Quickstep: Fast and accurate density functional calculations using a mixed gaussian and plane waves approach," *Comput. Phys. Commun.*, vol. 167, no. 2, pp. 103 – 128, 2005.

[117] S. Svelle, C. Tuma, X. Rozanska, T. Kerber, and J. Sauer, "Quantum chemical modeling of zeolite-catalyzed methylation reactions: Toward chemical accuracy for barriers," *J. Am. Chem. Soc*, vol. 131, no. 2, pp. 816–825, 2009.

[118] V. Van Speybroeck, *Chemie van Industriële processen*. University Ghent, 2015.

[119] D. S. Wragg, R. E. Johnsen, P. Norby, and H. Fjellvag, "The adsorption of methanol and water on sapo-34: in situ and ex situ x-ray diffraction studies," *Microporous Mesoporous Mater.*, vol. 134, no. 1-3, pp. 210–215, 2010.

[120] D. S. Wragg, D. Akporiaye, and H. Fjellvåg, "Direct observation of catalyst behaviour under real working conditions with x-ray diffraction: Comparing sapo-18 and sapo-34 methanol to olefin catalysts," *J. Catal.*, vol. 279, no. 2, pp. 397–402, 2011.

[121] M. Zokaie, D. S. Wragg, A. Grønvold, T. Fuglerud, J. H. Cavka, K. P. Lillerud, and O. Swang, "Unit cell expansion upon coke formation in a sapo-34 catalyst: A combined experimental and computational study," *Microporous Mesoporous Mater.*, vol. 165, pp. 1–5, 2013.